TANDEM MASS SPECTROMETRY AND COMPUTATIONAL CHEMISTRY OF ELUSIVE ORGANIC IONS AND NEUTRALS IN THE GAS PHASE

For Tony

For my parents and family

TANDEM MASS SPECTROMETRY AND COMPUTATIONAL CHEMISTRY OF ELUSIVE ORGANIC IONS AND NEUTRALS IN THE GAS PHASE

By

GEORGINA DIMOPOULOS, B. Sc.

A Thesis

Submitted to the School of Graduate Studies

In Partial Fulfillment of the Requirements

for the Degree

Master of Science

McMaster University

MASTER OF SCIENCE
(Chemistry)

McMaster University
Hamilton, Ontario

TITLE : Tandem mass spectrometry and computational chemistry of elusive organic ions and neutrals in the gas phase

AUTHOR : Georgina Dimopoulos (McMaster University)

SUPERVISOR : Dr. Johan K. Terlouw

NUMBER OF PAGES : x, 112

ABSTRACT

Small nitrogen or silicon containing molecules and their ionized counterparts have attracted a great deal of attention from both experimentalists and theoreticians. This is because such species may play an important role in interstellar chemistry. Small nitrogen containing heterocyclic molecules and ions are of biological importance and are of increasing interest to chemists and biochemists. Therefore, studying the chemistry of such species in the gas phase as solitary ions and neutrals is of considerable importance.

The ions studied in this thesis were generated in the rarefied gas phase of the mass spectrometer by (dissociative) electron ionization of selected precursor molecules. The characterization of their structure and reactivity was realized using a variety of tandem mass spectrometry based techniques. These include metastable ion spectra to probe the dissociation chemistry of the low energy ions and (multiple) collision experiments to establish the structure (atom connectivity) of the stable ions. The technique of neutralization-reionization mass spectrometry (NRMS) was used to probe the structure and stability of the neutral counterparts of the ions. The results of theoretical calculations involving the CBS-QB3 model chemistry formed an essential component in the interpretation of the experimental findings.

The above approach was used to study various isomers of the $CH_2N_2^{\bullet+}$ family of ions, in particular the elusive carbodiimide ion $HN{=}C{=}NH^{\bullet+}$. Unlike other isomers including ionized cyanamide $H_2N\text{-}C{\equiv}N^{\bullet+}$ and nitrilimine $HC{=}N{=}NH^{\bullet+}$, the carbodiimide ion could only be identified by a strategy that involved the use of the technique of collision-induced dissociative ionization (CIDI) mass spectrometry. Guided by the results of the theoretical calculations, the carbodiimide ion, the global minimum on the $CH_2N_2^{\bullet+}$ potential energy surface, could also be generated by the molecule-assisted isomerization of its 1,3-H shift isomer $H_2N\text{-}C{\equiv}N^{\bullet+}$. This occurs through an ion-molecule interaction with a single molecule of H_2O under conditions of chemical ionization : a process termed proton-transport catalysis.

The amino-substituted carbodiimide ion, $H_2N\text{-}N{=}C{=}NH^{\bullet+}$, and nine more isomers have all been calculated to be minima on the potential energy surface of the $CH_3N_3^{\bullet+}$ family of ions. Four of these, *viz.* the aminocarbodiimide ion, the aminonitrilimine ion, $H_2N\text{-}C{=}N{=}NH^{\bullet+}$, the cyclic C-aminoisodiazirine ion, and the ionized biradical, $H_2N\text{-}N{=}C(H){=}N^{\bullet+}$, were generated and characterized by tandem mass spectrometry as stable species in the gas phase. Neutralization-reionization experiments show, in agreement with the CBS-QB3 computational results, that aminocarbodiimide and aminonitrilimine are stable species in the gas phase.

Next, the α-distonic ions of a number of heterocyclic nitrogen-containing compounds including pyrazole, pyridazine and aminopyrazine, were characterized and differentiated by tandem mass spectrometry. The stabilities of the neutral counterparts of the ylid ions and their conventional isomers were probed by neutralization-reionization experiments. From these experiments, it follows that the ylid ions have stable neutral counterparts, as predicted by the theoretical calculations.

The final component of this work deals with the chemistry of a silicon containing species of potential interest in interstellar chemistry. The reactions of protonated silicic acid, $Si(OH)_3^+$, and the mechanisms of these reactions were studied using tandem mass spectrometric experiments and CBS-QB3 model chemistry. The low energy (metastable) ions of $Si(OH)_3^+$ dissociate by loss of H_2O and SiO_2 to form $O{=}SiOH^+$ and H_3O^+ ions. Neutralization-reionization experiments show that $Si(OH)_3^{\bullet}$ is a stable species in the rarefied gas phase.

ACKNOWLEDGEMENTS

Many people have been part of my graduate studies and this is the place where I can acknowledge those people. First and most importantly, I would like to thank my supervisor, Dr. Terlouw. He is an excellent and enthusiastic professor who is dedicated to his graduate students and their research. JKT, thank you very much for giving me the chance to work with you, for always leading me down the right path and for having confidence in me.

Many thanks to the members of the Mass Spec Group for their help over the past few years. This includes Kirk Green, Tadek Olech, Leah Allan, Lisa Heydorn, Richard Lee, Cathy Wong, Rashidah Pilus and Zahra Jama. To my good friend, Anna Trikoupis, I would like to thank you for all your help over the past couple of years and for being a great friend.

To my friends, Trisha Voth, Nada Reginato, Diane Stogiannes, Greg Potter, Matt Moran and Mark Marynowisz, thank you for being such wonderful friends and colleagues. To my friends at home, thank you for all the support, for listening to me and for always being there for me.

I would like to thank the most important people in my life, *my fans*, my family. To my parents, I am grateful for their love, support and encouragement that guided me through the many years. I am also lucky to have wonderful siblings who are my best friends, Giota and Tony. I am lucky to have three furry fans, Octavius, Hercules and Maximus because they always provide me with lots of unconditional love. They taught me that a wagging tail can cure stress instantly!! To the most wonderful person in the world, my husband, Tony, I thank you for the unlimited love and support. You are my angel and I love you.

TABLE OF CONTENTS

LIST OF FIGURES

LIST OF ABBREVIATIONS

B	=	magnetic sector
B3LYP	=	hybrid Hartree-Fock/density functional theory
CCSD(T)	=	coupled cluster singles doubles and triples
CI	=	chemical ionization
CID	=	collision-induced dissociation
CIDI	=	collision-induced dissociative ionization
CBS-QB3	=	complete basis set model chemistry
DFT	=	density functional theory
EI	=	electron ionization
ESA (E)	=	electrostatic analyzer
eV	=	electron Volt (1 eV=23.061 kcal/mol or 96.487 kJ/mol)
ffr	=	field-free region
G2	=	Gaussian-2 theoretical method
ΔH_f	=	enthalpy of formation
HF	=	Hartree-Fock
IE	=	ionization energy
KER	=	kinetic energy release
MI	=	metastable ion
MP	=	Möller-Plesset(perturbation theory)
MS	=	mass spectrometry
NDMA	=	N,N-dimethylaniline
m/z	=	mass to charge ratio
NR(MS)	=	neutralization-reionization(mass spectrometry)
PA	=	proton affinity
q	=	charge
r,R	=	radius
T	=	kinetic energy release (value)
TS	=	transition state
ZAB-R	=	BEE three-sector mass spectrometer
ZPVE	=	zero-point vibrational energy

Chapter 1

1.1 Introduction, scope of this thesis

The gas phase ion chemistry described in this thesis focuses on the study of gaseous ions of small organic molecules. A mass spectrometer is the instrument used to generate these species. Tandem mass spectrometry and computational chemistry are the techniques used to probe their structure and reactivity. Most of the ions studied are radical cations. In favourable cases these may be generated in the ion source of the mass spectrometer by direct electron ionization (EI) of their gaseous neutral counterpart. Alternatively, the ions can be generated by dissociative electron ionization of a carefully selected precursor molecule. One important aspect of such experiments is that the pressure in the ion source remains so low that the ions do not interact with (sample) molecules via ion-molecule reactions. This implies that the chemistry and reactivity of a given radical cation can be studied in a "solvent-free" environment.

Most radical cations have stable isomers of conventional and unconventional structure. Radical cations of unconventional structure include distonic ions, where the charge and radical sites are located on separate (adjacent or non adjacent) atoms within the molecule, ion-dipole complexes (two species interacting through the charge of one and the dipole of the other) and hydrogen bridged radical cations (two species, one ionic and one neutral interacting through a hydrogen bond). For example, ionized methanol, $CH_3OH^{\bullet+}$, has a stable distonic isomer, $CH_2OH_2^{\bullet+}$, whereas ionized formic acid, $H\text{-}C(=O)OH^{\bullet+}$, has the following stable isomers : the ionized carbene, $HO\text{-}C\text{-}OH^{\bullet+}$, the ion-dipole complex, $[H_2O\bullet\bullet\bullet CO]^{\bullet+}$, and the hydrogen-bridged radical cations $[OC\bullet\bullet\bullet H\bullet\bullet\bullet OH]^{\bullet+}$ and $[CO\bullet\bullet\bullet H\bullet\bullet\bullet OH]^{\bullet+}$.

The radical cations generated in the above low pressure experiments do not necessarily retain their structure identity : their internal energy content may be such that isomerization into other more stable isomers occurs, often via a H-shift. On the other hand, there are also many systems where the barrier for the H-shift associated with the interconversion of isomeric ions is so high that a unimolecular isomerization does not occur. However, recent work in our group and other laboratories has shown that such high interconversion barriers may be lowered if the ion is allowed to form an encounter complex with a carefully selected neutral molecule. In our experimental set-up, this is realized by performing the reaction under chemical ionization conditions, where the pressure in the ion source is much higher (by a factor of c. 10 000) than in a conventional electron ionization experiment. This phenomenon, that is the single (solvent) molecule assisted isomerization of a given radical cation into a more stable isomer, has been termed "proton-transport catalysis" and is discussed in more detail in Section 1.3.

Chapter 2 deals with the above scenario. It focuses on the isomerization of $H_2NCN^{\bullet+}$, the cyanamide radical cation, into its H-shift isomer, $HNCNH^{\bullet+}$, the carbodiimide ion, which the theoretical calculations predict to be the more stable isomer. This elusive ion was generated and characterized by tandem mass spectrometry and, in agreement with the calculations, it does not communicate with $H_2NCN^{\bullet+}$ prior to dissociation. However, under conditions of chemical ionization and using H_2O as the catalyst, the cyanamide radical cation can be promoted to isomerize into $HNCNH^{\bullet+}$, via a mechanism akin to proton-transport catalysis. One incentive to study this system is that cyanamide is one of the C, H and N containing molecules that has been identified as a key molecule in the ultra low pressure gas phase chemistry of the interstellar medium.

The generation of aminocarbodiimide and several other $CH_3N_3^{\bullet+}$ isomers is discussed in Chapter 3. Experiments involving collision-induced dissociation (CID) and neutralization-reionization (NR) mass spectrometry are used to probe the structure, stability and reactivity of these ions in the gas phase.

Chapter 4 describes the unimolecular chemistry of several N-containing heterocyclic species including pyrazole, pyridazine and a set of amino-substituted pyrazines and pyridines. Of particular interest are their 1,2-H shift isomers, the α-distonic or ylid isomeric ions. Earlier work had shown that the ylid isomer of ionized pyridine is a surprisingly stable species in the gas phase which does not interconvert with the pyridine radical cation. However, the pyridine radical cation does isomerize into its more stable α-distonic isomer in the presence of benzonitrile as the catalyst.

Precursor molecules were designed and synthesized to generate the α-distonic isomers of the above N-heterocyclic compounds by dissociative electron ionization reactions. The various α-distonic isomeric ions (as well as their neutral counterparts) could all be identified as stable species in the gas phase, confirming the predictions of the theoretical calculations. However, theory also predicts that these α-distonic ions are (slightly) higher in energy than their conventional counterparts and thus these systems appear to be less attractive to study molecule-assisted isomerization reactions.

Another species of potential interest in interstellar chemistry is described in Chapter 5. This Chapter deals with the reactions of protonated silicic acid $Si(OH)_3^+$, whose low energy (metastable) ions dissociate by loss of H_2O and SiO_2 to give $O{=}Si{-}OH^+$ and H_3O^+ ions, respectively. Secondary dissociation reactions generate $SiOH^{\bullet+}$ and $SiO^{\bullet+}$ ions which have been identified and detected in interstellar dust clouds.

The next two sections of this Chapter serve to provide the non-expert reader with background information on the mass spectrometry based techniques and the computational chemistry used in the studies reported in this thesis.

Section 1.2 presents a brief introduction to the instrumentation used in the experiments, a state-of-the-art tandem magnetic sector mass spectrometer. This section also discusses the various techniques that were used to generate and

characterize the ions and the computational tools used to assist in the interpretation of the experimental observations.

Section 1.3 presents a brief overview of the methodology to perform ion-molecule reactions under conditions of chemical ionization (CI) with an emphasis on the parameters that influence molecule-assisted isomerization reactions of radical cations.

The results described in Chapter 5 of this thesis have been reported in the literature. This project involved a mutually beneficial international collaboration with the Indian Institute of Technology in Hyderabad. The more sophisticated mass spectrometric experiments and all of the theoretical calculations associated with this project were performed in this laboratory. The computational chemistry of Chapter 2 was performed in collaboration with Prof. P.J.A. Ruttink (University of Utrecht, The Netherlands) whose expert advice and guidance I gratefully acknowledge. Most of the precursor molecules used in the study of Chapter 4 are not commercially available. They were synthesized by Thanasis Karapanayiotis and Dr. R.D. Bowen (University of Bradford, UK) in the context of a future joint project.

1.2 The generation and characterization of ions by tandem mass spectrometry

The VG Analytical ZAB-R Mass Spectrometer

The use of several sophisticated mass spectrometric techniques in conjunction with computational chemistry allows for the characterization of ions generated in the ion source of the mass spectrometer.

Figure 1.1 shows a schematic diagram illustrating the components of our ZAB-R mass spectrometer. This instrument is a multiple sector mass spectrometer and is comprised of an ion source and three mass analyzers : a magnet (B) and two electrostatic analyzers (E). This particular ZAB-R instrument is of BEE geometry in that the magnet precedes the two electrostatic analyzers. The mass

analyzers are separated by field-free regions (ffr) and within these field-free regions are the collision cells. In these field-free regions, we can perform sophisticated experiments such as CID and NR mass spectrometry.

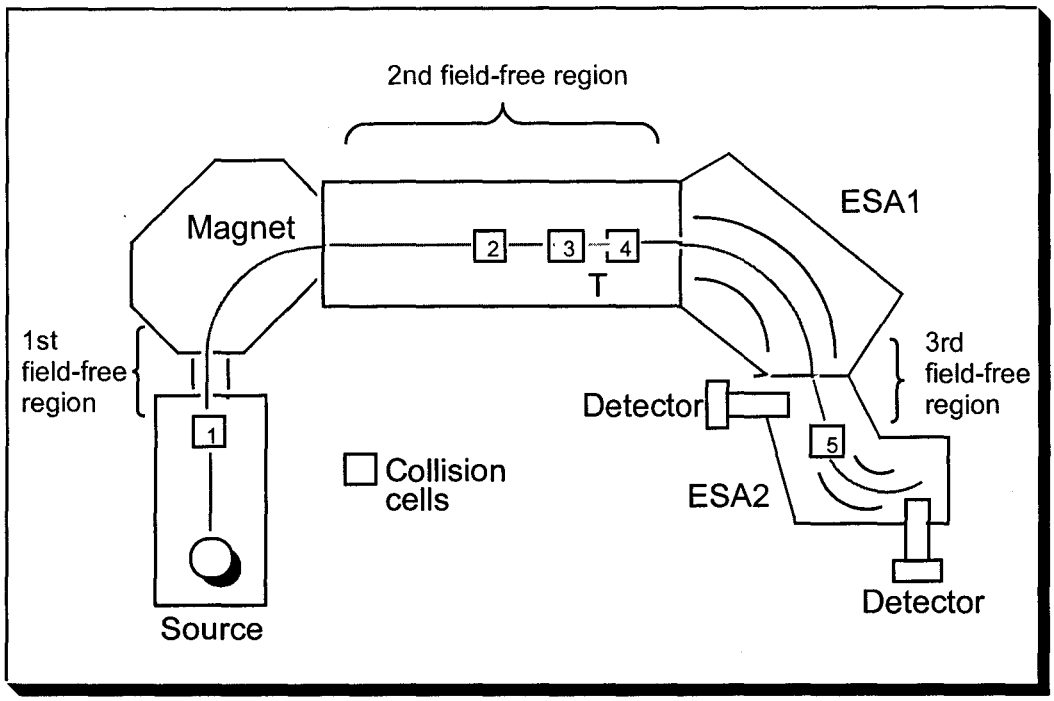

Figure 1.1. Schematic diagram depicting the geometry of the VG ZAB-R Mass Spectrometer.

In the source of the instrument, the compound of interest is introduced as a vapour directly via a leak valve into the ion source. Electrons that are produced from a tungsten filament are accelerated into the ion source by a potential set between the filament and the ion source (50 - 100 eV) [1]. Ions are generated when the traversing electrons collide with the neutral molecule on their way to hitting the trap (an electrode at a higher potential). Ionization can occur by direct contact or by close contact of the electron with the sample molecule. The removal of an electron from a neutral molecule leads to the generation of an ion and this process is referred to as electron impact ionization (EI). A positively charged ion is formed by this ionization process in the following manner: $M + e^- \rightarrow M^{\bullet+} + 2e^-$, where M is the neutral molecule and e^- is the electron. The resulting positive ion

is denoted as $M^{\bullet+}$ to indicate that it is a radical cation. This is because almost all organic molecules contain an even number of electrons and thus when an electron is ejected, an odd-electron ion is formed.

This form of ionization takes place within 10^{-16} sec, that is much faster than the movement of the nuclei in the molecule (the fastest molecular vibrations require 10^{-14} sec) [1]. The nuclei of the molecule can therefore be considered to be at rest during the ionization process. In other words, we are dealing with a vertical ionization process governed by the Frank-Condon principle. If the energy imparted by the electron is greater than the ionization energy (IE) of the molecule, the excess energy is deposited into the newly formed molecular ion as internal energy resulting in transitions to various excited vibrational, rotational and possibly electronic states. The energy imparted by the electrons in the ionization process is not the same for every ion. In fact, the molecular ions generated by electron ionization have a fairly wide range of internal energies. As a result, some of the ions may dissociate by direct bond cleavage or rearrangement whereas others remain intact.

The residence time for a given ion generated in the source is c. 1 μs and the time it takes for that ion to reach the detector is c. 10 μs. For dissociations of the incipient molecular ions to take place in the ion source of the mass spectrometer, they must occur within a 1 μs which translates into a minimum rate constant of 10^6 sec^{-1}. The type of reactions an ion undergoes depends on its internal energy content. Direct bond cleavage reactions have a maximum rate constant of 10^{14} sec^{-1} whereas rearrangement reactions typically have a maximum rate constant of 10^{10} sec^{-1}. Molecular ions that dissociate in the ion source do so with a rate constant of $10^6 < k < 10^{14}$ sec^{-1}. Such ions are termed "unstable" ions because they fragment before leaving the source. In contrast, "stable" ions are low internal energy ions that do not dissociate during the time required to reach the detector. Such ions are characterized by a rate constant of $k < 10^4$ sec^{-1}. Ions that do not have enough internal energy to dissociate in the source but nevertheless

fragment before reaching the detector are called metastable ions. The rate constant with which these ions dissociate lies in the range $10^4 < k < 10^6$ sec^{-1}. The behaviour of metastable ions is normally studied in one of the field free regions of the instrument.

The relationship of the rate constant k to the internal energy of an ion is well described by two statistical methods : the Quasi-Equilibrium Theory (QET) and the Rice, Rampsberger, Kassel and Marcus (RRKM) Theory. In a simplified version of the QET, the fragmentation reactions of ions can be characterized by reaction rate constants with the equation: $k=\nu[E_i-E_o / E_i]^{s-1}$, where E_i is the internal energy of the ion undergoing fragmentation, s is the number of effective oscillators in the ion, E_o is the activation energy and ν is the frequency factor [1].

Metastable Ion spectra

Metastable ion spectra are obtained by mass selecting the ion of interest with the magnet. A magnetic field is imposed on the beam of ions that are accelerated from the source in a direction perpendicular to the direction of the ions [1]. An ion of mass m_1, charge e and velocity v injected into a magnetic flux in this way will follow a circular path of radius r given by r = mv/Be [1]. The radius can be seen to be proportional to the momentum. Thus the magnet separates ions according to their momentum. The separation of ions by a magnetic field is given by the relationship : $m/z = B^2r^2/2v$ [1]. Upon selection of the precursor ions, $m_1^{\bullet+}$, they are transmitted into the 2ffr where a very small portion of these ions spontaneously dissociates into products, $m_2^{\bullet+}$ and m_3. The translational energy of a precursor ion, $m_1^{\bullet+}$, is distributed among the products based on their mass (m_2/m_1 x V_{acc} , where V_{acc} is the accelerating voltage). The product ions are subsequently mass analyzed by the first electrostatic analyzer (ESA1) according to their translational energy. The main beam of ions contains a mixture of stable and metastable ions and only about 1% of the intensity of the main beam corresponds to the overall intensity of the peaks in the MI spectrum.

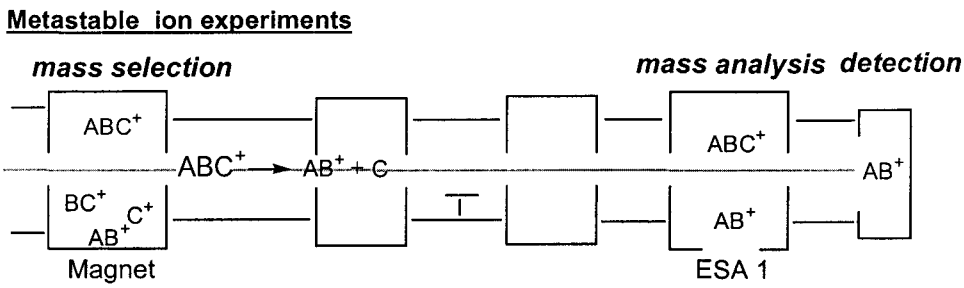

Figure 1.2. Schematic diagram illustrating the events in a metastable ion experiment.

In a metastable ion experiment, the metastable peaks arise from ions having a narrow range of internal energies but their width is invariably larger than that of the unperturbed main beam of non-dissociating ions [3]. This is a result of the conversion of internal energy of $m_1^{\bullet+}$ into kinetic energy of the products of the reaction ($m_2^{\bullet+} + m_3$). Another important contribution to the kinetic energy content of the products is the reverse activation energy.

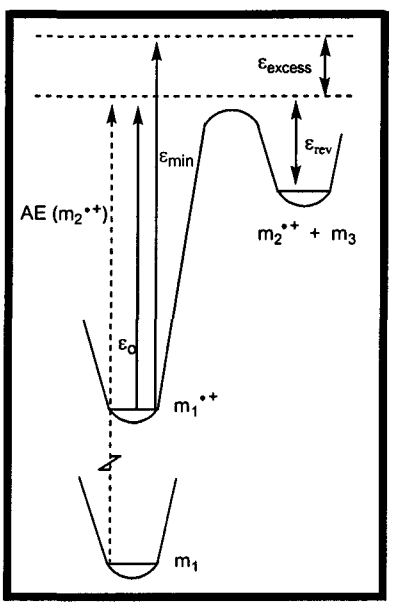

Figure 1.3. Potential energy diagram for an endothermic reaction in the gas phase.

Figure 1.3 depicts the energy diagram for an endothermic dissociation reaction associated with a significant barrier for the reverse process. The

minimum internal energy required to observe the dissociation of $m_1^{\bullet+}$ in the metastable time frame is ε_{min} [1]. The minimum internal energy requirement to meet this condition is larger than that of the forward activation energy, ε_o. The difference between ε_{min} and ε_o is the excess energy, ε_{excess}. The barrier for the reverse reaction is denoted by ε_{rev}. This barrier represents the difference between the enthalpy of formation of the dissociation products and that of the activated complex. The excess energy and the reverse activation energy both contribute to the energy that is converted to kinetic energy of the products, $m_2^{\bullet+} + m_3$.

The conversion of internal energy to translational energy of the products during the dissociation of a metastable ion may result in the release of kinetic energy (KER) T [1]. The KER can come from the excess energy of the activated complex [1] and the reverse activation energy. Reactions which can be expected to have substantial reverse activation energies include rearrangements, in which a neutral molecule and a stable ionic product are generated [1]. Simple direct bond cleavage reactions are expected to have no (or very little) reverse activation energies. A release in kinetic energy can be observed in MI spectra as a broadening of the metastable ion peak of a fragment ion relative to the width of the main beam of ions $m_1^{\bullet+}$. Dissociation reactions that have a small amount of energy release give metastable peaks having a Gaussian shape, whereas reactions having a large kinetic energy release may display flat-topped or dish-shaped peaks [1]. The peak shape gives information on the physicochemical aspects of ion fragmentations [3]. Metastable peak shapes can help probe the structure of fragmenting ions and they also yield information on the partitioning of internal energy of the decomposing ion into translational energy of the products [3]. The kinetic energy release, T, can be measured from the width of the metastable ion peak at a certain height, h : $T_h = (m_1^2/16\, m_2\, m_3)(V_{acc})[(\Delta E_h)^2/E^2]$, where E is the electric sector voltage at which the ions are transmitted, V_{acc} is the accelerating voltage and ΔE_h is the width of the metastable peak at height h. Kinetic energy

releases are commonly reported for the width at the half-height ($T_{0.5}$) of the metastable peak.

The MI spectrum provides valuable information on the low energy dissociation reactions available to a given ion.

Collision-Induced Dissociation spectra

Collision-induced dissociation reactions provide structural information upon inspection of the fragment ions produced. The ions of interest are generated in the ion source of the instrument, accelerated to typically 8keV translational energy and then mass-selected by the magnet. The beam of mass-selected ions is transmitted into the 2ffr where it passes through a collision chamber pressurized with an inert gas such as helium (He) or oxygen (O_2). These gases are called collision or target gases. Some of the fast moving ions collide with a gas molecule and in this process a small fraction of their high translational energy is converted into internal energy. The internal energy of the collisionally energized ions is characterized by a fairly broad distribution whose high energy tail extends to a few eV. As a result, these ions often undergo a variety of dissociation reactions and as a rule direct bond cleavage reactions prevail over rearrangement processes. Thus, unlike the situation with metastable ions where the spectrum is dominated by one or two low energy rearrangement processes, CID spectra are dominated by a number of direct bond cleavage reactions and/or rearrangement reactions. Direct bond cleavage reactions can be used to elucidate the structure of the ion and hence characterize the ion.

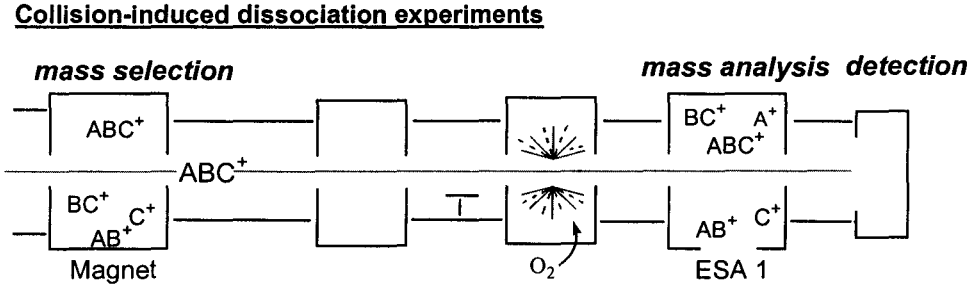

Figure 1.4. Schematic diagram illustrating the events in a collision-induced dissociation experiment.

The appearance of a CID spectrum is affected by many factors such as the nature of the collision gas, the collision gas pressure and the translational energy of the ions. Helium, argon, nitrogen and oxygen are commonly used as collision gases. Helium is the most widely used because it has a high target efficiency, (i.e. there is less concern that the ions are neutralized and scattered when using He as a target gas). In all experiments described in this thesis, oxygen is used as a collision gas. CID spectra obtained with O_2 are often similar to those obtained with He, although oxygen sometimes induces unique high energy reactions that give rise to minor peaks in the CID spectrum [4].

The pressure of the collision gas in a CID experiment is an important factor to consider since it determines whether the target ion is involved in a single or multiple collision event. In our experiments, the pressure is maintained very low to ensure that only single collision events occur.

The actual pressure of the collision gas is not measured directly : it is monitored by using a remote ionization gauge located outside the collision cell. The collision gas pressure can be estimated by observing the reduction of the main beam intensity as the pressure is varied. The optimal condition for a main beam reduction is c. 30 – 40 % : further reduction leads to an increase in multiple collision encounters and high energy dissociations [5]. Thus as the yield of fragment ions is increased, the ion structure-specific information may be significantly reduced [5].

The translational energy content of the collisionally activated ions plays a significant role in the appearance of a CID spectrum. As mentioned above, part of the translational energy of a fast moving ion may be converted into internal energy upon collision with a neutral molecule. When the translational energy of an ion is increased, the range of collisionally derived internal energy for that ion also increases and as a result, there is more collision induced fragmentation [5].

The most probable energy, E_{max}, transferred on collision is approximately given by the equation : $E_{max} = h/a(2eV/m)^{1/2}$, where h is Plank's constant (6.62×10^{-34} J•s) , a is the interaction distance, eV is the ion's translational energy and m is the ion's mass [5]. Energy deposition distribution functions were calculated using the above equation and some simplifying assumptions and from this, for example, it was estimated that an ion of m/z 40 will receive, as most probable energy, 0.9, 1.3 and 2.0 eV when its translational energy is 2, 4 and 8kV, respectively [5]. The mass of the neutral gas molecule or atom also affects the amount of energy transferred to an ion. It is generally true that heavier collision gases lead to more efficient energy deposition due to a large center-of-mass kinetic energy (E_{cm}) [6]. E_{cm} is the maximum available energy that can be converted to internal energy of the ion as given by the equation : $E_{cm} = E_{lab}m_t / (m_t + m_i)$, where E_{lab} is the translational energy of the ion in eV, m_t is the mass of the collision (target) gas and m_i is the mass of the ion [6].

Neutralization-Reionization spectra

Neutralization-reionization mass spectrometry (NRMS) has proved to be of enormous value for the formation of elusive and highly reactive neutrals which are difficult to generate by other means due to their tendency toward unimolecular fragmentations or fast bimolecular rearrangement [7a].

The key features in a NR experiment are displayed in Figure 1.5 :

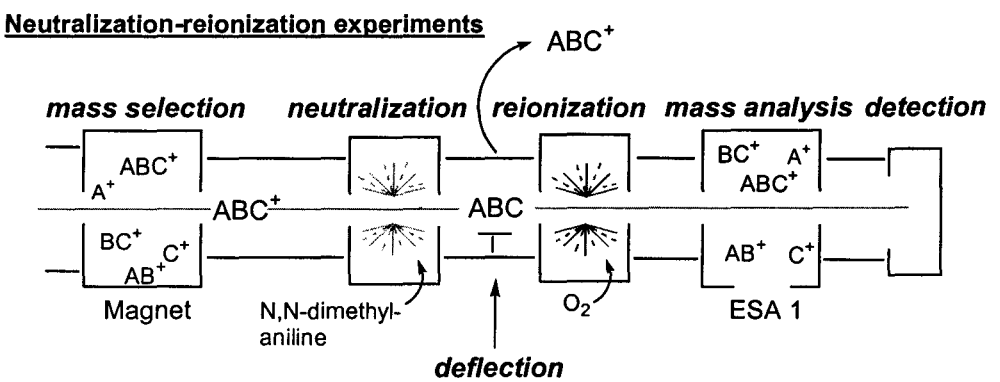

Figure 1.5. Schematic diagram illustrating the events in a neutralization-reionization experiment.

In a NR experiment, the ions under investigation are generated from a suitable precursor molecule in the source of the mass spectrometer. These ions are mass selected by the magnet and transmitted into the 2ffr of the instrument. This fast moving beam of ions is subjected to two sequential collision events with appropriate target gases in collision cells along the flight path, see Figure 1.5. The first collision cell is pressurized with Xe or an organic vapour (N,N,-dimethylaniline) which neutralizes the ions by a single electron transfer. The remaining ions are subsequently deflected away by a (positively) charged deflector electrode which is located between the two collision cells. The beam of neutral molecules (which may contain uncharged dissociation products) enters a second collision cell and is reionized by collision with oxygen gas. A portion of the reionized species will also dissociate in the collision cell. The resulting ions are mass analyzed by the second electrostatic analyzer (ESA2) and detected by the first detector to obtain a NR spectrum. The presence of a signal at the m/z value of the original mass-selected ions is called the "survivor ion signal". This signal corresponds to the mass-selected ions that have survived the neutralization-reionization process and shows that the neutrals generated in these experiments are stable species on the μs timescale.

In NR experiments, Xe gas can conveniently be used for neutralization although it has a high ionization energy (IE) and the electron transfer to many projectile ions from which $AB^+ + N \rightarrow AB + N^+$ is an endothermic process. This does not impair the efficiency of the reaction, since the energy deficit is easily made up by the large translational energy of the ion (8keV) [7b]. A "hard" target gas such as He can be used for reionization, $AB + He \rightarrow AB^+ + He + e^-$. It causes extensive fragmentation, whereas a "soft" target gas such as O_2, does not. Reionization with O_2 in part takes place via : $AB + O_2 \rightarrow AB^+ + O_2^-$. If He is used, the end product will be a high yield of structurally informative fragment ions, whereas a high yield of "survivor" ions results when O_2 is used.

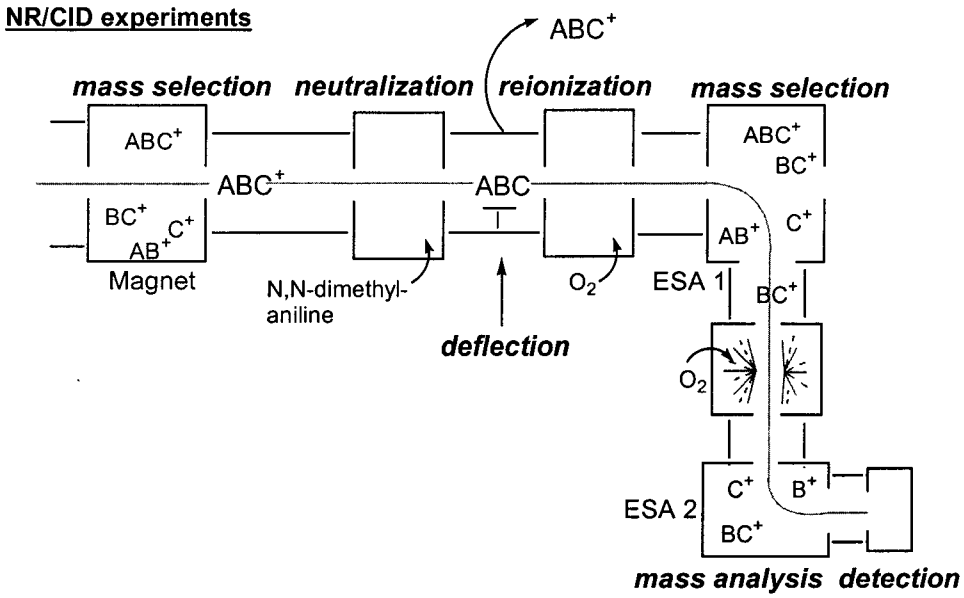

Figure 1.6. Schematic diagram illustrating the events in a neutralization-reionization/collision-induced dissociation experiment.

A CID spectrum of the survivor ions from an NR experiment makes it possible to determine if the incipient neutral species has retained its structural integrity or rearranged into a more stable isomer prior to reionization. Such an NR/CID spectrum is obtained by mass selecting the survivor ions with ESA1 and transmitting these ions into the 3ffr where they dissociate upon collision with O_2 gas in the collision cell. The resulting ions are mass analyzed by ESA2 and subsequently detected. To determine if the neutrals isomerized upon neutralization, the NR/CID is compared to the 3ffr CID spectrum of the source generated ions. The similarity of these two spectra provides evidence that the neutrals in the NR experiment are stable and have retained their structural identity. However, if these spectra are different, it may show that the neutral has isomerized into a more stable neutral isomer. This can be verified if a 3ffr CID spectrum of the more stable isomer is available as a reference. On the other hand, if there is an isomeric or isobaric impurity of the mass-selected source generated ions this would lead to isomerically or isobarically impure neutrals and a disparity between the NR/CID and 3ffr CID spectra would result.

Computational chemistry also plays a role in the interpretation of NR spectra. The heights of the dissociation and isomerization barriers in both the original ion and its neutral counterpart describes whether isomerization is a facile process of the neutral and ionic species in question.

Collision-Induced Dissociative Ionization spectra

A collision-induced dissociative ionization (CIDI) experiment is used to probe the structure and stability of the neutral species lost from a spontaneous dissociation reaction. The precursor ion is mass-selected by the magnet and transmitted into the 2ffr. Only a very small portion of the mass-selected ions spontaneously dissociates unimolecularly during the flight to the collision chamber [8]. All ions generated by these spontaneous dissociations ($m_2^{\bullet+}$) and the parent ions ($m_1^{\bullet+}$) are deflected away by a charged deflector electrode and the only species entering the collision cell are the fast moving neutrals [8]. The neutrals enter the collision cell and are collisionally ionized using O_2 gas. The collisionally ionized neutrals (and their dissociation products) are mass analyzed by the ESA1 and detected to give a CIDI spectrum. To probe the structure of an ionized neutral, it can be mass-selected by the ESA1 and transmitted into the 3ffr where it dissociates upon collision with oxygen gas in the collision cell. The resulting ions from this CID experiment in the 3ffr are mass analyzed by the ESA2.

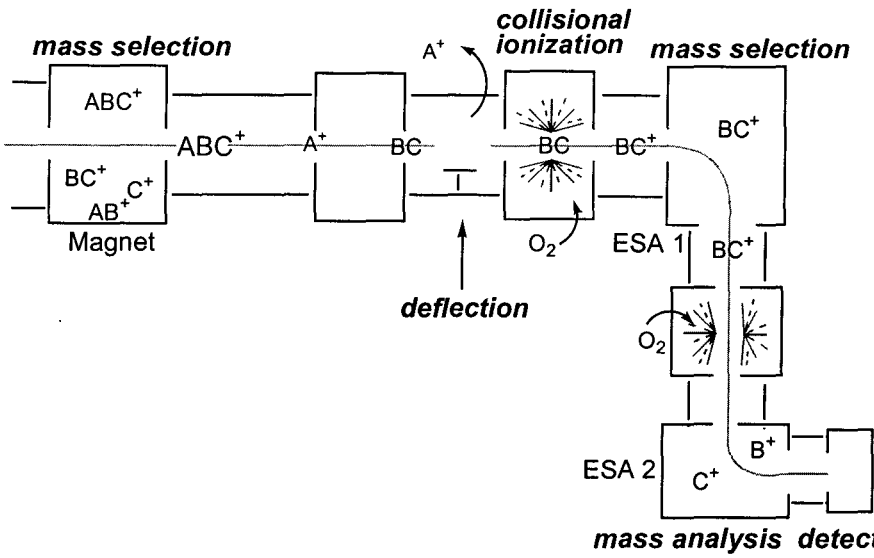

Figure 1.7. Schematic diagram illustrating the events in a collision-induced dissociative ionization experiment.

Computational Chemistry

Computational chemistry is used as a complementary tool in mass spectrometric studies. It is used as an aid in determining the structure of the ion in question and the mechanism of the reaction.

The CBS-QB3 model chemistry [9] is the type of calculation used in this thesis to calculate the theoretical energy values and transition states. This Complete Basis Set Quadratic configuration interaction (CBS-Q) model chemistry is a hybrid empirical correction/pair correlation energy extrapolation scheme which uses the B3LYP (B3) density functional method in combination with the 6-311G(2d,d,p) basis set for geometry optimization. This method yields the absolute enthalpies of formation for both minima and transition states. This model involves four calculations having different number of basis sets and at different levels of theory.

The first step in the calculation is the optimization of the input geometry of the structure of the ion or molecule under investigation. The input geometry is optimized to a stationary point on the potential energy surface (PES) [10]. The

optimized structure may correspond either to a minimum (i.e. have no imaginary frequencies) or a transition state (i.e. one imaginary frequency). The PES may contain many minima which correspond to stable isomers or conformers lying in energy wells of varying depth. Thus the choice of the input geometry is quite important. The energy calculated at the B3LYP level of theory is not used, only the optimized geometry is used in the next steps to obtain a final CBS-QB3 (298K) energy. The vibrational frequency is calculated after the geometry is optimized. For a given molecule, there are 3N-6 vibrational frequencies, where N is the number of atoms. However, in a transition state, one of the frequencies is negative in value and corresponds to the imaginary frequency of the transition state vibration. The frequency calculation also provides the zero-point vibrational energy (ZPVE) for the stable molecule, ion or transition state [11].

The following steps involve calculating the energy of the structure of the ion, molecule or transition state optimized in the first step. A Møller-Plesset (MP) calculation, at the MP2 level of theory, is carried out, which yields the corresponding Hartree-Fock (HF) energy. A coupled-cluster singles, doubles and a perturbative triple (CCSD(T)) calculation and an MP4 calculation follow; they operate at higher levels of theory. The energy is calculated at these two levels of theory to estimate the effect from higher-order electron correlation on the energy. Considering the electron-electron interaction in an energy calculation improves the accuracy of the calculated energy value and the molecular geometry [12].

The total energy is then calculated in the output in the final step as E(CBS-QB3) by using the MP2 energy and correcting this value using the CCSD(T) and MP4 values. This total energy value is the energy of the molecule (ionic or neutral) at 0K. The enthalpy of formation of the calculated neutral or ionic species is determined by the following equation:

$$\Delta H_{f,298} = \Delta H_{f,0}(\text{exp}) - E_{AT} + E(\text{CBS-QB3}) + E_{thermal} - ZPVE - \Delta H_{298}(\text{exp})$$

where $\Delta H_{f,0}(\text{exp})$ is the sum of the experimental $\Delta H_{f,0}$ values for each atom in the species, E_{AT} is the sum of the atomization energies for each atom in the species,

$E_{thermal}$ is the thermal energy correction (obtained from the frequency calculation), ZPVE is the zero point vibrational energy (obtained from the frequency calculation and scaled to a factor of 0.99) and $\Delta H_{f,298}(exp)$ is the sum of the experimental ΔH_{298} for each atom in the species. Ref. 13 lists the $\Delta H_{f,0}(exp)$ and $\Delta H_{298}(exp)$ values for first and second-row elements.

The estimated uncertainty in the accuracy of the calculated enthalpies of formation is ± 1-2 kcal/mol for minima and ± 4 kcal/mol for transition states [9,14]. One factor that may affect the accuracy is spin contamination. Spin contamination can be considered as having too much spin polarization; i.e. having a mixture of spin states for a particular species [12b]. More often, the occurrence of spin contamination in a calculation causes a slight increase in the total energy since a higher energy state is mixed in [12b]. High spin contamination may cause changes in the geometry and spin density of the calculated species [12b]. In CBS-QB3 calculations, the value for the total spin $<S^2>$ is included in the output and if no spin contamination occurs, this value should be equal to s(s + 1) where s is the number of unpaired electrons multiplied by ½. For radical cations, which have one unpaired electron, s is 0.5 and $<S^2>$ is 0.75. However, spin contamination with a value of less than 10% of s(s + 1) is negligible [12b].

1.3 Ion-molecule reactions and proton-transport catalysis

Biomolecular reactions of gas phase ions with neutral molecules is an area of extensive and on-going research [15]. Through the use of chemical ionization experiments, the interactions of ions and molecules can be investigated. Chemical ionization (CI) is a soft ionization method in which the pressure in the ion source is increased to 10^{-4} to 10^{-5} Torr ensuring that a sample molecule will undergo hundreds of collisions before leaving the source [2]. In CI experiments, the reagent gas, R, is introduced into the ion source and ionized by electron impact. It

can further react with other reagent molecules or a substrate molecule to form reactive ionic species [2].

$$R + e^- \rightarrow R^{\bullet+} + 2e^-$$

$$R^{\bullet+} + M \rightarrow [R\bullet\bullet\bullet M]^{\bullet+}$$

$$R^{\bullet+} + R \rightarrow [R\bullet\bullet\bullet R]^{\bullet+}$$

$$R^{\bullet+} + R \rightarrow RH^+ + [R\text{-}H]^{\bullet}$$

$$RH^+ + M \rightarrow [R\bullet\bullet H\bullet\bullet M]^+ \text{ (proton bound mixed dimer)}$$

$$RH^+ + M \rightarrow [R\bullet\bullet H\bullet\bullet R]^+ \text{ (proton bound dimer)}$$

$$R^{\bullet+} + M \rightarrow [R\bullet\bullet H\bullet\bullet (M\text{-}H)]^{\bullet+} \text{ (hydrogen-bridged radical cation)}$$

Depending on the nature of the reagent and the substrate, several ion-molecule reactions can occur in the ion source to afford different types of encounter complexes. Encounter complexes are generated when two species interact with one another via hydrogen bonding, electrostatic or van der Waals forces. Interaction of a reagent ion with the hydrogen atom of the neutral molecule generates a hydrogen-bridged radical cation (HBRC) $[R\bullet\bullet\bullet H\bullet\bullet\bullet (M\text{-}H)]^{\bullet+}$ whereby the hydrogen is bridging the two species. This type of adduct ion is formed in the CI experiments of cyanamide and water, see Chapter 2. A proton-bound dimer (PBD) arises from the interaction of a protonated reagent ion with a neutral substrate molecule (or reagent molecule) $[R\bullet\bullet\bullet H\bullet\bullet\bullet M(R)]^+$. The proton-bound dimer of SiO_2 and H_3O^+ is generated in the unimolecular experiments of protonated silicic acid and is the direct precursor to loss of SiO_2, see Chapter 4. Dimers can also be formed between the reagent ion and a neutral molecule (or a neutral reagent ion). An encounter complex between an ion and a neutral molecule having a dipole moment is called an ion-dipole complex and is held together through electrostatic forces.

Stabilization Energy

Prior to the development of model theories for use in computational analysis, the heat of formation of a proton-bound dimer was often determined

using an empirically derived equation relating the bond dissociation energies of the bonds in the PBD and the proton affinities (PA) of the individual molecules comprising the dimer.

PBDs are even electron ions in which two species are bound by a positively charged proton. In symmetrical PBDs, the two connecting molecules are the same species for example, $[H_2O{\bullet\bullet}H{\bullet\bullet}OH_2]^+$. In this particular case both H_2O species are molecules and the hydrogen carries the positive charge. In asymmetrical PBDs, the two connecting species are different molecules. An example of this type of mixed PBD is that of water and methanol, $[H_2O{\bullet\bullet}H{\bullet\bullet}O(H)CH_3]^+$, in which methanol and water are the neutrals and the bonding hydrogen is the proton (H^+).

Larson and McMahon [16] and Meot-Ner [17] derived an empirical relationship for experimentally determining the heat of formation of symmetrical and asymmetrical O••H••O proton-bound dimers. Using sophisticated mass spectrometric techniques at high pressures several PBDs have been generated and their base exchange equilibria have been examined. From this information the thermochemistry of the process (proton-bound dimer solvent-exchange equilibria) was also obtained, such as the Gibbs free energy and bond dissociation energy for each PBD (symmetric and asymmetric). The correlation of the difference in hydrogen bond energies of the two molecules being bound with the difference in their proton affinites gives an empirical relationship that can be applied to other O••H••O PBD systems not studied within the test group.

The empirical relationship derived by both groups are slightly different as both studies used different test sets of PBDs. Larson and McMahon's expression for the stabilization energy of O••H••O PBDs is 30.8–0.46[ΔPA] [16] and that derived by Meot-Ner [17], SE = 30.4 –0.30[ΔPA] in kcal/mol, is based on a test group of approximately 35-45 PBDs. The first term in the expression is the average bond dissociation energy of the series of PBDs studied to achieve the

correlation and the constant in the second term is the slope of the correlation plot (bond dissociation energy vs. ΔPA).

In the symmetrical PBD $[H_2O{\bullet\bullet}H{\bullet\bullet}OH_2]^+$, the stabilization energy is defined as the sum of the heats of formation of the dissociation products less the heat of formation of the PBD itself : $\Delta H_f(product_1) + \Delta H_f(product_2) - \Delta H_f(PBD^+)$. Since this is a symmetrical PBD, there is only one set of products, $H_3O^+ + H_2O$, and the heats of formation are well known. Moreover, for a symmetrical PBD, the ΔPA is zero since both molecules are the same and have the same PA, the stabilization energy is the average for the series sampled, 30.0 kcal/mol. This stabilization energy can be used to estimate the ΔH_f of the PBD.

However, for an asymmetrical PBD, such as $[H_2O{\bullet\bullet}H{\bullet\bullet}O(H)CH_3]^+$, there are two sets of dissociation products, $CH_3OH_2^+ + H_2O$ and $CH_3OH + H_3O^+$. In this case, the product combination of lowest energy is used to estimate the heat of formation of the PBD, shown in the scheme below:

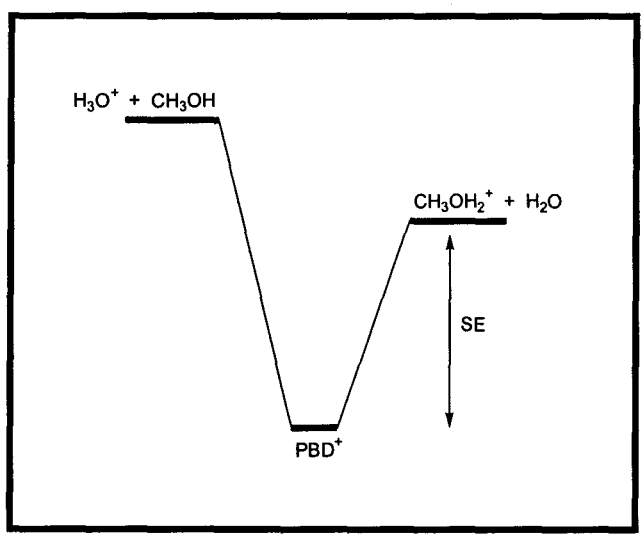

Also, the ΔPA is the difference in the PAs of the two molecules, CH_3OH and H_2O.

Meot-Ner [17] has extended his work to include ionic hydrogen bond and ion solvation measurements for PBDs of the type $[N{\bullet\bullet}H{\bullet\bullet}O]^+$ and $[N{\bullet\bullet}H{\bullet\bullet}N]^+$. Thus the equations for these types of PBDs have been determined :

$[N\bullet\bullet H\bullet\bullet O]^+$ $SE = 30.0 - 0.26[\Delta PA]$

$[N\bullet\bullet H\bullet\bullet N]^+$ $SE = 23.2 - 0.25[\Delta PA]$

In this study [17], it is reported that some deviations from this relationship cause errors in the calculated stabilization energy and reasons for such deviations are also presented.

The same relationship can be applied to odd-electron ions known as hydrogen-bridged radical cations (HBRC). An example of an HBRC is $[CH_3O\bullet\bullet H\bullet\bullet OH_2]^{\bullet+}$ where the hydrogen in methanol is the bridging hydrogen. Using the same relationship, $SE = 30.4 - 0.30[\Delta PA]$, the estimated heat formation of this HBRC can be obtained. In the case of HBRCs, the ΔPA is the difference in the PA of the radical ($CH_3O^{\bullet}$) and the PA of the molecule (H_2O) because the methanol hydrogen is the bridging hydrogen. Since there are two possible dissociation reactions in HBRCs, the product combination that is lowest in energy of the pair is the one in which the stabilization energy is subtracted from to obtain the empirically derived heat of formation of the HBRC.

Catalyzed Isomerization Reactions

In certain cases, the interaction of an ion with a neutral molecule can alter the nature of the reacting ion. It is increasingly becoming clear that the interconversion of isomeric ions may be catalyzed by their interactions with an appropriate neutral molecule [15].

One of the most common isomeric pairs of ions in which catalysis has been observed are distonic radical cations. The term distonic ion was first introduced by the Radom group [18], who defined such an ion as a radical cation in which the charge and radical are separated and reside on different atoms. Distonic radical cations, while often more stable than their conventional counterparts, are usually separated from these isomers by large energy barriers, enabling the two isomeric forms to be observed independently [18]. An example of this is the investigation of the methylene oxonium ion $^{\bullet}CH_2OH_2^+$, by Radom et

al [19a] and by the Holmes and Terlouw group [19b]. This distonic ion is more stable than its conventional isomer, $CH_3OH^{\bullet+}$, but the two isomers do not interconvert because the 1,2-H shift involved imposes a high barrier. However, a molecule of water catalyzes this shift and promotes a smooth transformation of $CH_3OH^{\bullet+}$ into $^{\bullet}CH_2OH_2^{+}$ by proton-transport catalysis.

Proton-transport catalysis (PTC) [20] is a mechanism by which a gaseous conventional radical cation $[H\text{-}X\text{-}Y]^{\bullet+}$ may rearrange into an isomer $[X\text{-}Y\text{-}H]^{\bullet+}$ via a two-step proton-transfer through interaction of a single solvent molecule that acts as a "base", B. The reaction $[H\text{-}X\text{-}Y]^{\bullet+} + B \rightarrow B{\bullet\bullet}H^{+}{\bullet\bullet}[X\text{-}Y]^{\bullet} \rightarrow B{\bullet\bullet}H^{+}{\bullet\bullet}[Y\text{-}X]^{\bullet} \rightarrow B + [X\text{-}Y\text{-}H]^{\bullet+}$ shows how the base "transports" the proton from the high-energy site to the low-energy site of the molecule thereby catalyzing the isomerization. If the base has a proton affinity (PA) intermediate between those of the sites X and Y of the molecule X-Y, it can pick up the proton from site X and the molecule X-Y simply needs to rotate within a weakly-bound adduct for the proton to be deposited at site Y and so for the isomerization from $[H\text{-}X\text{-}Y]^{\bullet+}$ to $[X\text{-}Y\text{-}H]^{\bullet+}$ to take place. If the PA[B] is significantly lower than the PA[X-Y] at X, the first step in the reaction, $[H\text{-}X\text{-}Y]^{\bullet+} + B \rightarrow B{\bullet\bullet\bullet}H^{+}{\bullet\bullet\bullet}[X\text{-}Y]^{\bullet}$, will not take place. If on the other hand, the PA[B] is significantly larger than the PA[X-Y] at Y, than the intermediate complex. $B{\bullet\bullet\bullet}H^{+}{\bullet\bullet\bullet}[X\text{-}Y]^{\bullet}$, will dissociate to $[X\text{-}Y]^{\bullet}$ and HB^{+} via a unidirectional proton transfer. Through evaluation of the conditions required for efficient catalysis, Gauld and Radom [15a] observed that if the PA[B] is intermediate, the barrier becomes negative relative to the separated reactants and products and the base successfully catalyzes the isomerization.

Not all isomerization reactions involve distonic pairs of ion. Chapter 2 describes the catalyzed isomerization reaction of the cyanamide ion, $H_2NCN^{\bullet+}$, into its more stable isomer, the carbodiimide ion, $HNCNH^{\bullet+}$ by proton-transport catalysis.

References

[1] R.G.Cooks, J.H. Beynon, R.M. Caprioli, G.R. Lester. *Metastable Ions.* Elsevier. Amsterdam. 1973.

[2] F.W. McLafferty, F. Turecek. *Interpretation of Mass Spectra.* Fourth Edition. University Science Books. California. 1993.

[3] J.L. Holmes , J.K. Terlouw. Org. Mass Spectrom. 15 (1980) 383.

[4] a) R. Flammang, V. Henrotte, P. Gerbaux, M.T. Nguyen. Eur. J. Mass Spectrom. 6 (2000) 3; b) G.A. McGibbon, P.C. Burgers, J. K. Terlouw. Int. J. Mass Spectrom. Ion Process. 136 (1994) 191.

[5] J.L. Holmes. Organic Mass Spectrometry. 20 (1985) 169.

[6] a) K.M. Stirk, P. Lin, T.D. Ranatunga, L.C. Zeller, J.T. Farrell Jr., H.I. Kenttamaa. Int. J. Mass Spectrom. Ion Process. 130 (1994) 187; b) K.L. Schey, H.I. Kenttamaa, V.H. Wysocki, R.G. Cooks. Int. J. Mass Spectrom. Ion Process. 90 (1989) 71.

[7] a) C.A. Schalley, G. Hornung, D. Schröder, H. Schwarz. Chem. Soc. Rev. 27 (1998) 91; b) F. Cacace. Chem. Eur. J. 8 (2002) 3838.

[8] J.K. Terlouw, H. Schwarz. Angew. Chem. Int. Ed. Engl. 26 (1987) 805.

[9] a) J.A. Montgomery, Jr., M.J. Frisch, J.W. Ochterski, G.A. Petersson. J. Chem. Phys. 110 (1999) 2822; b) ibid. 112 (2000) 6532.

[10] J.B.Foresman, A.Frisch. *Exploring Chemistry with Electronic Structure Methods.* Second Edition. Gaussian, Inc. Pennsylvania. 1996.

[11] a) A.D.Becke. J. Chem. Phys. 98 (1993) 1372; b) ibid. 98 (1993) 5648.

[12] a) F. Jensen. *Introduction to Computational Chemistry.* John Wiley and Sons. New York. 1999; b) D.Young. *Computational Chemistry; A Practical Guide for Applying Techniques to Real World Problems.* John Wiley and Sons. New York. 2001.

[13] A. Nicolaides, A. Rauk, M.N. Glukhovstev, L. Radom. J. Phys. Chem. 100 (1996) 17640.

[14] L.N. Heydorn, Y. Ling, G. de Oliveira, J.M.L. Martin, C. Lifshitz, J.K. Terlouw. Zeitschrift für Physikalische Chemie. 215 (2001) 141.

[15] a) D.K. Bohme. Int. J. Mass Spectrom Ion Processes. 115 (1992) 95; b) J.W. Gauld, L. Radom. J. Am. Chem. Soc. 119 (1997) 9831; c) M.A. Trikoupis, J.K. Terlouw, P.C. Burgers. J. Am. Chem. Soc. 120 (1998) 12131; d) M.A. Trikoupis, P.C. Burgers, P.J.A. Ruttink, J.K. Terlouw. Int. J. Mass Spectrom. 217 (2002) 97 and references cited therein.

[16] J.W. Larson, T.B. McMahon. J. Am. Chem. Soc. 104 (1982) 6255.

[17] M. Meot-Ner. J. Am. Chem. Soc. 106 (1984) 1257.

[18] L. Radom, W.J. Bouma, R.H. Nobes, B.F. Yates. Pure & Appl. Chem. 56 (1984) 1831.

[19] a) W.J. Bouma, J.K. MacLeod, L. Radom. J. Am. Chem. Soc. 104 (1982) 2930; b) J.L. Holmes, F.P. Lossing, J.K. Terlouw, P.C.Burgers. J. Am. Chem. Soc. 104 (1982) 2931.

Chapter 2

The gas-phase dissociation chemistry of the system of $CH_2N_2^{\bullet+}$ ions studied by theory and experiment : the quest for the elusive carbodiimide ion, $HN=C=NH^{\bullet+}$, and its generation from ionized cyanamide by proton transport catalysis.

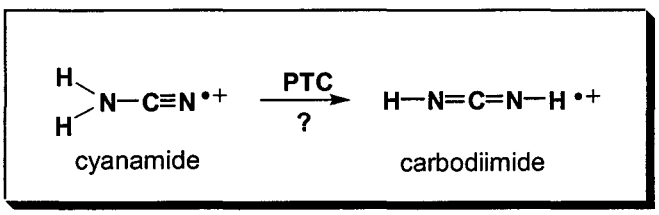

A study of the $CH_2N_2^{\bullet+}$ system of ions using the CBS-QB3 model chemistry predicts that the cyanamide ion, $H_2NCN^{\bullet+}$ (**1**) is a stable species in the gas phase. In line with this, ion **1**, which can readily be generated by electron impact ionization of the neutral molecule, shows a structure characteristic CID mass spectrum. The calculations further indicate that **1** is separated by a high barrier (87 kcal/mol) from its 1,3-H shift isomer $HN=C=NH^{\bullet+}$ (**6**), the carbodiimide radical cation. The latter isomer represents the global minimum on the $CH_2N_2^{\bullet+}$ potential energy surface. Nevertheless, apart from an inconclusive study [15], the generation and characterization of this elusive ion has not been reported. It will be shown that **6** can be cleanly generated in a collision induced dissociative ionization (CIDI) experiment on the neutral generated by the dissociative ionization of ionized aminoguanidine, $H_2NC(=NH)NHNH_2^{\bullet+}$, into $N_2H_4^{\bullet+}$ + HN=C=NH.

Ion **6** displays a unique CID spectrum that is characteristically different from that of **1.** This information was used to corroborate the computational prediction that, in the presence of a single H_2O molecule as the catalyst, the cyanamide ion **1** isomerizes into the carbodiimide radical cation **6.**

Introduction

As pointed out by Cacace et al. [1], cyanamide, H_2N-C≡N, is a molecule whose gas-phase ion chemistry is of considerable interest. It is a key molecule in prebiotic synthesis [2-4] and is one of a small group of molecules that are abundant in interstellar space [5,6], where its formation is traced to **ionic** reactions [7].

The neutral molecule is slightly more stable than its tautomer HN=C=NH, carbodiimide. However, calculations using the CBS-QB3 model chemistry [8,9], this work, Table 1, indicate that the reverse is true for the ions : $HN=C=NH^{\bullet+}$ is more stable than H_2N-C≡$N^{\bullet+}$, by 4 kcal/mol. The two ions are separated by a very high isomerization barrier : the associated 1,3-H shift requires 87 kcal/mol, see Table 2.1 and Figure 2.1. Thus, the two species do not interconvert as solitary ions. This raises the question whether the isomerization can be achieved by catalysis. Theory predicts that a single molecule of water may catalyze this H-shift reaction and promote the isomerization of cyanamide **1**, $H_2NCN^{\bullet+}$, into carbodiimide **6**, $HN=C=NH^{\bullet+}$. The calculations further indicate that hydrogen-bridged radical cations (HBRCs) play an important role in this isomerization, a process termed proton-transport catalysis [10].

The neutral CH_2N_2 system has been examined in considerable detail, by both theory and experiment [7,11-13]. In brief, cyanamide, H_2N-C≡N (**1N**), isocyanamide, H_2N-N=C (**2N**), diazomethane, CH_2N=N (**3N**), and its cyclic isomer diazirine, H_2C-N=N (**4N**), are all stable species in the gas phase. Of these, see the CBS-QB3 results of Table 1a, cyanamide is clearly the isomer of lowest energy. Nitrilimine, HC=N=NH (**7N**), has also been reported, in a NR study by Schwarz and co-workers [11], to be a stable molecule in the gas phase. Other isomers, such as isodiazirine, HC=N-NH (**5N**) and carbodiimide HN=C=NH (**6N**) have not been identified as pure species, but they are reported as chemically viable species [12]. Carbodiimide has been shown by Fourier Transform Infrared Spectroscopy (FT-IR) to exist in the gas phase in admixture with its tautomer

cyanamide [13]. Moreover, substituted carbodiimides are well known intermediates in organic and biochemical synthesis [14].

Ionized isodiazirine HC=N-NH$^{\bullet+}$ (**5**) and carbodiimide HNCNH$^{\bullet+}$ (**6**) have so far eluded experimental observation. Our calculations on the CH_2N_2 system of ions, see Table 2.1 and Scheme 2.1 for the various structures, predict that **5** and **6** are both stable ions in the gas phase as are the ionic counterparts of the stable molecules cyanamide, isocyanamide, diazomethane, diazirine, and nitrilimine.

Scheme 2.1. Isomeric CH_2N_2 radical cations. Structures **8** and **9** are not minima on the PES; D = doublet, Q = quartet.

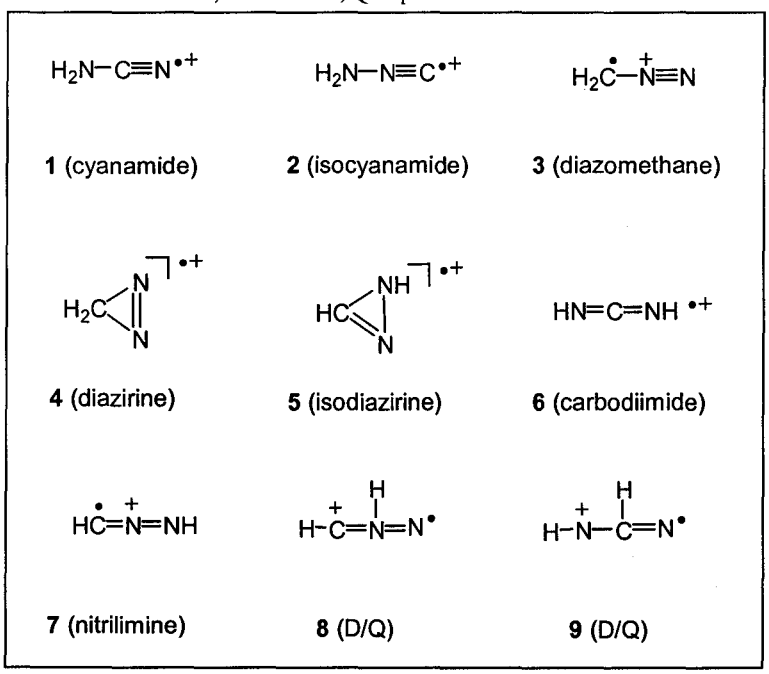

This study describes the generation and characterization of the cyanamide ion $H_2NCN^{\bullet+}$(**1**), and its elusive carbodiimide isomer HNCNH$^{\bullet+}$ (**6**), using tandem mass spectrometric techniques including collision-induced dissociation (CID) and collision-induced dissociative ionization (CIDI). Previously reported experimental results on the gas phase ion chemistry of ions **1**, **2**, **3**, **4** and **7** using MI and CID mass spectrometry [15] are also briefly discussed. The second part of this Chapter describes chemical ionization (CI) type experiments of cyanamide and water in

the presence of a bath gas, by which the cyanamide ion **1** isomerizes into the more stable carbodiimide ion **6**.

The introduction of the neutrals into the source of the mass spectrometer provides one route to generating $CH_2N_2^{\bullet+}$ radical cations ; dissociative ionization under EI conditions provides another route. Cyanamide **1** is generated by electron impact ionization of the neutral molecule whereas the elusive carbodiimide ion **6** is generated as a neutral via dissociation of a suitable precursor ion.

Experimental and Theoretical Methods

The mass spectrometric experiments were performed on the VG Analytical ZAB-R mass spectrometer of BEE geometry (E = electric sector, B = magnet).

The metastable ion spectra were recorded in the second field free region (2ffr) and the collision-induced dissociation spectra were recorded in the 2 and 3ffr using oxygen as the collision gas. The CID mass spectra of the 2ffr metastable or collision-induced peaks were obtained in the 3ffr using O_2 as the collision gas. Unless otherwise noted, for the experiments described in this thesis, an accelerating voltage of 8 kV was used. CID spectra of reference ions having a translational energy close to that of product ions resulting from (MI or CID) dissociations in the 2ffr, were also obtained in the 3ffr. Neutralization-Reionization (NR) mass spectra were recorded using N,N-dimethylaniline as the reducing agent and oxygen gas for reionization. All spectra were recorded using a small PC-based data system developed by Mommers Technologies Inc. (Ottawa).

Samples were introduced into the mass spectrometer via a direct insertion-type solid probe. In the EI experiments at indicated pressures (monitored by a remote ionization gauge) of typically 10^{-6} to 10^{-7} Torr, ions were formed by electron ionization (70 eV) at a source temperature ranging from 100 - 150°C.

In the CI experiments, nitrous oxide (N_2O) was used as a bath gas. This gas was introduced into the source via a Negretti leak valve at an indicated

pressure of c. 4 x 10^{-5} Torr. Cyanamide was introduced by the direct insertion probe for solids at an estimated pressure of 2 x 10^{-6} Torr. The water vapour was introduced via the all quartz direct insertion probe for liquids at an indicated pressure of 2 x 10^{-6} Torr.

Cyanamide and the precursor molecules listed in the Chart below were obtained from Aldrich.

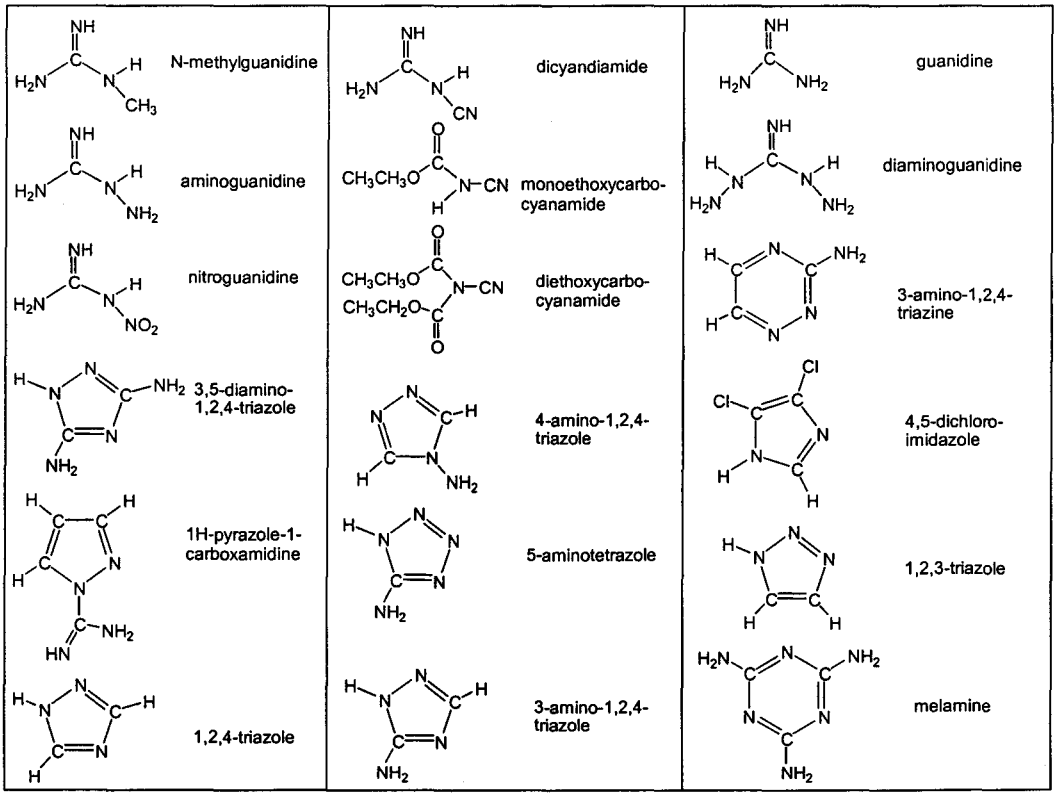

The structures and energies of the $CH_2N_2^{\bullet+}$ ions, neutrals, connecting transition states and dissociation products pertinent to this study, were probed by the standard CBS-QB3 model chemistry [8]. The calculations were performed using Gaussian 98 Revision A11.3 [9]. The calculated energies are presented in Tables 2.1 and 2.2 (see Appendix) and in the potential energy diagrams of Figures 2.1, 2.4 and 2.6. Detailed geometries of selected species are given in the Appendix. Frequency calculations indicated the correct number of negative

eigenvalues for all minima and transition states and the spin contamination was within the acceptable range (any exceptions are noted in the Tables). The connections of the transition states were verified by geometry optimizations and frequency calculations.

Results and Discussion

1. Characterization of $CH_2N_2^{\bullet+}$ ions using MI and CID mass spectrometry.

In our analysis of the experimental results we will use the potential energy diagram of Figure 2.1, which summarizes our theoretical calculations on the $CH_2N_2^{\bullet+}$ system of ions, as a guide.

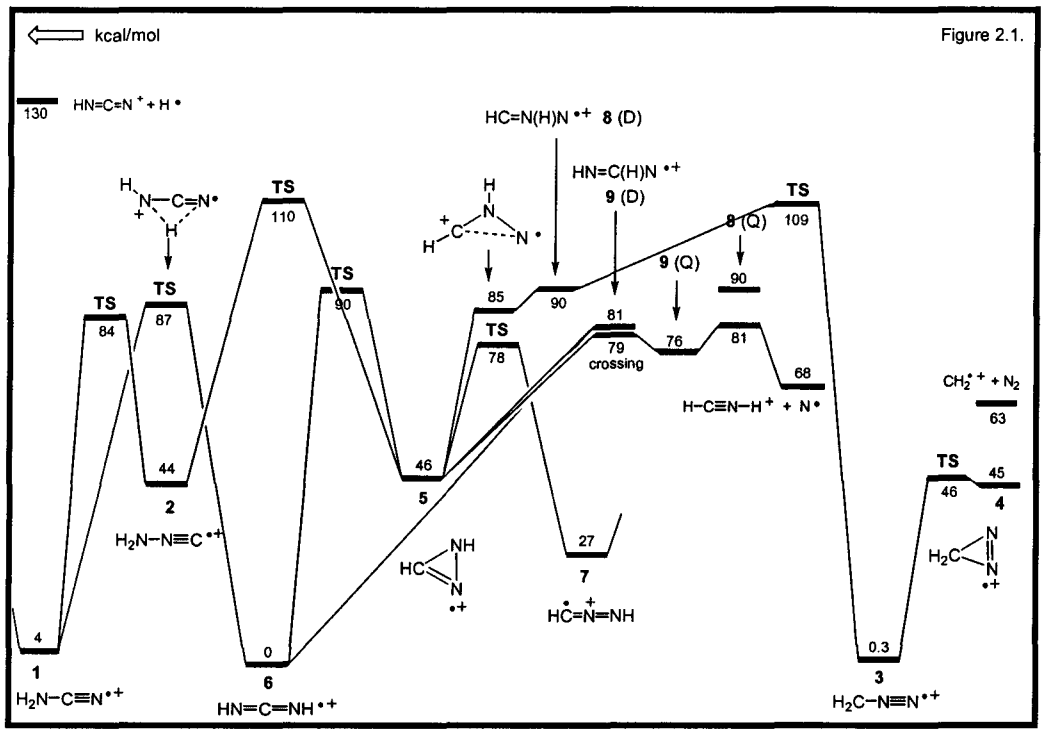

It is seen that the cyanamide ion **1** lies in a deep potential well and that the barriers for isomerization into the isocyanamide ion **2** and the carbodiimide ion **6** are quite high. The carbodiimide ion **6**, which represents the global minimum on the PES, also lies in a deep well : communication by ring closure/opening with

the stable ions **5** (isodiazirine) and **7** (nitrilimine) requires 90 kcal/mol. The dissociation reaction of lowest energy requirement for these five isomeric ions, **1**, **2**, **5**, **6** and **7**, involves the loss of $N^{\bullet}$ to yield m/z 28 ions of structure $HCNH^{+}$. The minimum energy requirement for this reaction is 68 kcal/mol (starting from ion **6**) but, see Figure 2.1, the reaction is calculated to have a significant barrier for the reverse reaction which lies at 81 kcal/mol. That this reaction is associated with a significant reverse activation energy is reflected in the magnitude of the kinetic energy released in the dissociation. Both ionized cyanamide **1** and ionized isocyanamide **2** have been reported to display a dish-shaped metastable ion peak in their MI spectrum at m/z 28 corresponding to the formation of $HCNH^{+}$ ions [15]. For **1**, the kinetic energy release in the formation of $N^{\bullet}$ and $HCNH^{+}$, as measured from the width of the peak at half height is c. 500 meV (11 kcal/mol). We further note that the height of the reverse barrier is close to that of the isomerization barriers that interconnects ions **1**, **2**, **5**, **6** and **7**. This implies that all five ions, including the elusive carbodiimide ion **6**, will have closely similar metastable ion characteristics: they are all expected to dissociate by loss of $N^{\bullet}$ with a broad dish-shaped metastable peak. Thus, the MI spectrum cannot be used to differentiate ions **1**, **2**, **5**, **6** and **7**. In contrast, see Figure 2.1, the isomeric ions **3** and **4** are expected to behave differently: these ions can only lose $N^{\bullet}$ via a rearrangement whose energy requirement greatly exceeds that calculated for the direct bond cleavage into $CH_2^{\bullet+} + N_2$. This is indeed borne out by the experimental observations [15] : **3** and **4** both show a single (narrow) peak in their MI spectrum at m/z 14.

One further point deserves comment : the cyclic isodiazirine ion **5** has been proposed to be generated from (substituted) azoles [16]. However, in a later study by Schwarz and coworkers [11], it was established that 1,2,4-triazole generates m/z 42 ions having the structure of the nitrilimine ion **7**. The MI spectrum of ionized 1,2,4-triazole, m/z 69, shows an intense peak at m/z 42 corresponding to the formation of $CH_2N_2^{\bullet+}$ ions. These $CH_2N_2^{\bullet+}$ ions show a

dished metastable ion peak for the formation of m/z 28 ($HCNH^+$) by loss of $N^\bullet$. As pointed out above, the MI spectrum cannot be reliably used to differentiate the isomers **1**, **2**, **5**, **6** and **7.** However, all these ions lie in deep potential wells and thus it is not surprising that their CID spectra contain peaks of structure diagnostic value.

The CID spectra of isomers **1, 2, 3, 4** have been reported in ref. 15 while those of **4** and **7** are discussed in ref. 11. A representative spectrum of the cyanamide ion **1** obtained in this study is shown in Fig. 2.2a.

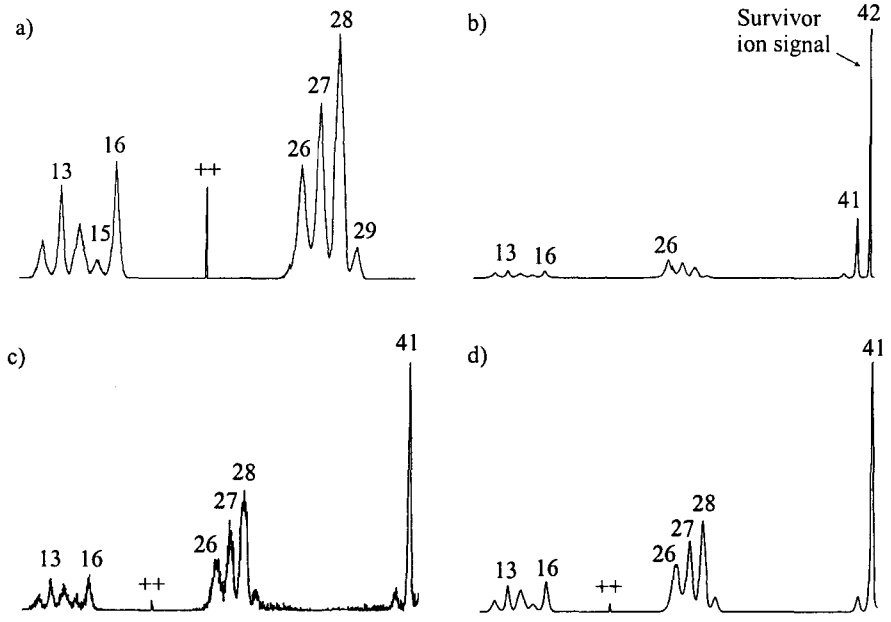

Figure 2.2. a) Partial CID spectrum (2ffr) of the source generated m/z 42 ions of cyanamide **1**; b) NR spectrum of cyanamide **1**; c) NR/CID spectrum of the survivor m/z 42 ions and d) CID spectrum (3ffr) of source generated m/z 42 ions of cyanamide **1.**

The reported CID spectra are all dominated by an intense $H^\bullet$ radical loss at m/z 41, which is not of any structure diagnostic value. However, the weaker clusters of peaks in the m/z 26-30 and m/z 12-17 regions are clearly characteristic of the structure of the isomer. For example, a unique peak at m/z 30 ($N_2H_2^{\bullet+}$), corresponding with the high energy loss of C, easily differentiates the

isocyanamide ion **2** from **1** and all other isomers. In the same vein, in the m/z 12-16 region of the CID spectrum, the spectrum of the nitrilimine ion **7** is dominated by m/z 13 (CH^+), while m/z 14 dominates the spectra of **3** and **4**. Finally, the CID spectrum of **1** displays a fairly intense signal at m/z 16 (NH_2^+), indicative of the structural connectivity of the cyanamide ion, $H_2N\text{-}CN^{\bullet+}$.

Although there is little doubt that carbodiimide **6N** is a stable molecule in the rarefied gas phase, it is not a "bottleable' molecule that can be introduced into the mass spectrometer to generate a beam of pure ions **6** by direct electron ionization. It was therefore attempted to generate ion **6** via dissociative ionization of a suitable precursor molecule. The quest for generating this elusive ion involved examining fourteen different precursor molecules. Neither of these molecules was useful : they all generated m/z 42 ions having the structure of either cyanamide **1** or a mixture of isomers. Of these precursor molecules, nitroguanidine, 1,3-diaminoguanidine and 3-amino-1,2,4-triazine produced m/z 42 ions whose CID spectrum is virtually identical to that of **1**.

A more promising approach to the formation of the carbodiimide ion involved the analysis of selected precursor molecules that upon ionization lose mass 42 as a neutral. To probe the structure of the mass 42 neutral generated by dissociative ionization of a precursor molecule, the technique of collision induced dissociative ionization was used. The selected precursor molecules were aminoguanidine and N-methylguanidine as a potential source of carbodiimide neutrals while 3,5-diaminoguanidine and 1H-pyrazole-1-carboxamidine were used to generate cyanamide for the CIDI experiments. The structures of these precursor molecules are presented in the Chart.

The electron impact mass spectrum of ionized 3,5-diamino-1,2,4-triazole displays the molecular ion as the most abundant peak at m/z 99. Other intense peaks are present m/z 57, 43 and 28. The MI spectrum of the molecular ion displays a dish-shaped peak at m/z 71 for loss of N_2 and also a Gaussian peak at m/z 57 for loss of CH_2N_2. The CIDI spectrum of the molecular ion shows an

intense peak at m/z 42 and less prominent peaks at m/z 67, 56, 28 and 27. Next, the CID spectrum of the m/z 42 ions generated in this CIDI experiment was obtained. The resulting spectrum, see Fig. 2.3c, is closely similar to that of the cyanamide ion **1**, obtained by electron ionization presented in Fig. 2.2a.

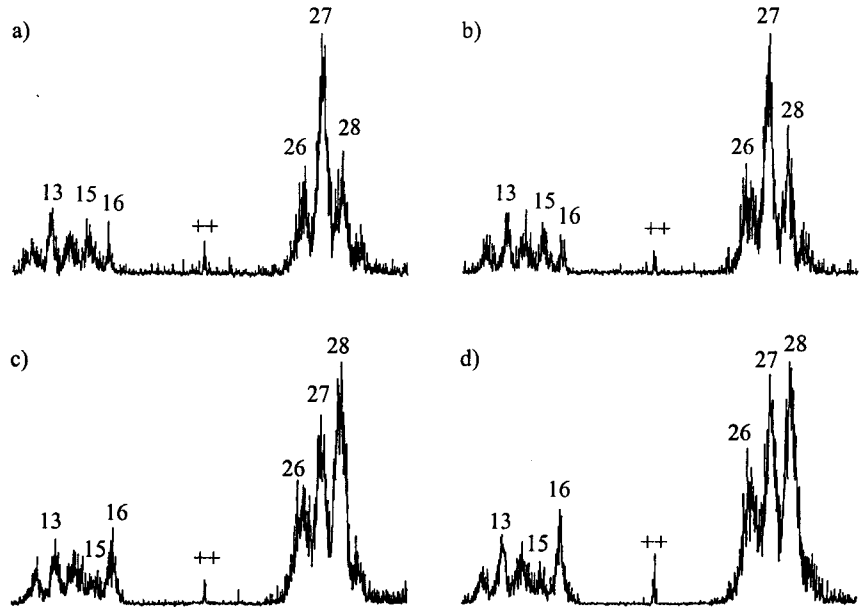

Figure 2.3. Partial CID spectra of the m/z 42 ions generated in the CIDI experiments of the molecular ions of a) aminoguanidine, b) N-methylguanidine, c) 3,5-diamino-1,2,4-triazole and d) 1H-pyrazole-1-carboxamidine.

This experiment provides compelling evidence that cyanamide is lost as a neutral in the above dissociation. It also shows that the collisional ionization process does not promote the isomerization of the incipient ion **1** into its more stable counterpart **6**.

1-H-pyrazole-1-carboxamidine was also investigated as a possible precursor for generating cyanamide as a neutral. Its mass spectrum displays an intense molecular ion at m/z 110, while the fragment ion at m/z 68 represents the base peak. The MI spectrum of the molecular ion contains a single peak at m/z 68 which corresponds to the formation of pyrazole by loss of a CH_2N_2 neutral. The structure of the m/z 68 ions was confirmed by comparison with a reference CID

spectrum of pyrazole. The CIDI spectrum of the molecular ion is dominated by ions at m/z 42. The CID spectrum of these m/z 42 ions is closely similar to that of ionized cyanamide, compare Fig. 2.3d and 2.2a. Thus, here too, the CH_2N_2 neutral lost from the molecular ion is neutral cyanamide.

Next, aminoguanidine and N-methylguanidine were examined as potential precursor molecules for the generation of mass 42 neutrals having the carbodiimide structure.

The mass spectrum of aminoguanidine, $H_2NC(=NH)NHNH_2$, displays prominent signals at m/z 74 ($M^{\bullet+}$), 44, 43, 32 and 18. The loss of mass 42 neutrals is the only low energy reaction of the aminoguanidine molecular ion, which is apparent from the intense peak at m/z 32 in its MI spectrum. The signal at m/z 32 may correspond to $H_2NNH_2^{\bullet+}$ ions generated via a 1,3-H shift and subsequent dissociation of the molecular ion. Ionized aminoguanidine can in principle undergo several hydrogen-shift reactions to lose either carbodiimide or cyanamide as a neutral species. The potential energy diagram of Figure 2.4 shows the possible hydrogen-shift reactions. It is seen that a 1,5-H transfer generating ion **Ac**, the direct precursor to the loss of carbodiimide **6N**, is the least energy demanding reaction. This suggests that ionized aminoguandine preferentially undergoes a 1,5-H shift to form ions **Ac**, which further dissociate by loss of carbodiimide, HN=C=NH.

CIDI experiments on the molecular ions of aminoguanidine are in line with this prediction. The mass-selected molecular ions of aminoguanidine yielded a CIDI spectrum that displays an intense peak at m/z 42. The CID spectrum of these m/z 42 ions, see Fig. 2.3a, is characteristically different from the CID spectra of cyanamide presented in Fig 2.3c/d. The spectrum is also different from the CID spectra of the isomers **2**, **3**, **4** and **7**. It is characterized by an intense peak at m/z 27 ($HNC^{\bullet+}$) in the cluster of peaks in the m/z 26-30 region, compatible with the loss of NH from the carbodiimide ion by direct bond cleavage. In the same vein, the peak at m/z 15 ($NH^{\bullet+}$) is more pronounced than the peak at m/z 16

(NH_2^+). These peaks correspond to structure specific ions that are indicative of the connectivity of the atoms in carbodiimide, HN=C=NH. Thus, this spectrum may provide evidence for the formation of carbodiimide from ionized aminoguanidine, in support of the computational results.

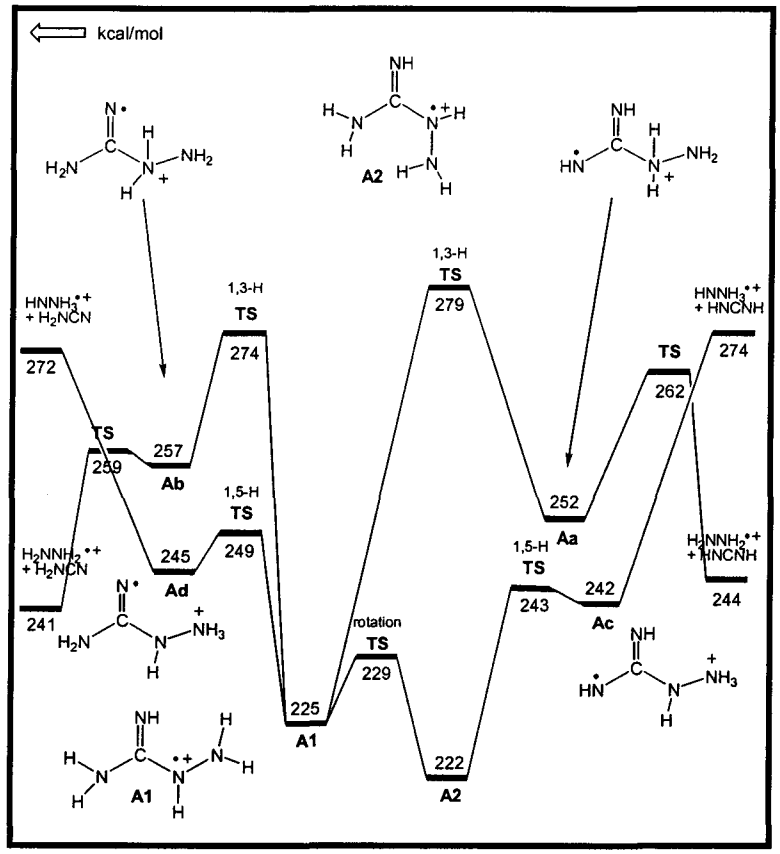

Figure 2.4. Potential energy diagram derived from CBS-QB3 (298K) calculations of aminoguanidine, its isomers and dissociation products.

Next, N-methylguanidine, $H_2NC(=NH)NHCH_3$, was examined as another potential precursor molecule for the formation of carbodiimide. Its 70 eV EI mass spectrum displays an intense molecular ion at m/z 73, in addition to prominent fragment ions at m/z 72, 57, 43 and 30. The MI spectrum of the molecular ions is dominated by peaks at m/z 72 ($H^\bullet$ loss) and m/z 56 (NH_3 loss). Also present in this spectrum are weak peaks at m/z 30 and 31. These correspond to the loss of

neutrals of mass 43 and 42, respectively. Upon collisional ionization, the mass 43 neutrals of putative structure H_2N-C=$NH^{\bullet}$ may dissociate by loss of a $H^{\bullet}$ radical to form m/z 42 ions of structure HN=C=NH and/or H_2N-C$\equiv N^{\bullet+}$. Therefore, a CIDI experiment to probe the structure of the mass 42 neutrals generated from the molecular ions may not be very informative, in that there are two contributing precursors to the mass m/z 42 peak in the CIDI experiment.

On the other hand, the prominent fragment ions at m/z 72 which result from the loss of $H^{\bullet}$ from the molecular ions, can be used to generate mass 42 neutrals in a CIDI experiment. This is because the $[M-H]^+$ ion shows a fairly intense peak at m/z 30 in its MI spectrum corresponding to a loss of mass 42. Indeed, a peak at m/z 42 dominates the CIDI mass spectrum of the m/z 72 ion. These m/z 42 ions, upon collisional activation, give a spectrum, see Figure 2.3b, that is very close to the CID spectrum of the m/z 42 ions from the CIDI experiment of aminoguanidine. This confirms that the $[M-H]^+$ ion of ionized N-methylguanidine loses mass 42 neutrals having the structure of carbodiimide. A tentative mechanistic proposal for this reaction is presented in the Scheme below :

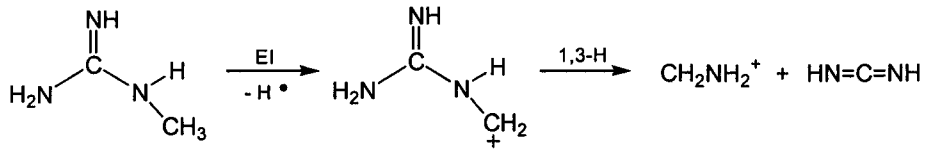

2. Characterization of CH_2N_2 neutrals using NR mass spectrometry.

The neutralization-reionization spectrum of ionized cyanamide **1** is presented in Figure 2.2b. The narrow survivor ion signal at m/z 42, which represents unfragmented reionized neutrals, is the base peak in this spectrum. The CID spectrum of the survivor ion presented in Fig. 2.2c is closely similar to the 3ffr CID spectrum of source generated cyanamide ions **1**, see Fig. 2.2d. Thus the cyanamide ion **1** survives the neutralization-reionization process. More importantly, these experiments reveal that cyanamide does not show any sign of

communication with the carbodiimide isomer prior to dissociation, either as a neutral or as an ion.

From the theoretical calculations presented in Table 2.1, it appears that neutral cyanamide **1N** is the most stable of the neutrals **1N-7N**. NR experiments on some of the other isomers, isocyanamide **2N** [15], diazomethane **3N** [11,15] and nitrilimine **7N** [11] have been previously reported. The spectrum of the reionized isocyanamide neutrals **2N** displays an abundant survivor ion signal at m/z 42 and the presence of this signal is an indication that these neutrals survive the neutralization-reionization process. The NR spectrum of isocyanamide **2** shows slight similarities to the NR spectrum of cyanamide **1**. The base peak in this spectrum lies at m/z 41 and in the low mass region, there are moderately intense peaks at m/z 12-16 and 26-29.

Neutralization-reionization experiments on the diazomethane ion **3** are discussed in a paper by Schwarz and coworkers [11]. The NR spectrum of **3** is shown in ref. [11] and, in addition to the abundant survivor ion signal at m/z 42, it is dominated by a signal at m/z 28. This spectrum does not display peaks at m/z 15 and 16 (which appear in the NR spectrum of **2**) and the peaks at m/z 26, 27 and 29 are almost negligible. It can be inferred from the intense survivor ion signal that diazomethane is a stable species in the gas phase. The theoretical calculations on the neutral CH_2N_2 system predict that diazomethane **3N** is more stable than isocyanamide **2N** by about 13 kcal/mol (see Table 2.1), in fairly good agreement with that found by Schwarz et al., about 15 kcal/mol (B3LYP/6-311+g(d,p) level of theory) [11].

Schwarz and coworkers [11] have also reported that neutral nitrilimine **7N** is less stable than neutral diazomethane **3N,** by about 24 kcal/mol, in good agreement with the CBS-QB3 calculations on this system (25 kcal/mol). It is observed that neutrals **3N** and **7N** lie in deep potential wells since they are separated by a relatively high energy barrier of 72 kcal/mol (B3LYP/6-311+g(d,p) level of theory) [11] possibly indicating that isomerization of the neutrals does not

occur. These theoretical calculations on the neutral system support the experimental findings. In ref. [11], it is reported that the base peak in the NR spectrum of the reionized nitrilimine ion **7** corresponds to the survivor ion signal. The subsequent CID experiment on the survivor ion signal gives a NR/CID spectrum that is nearly identical to the CID spectrum of the source generated nitrilimine ions **7** providing further evidence that neutral nitrilimine **7N** does not interconvert with a more stable neutral isomer.

3. Proton Transport Catalysis in the cyanamide radical cation.

As mentioned previously, the cyanamide radical cation **1**, $H_2NCN^{\bullet+}$, has one stable hydrogen shift isomer, the carbodiimide radical cation **6**, $HNCNH^{\bullet+}$. This 1,3-H shift isomer of cyanamide is more stable by approximately 4 kcal/mol but theory predicts that the unassisted isomerization reaction of the cyanamide ion **1** into the more stable carbodiimide ion **6** does not occur spontaneously. This is corroborated by our experiments which show that ions **1** and **6** have uniquely different CID spectra.

However, the proton-transport catalysis criterion discussed in Chapter 1, Section 1.3 , predicts that an efficient isomerization of ions **1** can be realized in an ion-molecule encounter complex with a neutral base, whose PA lies between the PA of $HNCN^{\bullet}$ at HN and N. From the ΔH_f values for $[HNCN^{\bullet}]$ = 76 kcal/mol, $[H_2NCN^{\bullet+}]$ = 275 kcal/mol, $[HN{=}C{=}NH^{\bullet+}]$ = 271 kcal/mol (Table 2.1) and $[H^+]$ = 366 kcal/mol [17], the PA values for protonation of $HNCN^{\bullet}$ at HN and N are estimated to be 167 and 171 kcal/mol, respectively.

Water is an abundant molecule on earth and in the atmosphere. It has a PA of 165 kcal/mol [18], which lies only slightly below the above-mentioned PA range. Therefore, it was considered as a potentially relevant catalyst ("base") for the isomerization of the cyanamide ion **1** into the carbodiimide ion **6**. The CBS-QB3 calculations presented in Fig. 2.5 suggest that a facile isomerization reaction of $H_2NCN^{\bullet+}$ into $HNCNH^{\bullet+}$, using H_2O as the catalyst, is feasible.

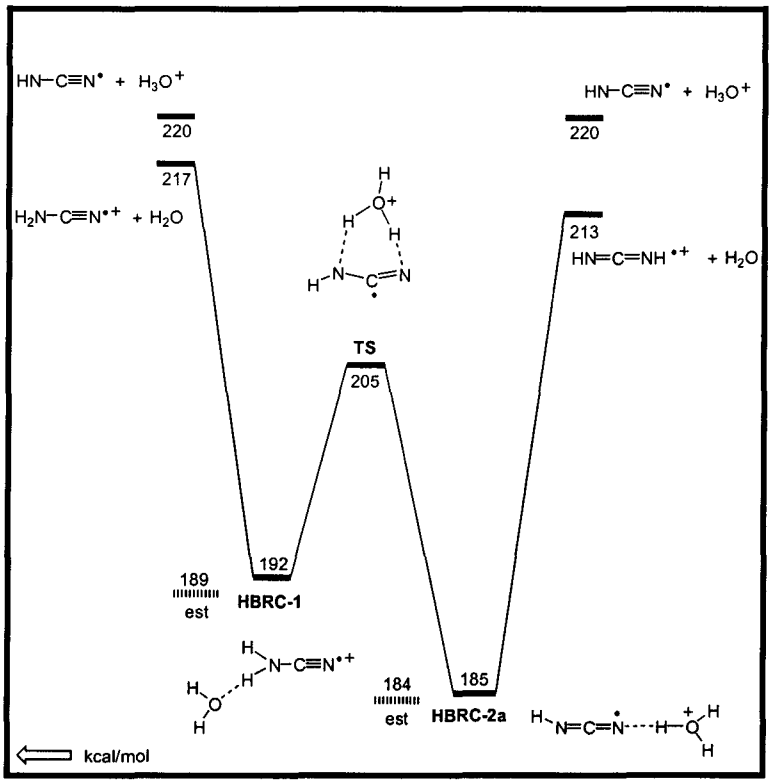

Figure 2.5. Potential energy diagram derived from CBS-QB3 (298K) calculations describing the proton transport catalysis reactions of cyanamide and carbodiimide using water as the catalyst (base).

The potential energy diagram indicates that the initial reactants can form a stabilized encounter complex of cyanamide and water, **HBRC-1**, $[H_2NCN{\bullet\bullet\bullet}H_2O]^{\bullet+}$. Once formed, these **HBRC-1** ions can easily overcome the isomerization barrier to generate the more stable encounter complex, **HBRC-2**, $[HNCNH{\bullet\bullet\bullet}H_2O]^{\bullet+}$, since the transition state lies lower in energy than the initial reactants. It appears that the stable **HBRC-2** ions can then dissociate by loss of H_2O to give carbodiimide ions $HNCNH^{\bullet+}$. Loss of $HNCN^{\bullet}$ neutrals from **HBRC-2** can also occur to form H_3O^+ ions. However, the formation of H_3O^+ ions lies slightly higher in energy than that for the formation of **6**.

In preliminary chemical ionization experiments of H_2NCN and H_2O in the presence of N_2O as a bath gas, a mass spectrum was obtained that features a weak

peak at m/z 60. This peak could result from the formation of an adduct ion of composition $[CH_2N_2 \bullet\bullet\bullet H_2O]^{\bullet+}$. The CID spectrum of these m/z 60 ions is presented in Fig. 2.6a.

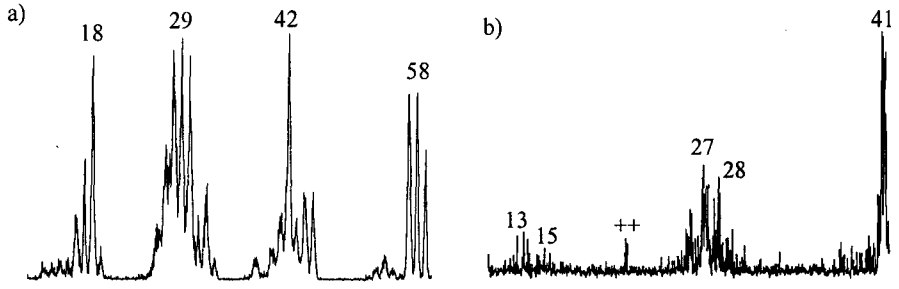

Figure 2.6. a) CID spectrum of the m/z 60 ions generated in the CI experiments of cyanamide and H_2O in the presence of a bath gas; b) CID spectrum of the m/z 42 ions from the CID spectrum of the m/z 60 ions.

Although this spectrum is far from pure, it does display an intense signal at m/z 42, suggesting that an encounter complex has been formed. The CID spectrum of these m/z 42 ions, obtained from a double-collision experiment, is shown in Fig. 2.6b. The spectrum suffers from a very low signal to noise ratio but it is nevertheless compatible with that of ionized carbodiimide, see Fig. 2.3a/b. Therefore, we tentatively propose that the encounter complex of carbodiimide and water, **HBRC-2** $[HNCNH \bullet\bullet\bullet H_2O]^{\bullet+}$, has been generated and that the H_2O molecule has promoted the isomerization of **1** into **6**.

Finally, it should be noted that the proposed mechanism of this isomerization, see Figure 2.5, involves the abstraction of a proton from the NH_2 moiety of the cyanamide ion by the H_2O molecule followed by a back-donation of another proton of the protonated base. This represents a variant of the proton transport catalysis mechanism. It has been coined as a quid-pro-quo mechanism [19].

Conclusion

Tandem mass spectrometry based experiments on the $CH_2N_2^{\bullet+}$ family of ions allow for the characterization and differentiation of the various isomers. In particular, persuasive evidence has been presented for the generation and characterization of the elusive carbodiimide ion $HNCNH^{\bullet+}$ (**6**). In line with theoretical calculations using the CBS-QB3 model chemistry, it is tentatively proposed that a single water molecule catalyzes the isomerization of the cyanamide ion **1** into its more stable counterpart, the carbodiimide ion **6**.

References

[1] F. Cacace, G. de Petris, F. Grandinetti, G. Occhiucci. J. Phys. Chem. 97 (1993) 4239.
[2] A. Schimpl, R.M. Lemmon, M. Calvin. Science. 147 (1965) 149.
[3] C. Ponnamperuma, E. Peterson. Science. 147 (1965) 1572.
[4] B.E. Turner, A.G. Kislyakov, H.S. Liszt, K. Kaifu. Astrophys. J. 201 (1975) L149.
[5] P.G. Wannier, R.A. Linka. Astrophys. J. 226 (1978) 817.
[6] H.E. Matthews, T.J. Sears. Astrophys. J. 300 (1986) 766.
[7] M. Birk, M. Winnewisser, A.Z. Cohen. J. Mol. Spectrosc. 136 (1989) 444.
[8] a) J.A. Montgomery Jr., M.J. Frisch, J.W. Ochterski, G.A. Petersson, J. Chem. Phys. 110 (1999) 2822; b) ibid, 112 (2000) 6532.
[9] M.J. Frisch, et al. Gaussian 98, Revision A.11.3, GAUSSIAN Inc., Pittsburgh PA, 2002.
[10] M.A. Trikoupis, P.C. Burgers, P.J.A. Ruttink, J.K. Terlouw. Int. J. Mass Spectrom. 217 (2002) 97.
[11] N. Goldberg, A. Fiedler, H. Schwarz. Helv. Chim. Acta. 77 (1994) 2354.
[12] a) B.T. Hart. Aust. J. Chem. 26 (1973) 461; idem. p. 477; b) J.B. Moffat. J. Mol. Struct. 52 (1979) 275; c) C. Thomson and C. Glidewell. J. Comput. Chem. 4 (1983) 1.
[13] a) M. Birk and M. Winnewisser. Chem. Phys. Lett. 123 (1986) 386; b) A.W. Allaf, R.J. Suffolk. J. Chem. Research (S) 1993, 269.
[14] a) A. Williams and I.T. Ibrahim. Chem. Rev. 81 (1981) 590; b) D. Tahmassebi. J. Chem. Soc., Perkin Trans. 2 (2001) 613; c) P. Sanchez-Andrada, I. Alkorta, J. Elguero. J. Molec. Struct. (Theochem). 541 (2001) 5 and references therein.
[15] B.L.M. van Baar. Ph.D. Dissertation. University of Utrecht, The Netherlands. 1988. Chapter 1.
[16] a) A. Maquestiau, Y. van Haverbeke and R. Flammang. Org. Mass Spectrom. 6 (1972) 1139; b) A. Maquestiau, Y. van Haverbeke, R. Flammang and J. Elguero. Org. Mass Spectrom. 7 (1973) 271.
[17] S.G. Lias, J.E. Bartmess, J.F. Liebman, J.L. Holmes, R.O. Levin, W.G. Mallard, J. Phys. Chem. Ref. Data 17 (1988) Supplement 1.
[18] E.P.L. Hunter, S.G. Lias. J. Phys. and Chem. Ref. Data 27 (1998) No. 3.
[19] L.N. Heydorn, P.C. Burgers, P.J.A. Ruttink, J.K. Terlouw. Int. J. Mass Spectrom. 227 (2003) 453.

Appendix to Chapter 2

Table 2.1a. CBS-QB3 computational results for various $CH_2N_2^{\bullet+}$ isomers, their neutral counterparts and transition states.

Structure			B3LYP/ CBSB7	ZPVE	CBS-QB3 (0 K)	ΔH_f (298 K)	E_{rel}
$H_2NCN^{\bullet+}$	**1**	[a]	-148.45097	20.6	-148.17928	275.2	4.1
$H_2NNC^{\bullet+}$	**2**		-148.38880	20.0	-148.11685	314.7	43.6
$H_2CNN^{\bullet+}$	**3**		-148.45047	19.5	-148.18492	271.7	0.6
$H_2\underline{CNN}^{\bullet+}$	**4**		-148.37637	if	-148.11406	315.9	44.8
$H\underline{CNN}H^{\bullet+}$	**5**		-148.37703	19.6	-148.11196	317.2	46.1
$HN{=}C{=}NH^{\bullet+}$	**6 cis**	[a]	-148.45623	18.2	-148.18642	271.1	0
	6 tr	[a]	-148.45548	if	-148.18641	270.1	-0.4
$HCNNH^{\bullet+}$	**7**		-148.41172	18.9	-148.14223	298.5	27.4
$HCNHN^{\bullet+}$	**8(D)**		-148.31251	18.6	-148.04085	362.1	91.0
	8(Q)		-148.31801	18.8	-148.04272	360.7	89.6
$HNCHN^{\bullet+}$	**9(D)**		-148.32628	17.0	-148.05769	351.7	80.6
	9(Q)		-148.33943	17.9	-148.06542	346.6	75.5
TS (1-2)			-148.31829	19.0	-148.05165	355.2	84.1
TS (1-6)			-148.31286	15.2	-148.04832	357.6	86.5
TS (2-5)			-148.26975	16.4	-148.00993	381.2	110.1
TS (3-4)			-148.37404	17.9	-148.11184	317.5	46.4
TS (3-8)			-148.27194	14.9	-148.01157	380.4	109.3
TS (5-6)			-148.31946	16.4	-148.04080	362.0	90.9
TS (5-7)			-148.32669	17.6	-148.06164	349.0	77.9
TS (5-8D)			-148.30595	17.2	-148.04988	356.4	85.3
TS (5-9D)			-148.32560	16.9	-148.05786	351.4	80.3
TS (6-9D)			-148.32614	16.3	-148.05641	352.2	81.1
H_2NCN	**1N**		-148.82942	21.4	-148.56529	33.0	-2.5
H_2NNC	**2N**		-148.75801	21.2	-148.49446	77.5	42.0
H_2CNN	**3N**		-148.78171	19.9	-148.51526	64.4	28.9
$H_2\underline{CNN}$	**4N**		-148.75780	20.9	-148.49755	75.1	39.6
$H\underline{CNN}H$	**5N**		-148.72338	20.4	-148.46572	95.2	59.7
$HN{=}C{=}NH$	**6N**		-148.82830	20.5	-148.56118	35.5	0
HCNNH	**7N**				-148.47148	89.0	53.5

[a] Spin contamination occurs in the CBS-QB3 calculation above a value of 0.825.

[b] B3LYP/CBSB7 and CBS-QB3 (0 K) values in Hartrees; ΔH_f (298 K) values in kcal/mol.

Table 2.1b. CBS-QB3 computational results for the dissociation products of the $CH_2N_2^{\bullet+}$ system.

Structure			B3LYP/ CBSB7	ZPVE	CBS-QB3 (0 K)	ΔH_f (298 K)	Exp. [c]
$HNCN^+$	m/z 41		-147.73226	11.7	-147.48071	349.3	
H_2NNH^+	m/z 31				-110.77246	229.3	
$HNNH^{\bullet+}$	m/z 30				-110.13127	269.8	272
HN_2^+	m/z 29						247.5
$HCNH^+$	m/z 28		-93.73316	17.5	-93.55430	226.4	226
$HCN^{\bullet+}$	m/z 27	[a]			-93.77376	354.0	346
$HNC^{\bullet+}$	m/z 27	[a]			-92.82363	323.1	336
NH_2^+	m/z 16				-55.38062	302.8	302
$NH^{\bullet+}$	m/z 15				-54.65080	396.1	401
$CH_2^{\bullet+}$	m/z 14		-38.78287	10.2	-38.69018	332.9	331
$HNCN^{\bullet}$			-148.17094	12.3	-147.91569	76.2	
HCN					-93.28750	31.7	32.3
HNC					-93.26616	45.5	48
$CN^{\bullet}$		[a]			-92.58753	106.6	104
NH					-55.14448	86.1	90
$N^{\bullet}$		[a]	-54.59854	0	-54.52055	113.0	113
$H^{\bullet}$			-0.50215	0	-0.49982	52.1	52.1

[a] Spin contamination occurs in the CBS-QB3 calculation above a value of 0.825.
[b] B3LYP/CBSB7 and CBS-QB3 (0 K) values in Hartrees; ΔH_f (298 K) values in kcal/mol.
[c] Ref. 17.

Table 2.2. CBS-QB3 computational results for the isomerization of $H_2NCN^{\bullet+}$ into $HN{=}C{=}NH^{\bullet+}$, using H_2O as the base.

Structure			CBS-QB3 (0 K)	CBS-QB3 (Enthalpy)	ΔH_f (298 K)
$H_2O{\bullet\bullet\bullet}H_2NCN^{\bullet+}$	**HBRC-1**	[a]	-224.55540	-224.54814	192.1
$H_2O{\bullet\bullet\bullet}HNCNH^{\bullet+}$	**HBRC -2**	[a]	-224.56697	-224.55900	185.3
TS(HBRC-1 to 2a)$^{\bullet+}$			-224.53374	-224.52748	205.0

[a] Spin contamination occurs in the CBS-QB3 calculation above the value of 0.825.
[b] CBS-QB3 (0 K) values in Hartrees; ΔH_f (298 K) values in kcal/mol.

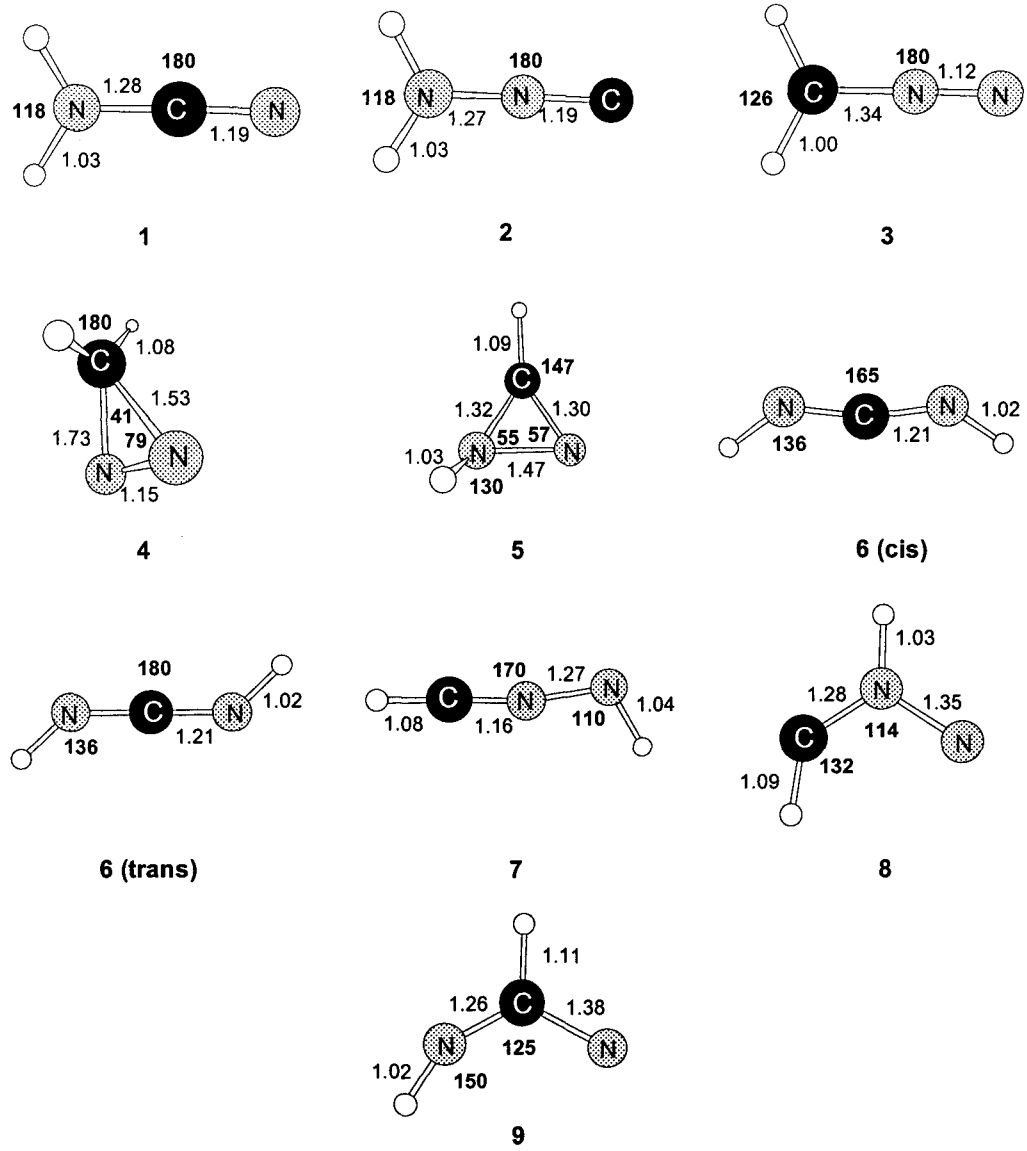

Figure A2.1. Selected optimized geometries of cyanamide and several isomers. Bond angles in degrees and bond lengths in Angstroms.

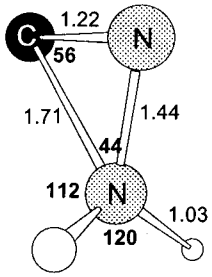

TS (1 to 2)

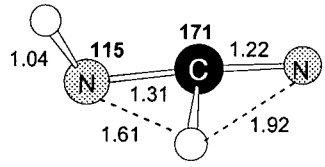

TS (1 to 6)

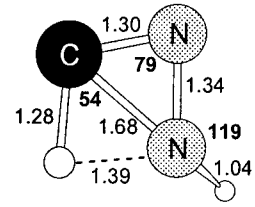

TS (2 to 5)

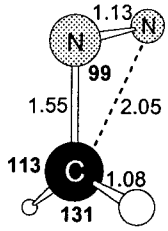

TS (3 to 4)

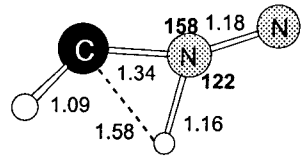

TS (3 to 8)

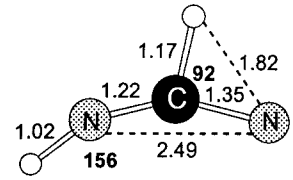

TS (5 to 6a)

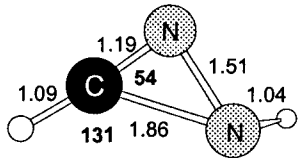

TS (5 to 7)

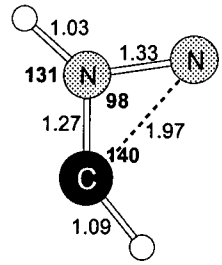

TS (5 to 8)

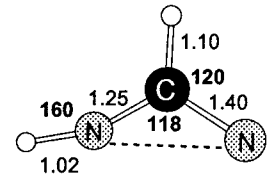

TS (5 to 9)

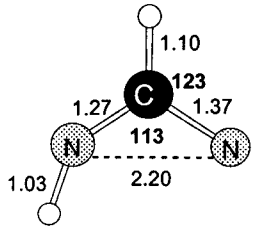

TS (5 to 9) crossing

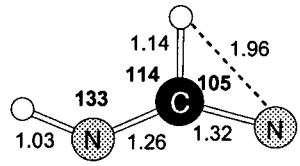

TS (6 to 9)

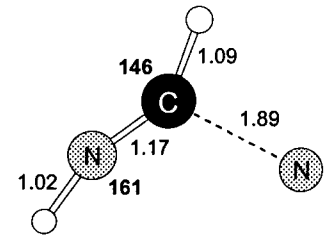

TS (9 to diss.)

Figure A2.2. Selected optimized geometries of the transition states linking the isomers in the cyanamide system. Bond angles in degrees and bond lengths in Angstroms.

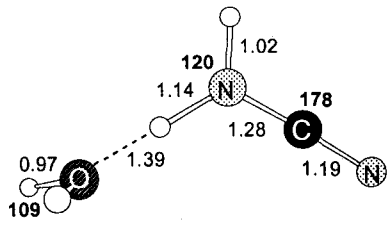

HBRC-1

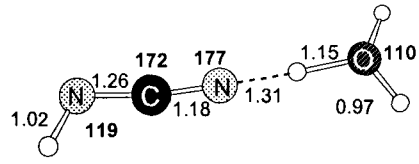

HBRC-2

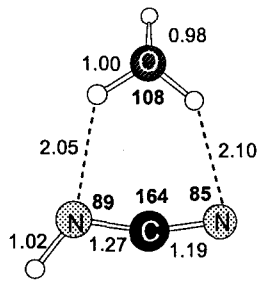

TS (HBRC-1 to 2)

Figure A2.3. Selected optimized geometries of the encounter complexes in the catalyzed isomerization reaction of cyanamide into carbodiimide using water as the catalyst. Bond angles in degrees and bond lengths in Angstroms.

Chapter 3

The generation and characterization of the aminocarbodiimide ion $H_2N\text{-}N{=}C{=}NH^{\bullet+}$ and some of its isomers by tandem mass spectrometry and computational chemistry.

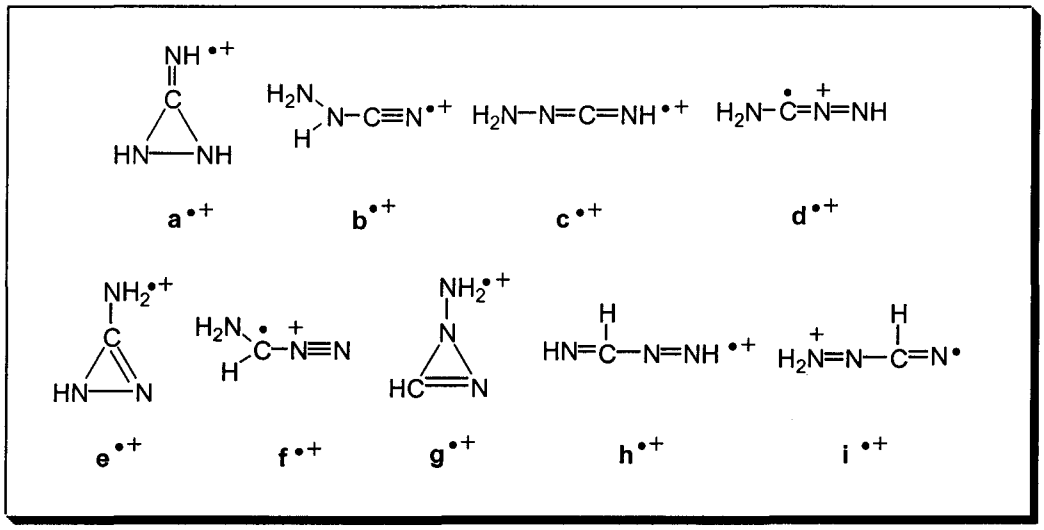

Using the results of a CBS-QB3 computational study on the $CH_3N_3^{\bullet+}$ isomeric ions shown in the Scheme above, this Chapter further describes experiments aimed to generate and characterize some of these ions in the gas phase. It is shown that the amino-carbodiimide ion $\mathbf{c}^{\bullet+}$, the aminonitrilimine ion $\mathbf{d}^{\bullet+}$, the C-aminoisodiazirine ion $\mathbf{e}^{\bullet+}$ and the ionized biradical, $\mathbf{i}^{\bullet+}$ can be generated via dissociative ionization of selected precursor molecules. Ions $\mathbf{c}^{\bullet+}$, $\mathbf{e}^{\bullet+}$ and $\mathbf{i}^{\bullet+}$ can readily be characterized on the basis of their CID spectra, but the characterization of $\mathbf{d}^{\bullet+}$ remains problematic. Neutralization-reionization experiments show, in agreement with the computational results, that the neutral counterparts of **c** and **e,** but not **i**, are stable species in the rarefied gas phase.

Introduction

Carbodiimides are an important class of heterocumulenes which contain two carbon-nitrogen double bonds and an orthogonal disposition of the substituents at the nitrogen atoms [1]. These compounds have become of great interest due to their involvement in synthetic organic chemistry but also due to their molecular structure : they are isoelectronic with allenes, ketenes and ketenimines [2]. Carbodiimides exhibit a high reactivity due to the electrophilic character of the central carbon atom to the nucleophilicity of the nitrogen atoms. Thus the carbon-nitrogen double bond is easily attacked by a variety of nucleophiles and electrophiles [1].

Cyanamide derivatives such as N-halo-amidines are unique in reactivity and useful as transient intermediates [3]. Diazo-compounds and the isomeric diazirines are also important substrates in synthetic studies and substituent affects on all these species is a topic of major interest [4]. Nitrilimines are important reagents in organic synthesis particularly in regioselective, 1,3-dipolar cycloadditions, however, for a long time they could only be observed as transient intermediates in low temperature matrices [5]. By selecting the appropriate substituents, nitrilimines can exist as stable compounds in the solid or liquid states [5].

It is apparent that CH_2N_2 derivatives are important compounds used in solution phase chemistry. This study focuses on generating and characterizing several $CH_3N_3^{\bullet+}$ ions (amino-substituted $CH_2N_2^{\bullet+}$ ions) in the gas phase. These isomeric ions are generated via dissociative ionization of aminoguanidine, 3-amino-1,2,4-triazole, 3,5-diamino-1,2,4-triazole, 5-aminotetrazole and 4-amino-1,2,4-triazole. The structure of the CH_3N_3 ions and neutrals are probed by collision-induced dissociation (CID) and neutralization-reionization (NR) mass spectrometry.

Experimental and Theoretical Methods

The mass spectrometric experiments were performed on the VG Analytical ZAB-R mass spectrometer of BEE geometry (E = electric sector, B = magnet).

Collision-induced dissociation mass spectra were recorded in the 2nd and 3rd ffr using oxygen as collision gas. The CID mass spectra of the 2ffr metastable or collision-induced peaks were obtained in the 3ffr using O_2 as collision gas. For these experiments an accelerating voltage of 8 kV was used unless otherwise noted. CID spectra of reference ions having a translational energy close to that of product ions resulting from (MI or CID) dissociations in the 2ffr, were also obtained in the 3ffr. Neutralization-reionization mass spectra were recorded using N,N-dimethylaniline as the reducing agent and oxygen gas for reionization. All spectra were recorded using a small PC-based data system developed by Mommers Technologies Inc. (Ottawa).

Samples were introduced into the mass spectrometer via a direct insertion-type probe for solids. At indicated pressures (monitored by a remote ionization gauge) of typically 10^{-6} to 10^{-7} Torr, ions were formed by electron ionization (70 eV) at a source temperature ranging from 100 - 150°C.

Aminoguanidine, 3-amino-1,2,4-triazole, 3,5-diamino-1,2,4-triazole, 5-aminotetrazole and 4-amino-1,2,4-triazole were obtained from Aldrich.

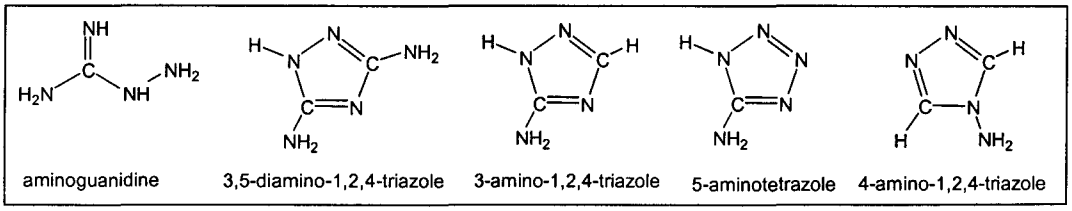

Structures and energies of the $CH_3N_3^{\bullet+}$ ions and neutrals pertinent to this study, connecting transition states and dissociation products were probed by the standard CBS-QB3 model chemistry [6]. The calculations were performed using

Gaussian 98 Revision A11.3 [7]. The calculated energies are presented in Table 3.1 (see Appendix) and the potential energy diagrams of Figures 3.2 and 3.3. Frequency calculations gave the correct number of negative eigenvalues for all minima and transition states and the spin contamination was generally within the acceptable range (any exceptions are noted in the tables). The connections of the transition states have been checked by geometry optimizations and frequency calculations.

Results and Discussion

Upon collisional activation, ionized aminoguanidine, H_2N-C(=NH)-NH-$NH_2^{\bullet+}$, generates ions at m/z 57 by loss of NH_3. The CID spectrum of these m/z 57 ions, shown in Figure 3.1a, is dominated by an intense signal at m/z 28. This peak corresponds to the formation of $HCNH^+$ ions by the loss of N_2 and $H^\bullet$. The theoretical calculations predict that the reaction $HCNH^+ + N_2 + H^\bullet$ is the least energy demanding dissociation reaction, see Figure 3.2 and Table 3.1. In the high mass region, this spectrum displays peaks for the loss of $NH_2^\bullet$ and NH at m/z 41 and 42, respectively. The ratio of these peaks is 1 : 0.75 for m/z 41 : 42, indicating a more facile loss of $NH_2^\bullet$ relative to the loss of NH from the m/z 57 ions.

In principle, ionized aminoguanidine can lose NH_3 via three different pathways to generate m/z 57 ions having the structure of either ionized aminocarbodiimide $\mathbf{c}^{\bullet+}$, its H-shift isomer ionized aminocyanamide $\mathbf{b}^{\bullet+}$, or the cyclic isomer ionized 2H-imidoisodiazirine $\mathbf{a}^{\bullet+}$:

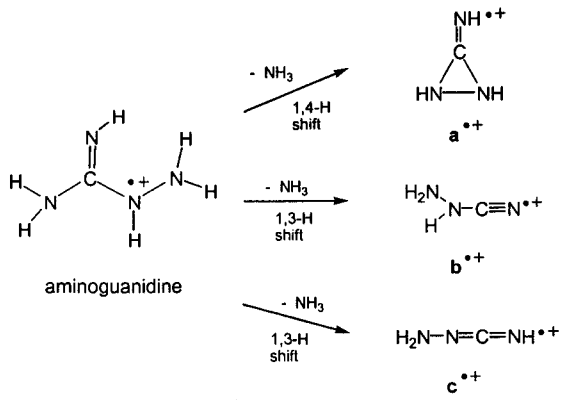

The above Scheme shows the structures of ions $\mathbf{a}^{\bullet+}$, $\mathbf{b}^{\bullet+}$ and $\mathbf{c}^{\bullet+}$. It is seen that loss of $NH_2^{\bullet}$ is a simple bond cleavage from ions $\mathbf{b}^{\bullet+}$ and $\mathbf{c}^{\bullet+}$, whereas ions $\mathbf{a}^{\bullet+}$ must rearrange via a 1,3-H transfer prior to this dissociation. The structures of these ions suggest a facile loss of NH from $\mathbf{a}^{\bullet+}$ and $\mathbf{c}^{\bullet+}$ but not from $\mathbf{b}^{\bullet+}$. Therefore, it is proposed that the m/z 57 ion has the structure of the aminocarbodiimide ion H_2N-N=C=$NH^{\bullet+}$ ($\mathbf{c}^{\bullet+}$).

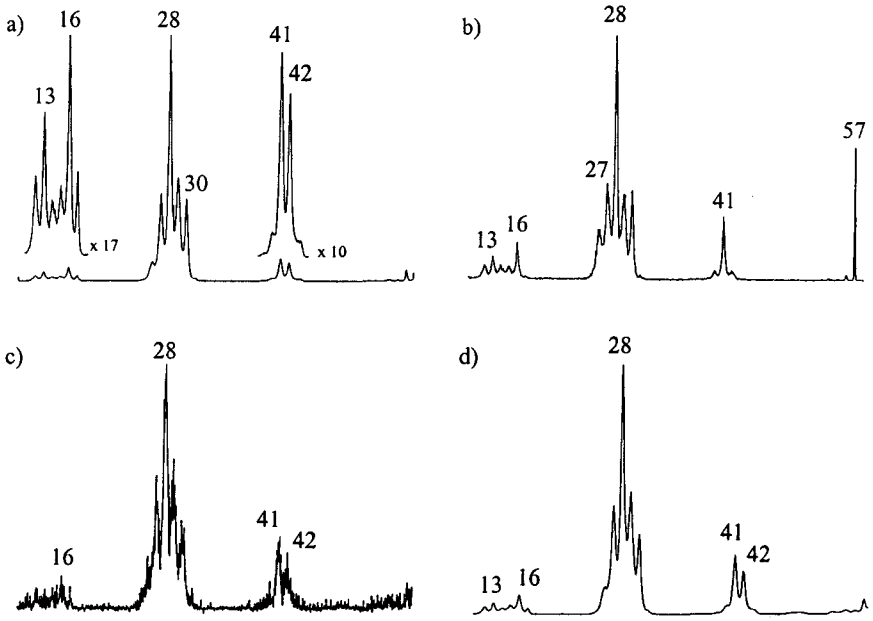

Figure 3.1. a) 2ffr CID spectrum; b) NR spectrum; c) NR/CID spectrum and d) 3ffr CID spectrum of the m/z 57 ions of ionized aminoguanidine.

The potential energy diagram of Figure 3.2 displays the CBS-QB3 computational results for the $CH_3N_3^{\bullet+}$ system of ions. It is seen that the stable aminocyanamide and aminocarbodiimide ions $\mathbf{b}^{\bullet+}$ and $\mathbf{c}^{\bullet+}$ are far lower in energy than the cyclic 2H-imidoisodiazirine ion $\mathbf{a}^{\bullet+}$. Moreover, ion $\mathbf{a}^{\bullet+}$ does not readily communicate with $\mathbf{b}^{\bullet+}$ or $\mathbf{c}^{\bullet+}$: the transition state (TS) for the route $\mathbf{a}^{\bullet+} \rightarrow \mathbf{e}^{\bullet+}$, the first step in the isomerization sequence, $\mathbf{a}^{\bullet+} \rightarrow \mathbf{e}^{\bullet+} \rightarrow \mathbf{d}^{\bullet+} \rightarrow \mathbf{c}^{\bullet+}$, is prohibitively

high. The isomerization $\mathbf{b}^{\bullet+} \rightarrow \mathbf{c}^{\bullet+}$ involves a 1,3-H shift. So far, all attempts to calculate the TS for this shift have been unsuccessful. This is because the input structures optimized to a 1,2-H shift TS. This TS represents a H-transfer from the amide N atom to the C atom, whereas the desired TS involves the transfer of the amide H atom to the cyano N atom. Even when the distance between the shifting H atom and the C atom in the four-membered ring input geometry was greatly increased, the optimized geometry remained associated with the 1,2-H shift TS.

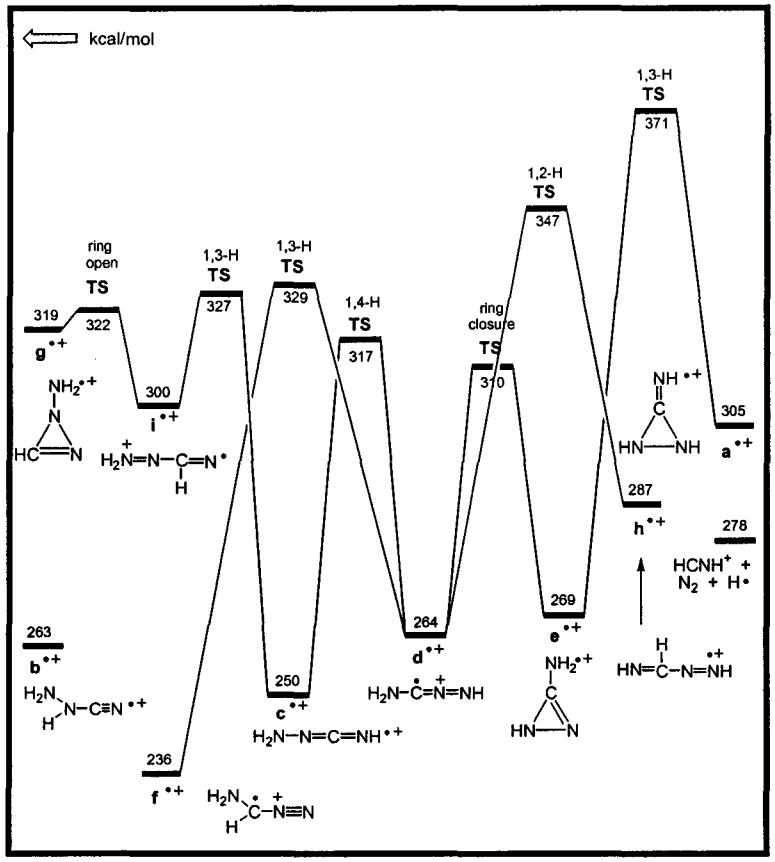

Figure 3.2. Potential energy diagram derived from the CBS-QB3 (298K, Table 1) calculations describing the isomerization reactions of the $CH_3N_3^{\bullet+}$ system of ions.

The potential energy diagram of Figure 3.3 shows the possible reaction pathways for the loss of NH_3 from ionized aminoguanidine. The least energy demanding pathway is that for the formation of ion $\mathbf{c}^{\bullet+}$. It can be seen that the

ionized aminoguanidine conformer, **A2**, rotates into conformer **A1** via a low lying rotational energy barrier (8 kcal/mol). Ion **A1** undergoes a 1,3-H shift to generate ion **Ag** which is the direct precursor for the formation of the aminocarbodiimide ion $\mathbf{c}^{\bullet+}$. Thus, the computational results provide further support for the formation of the proposed ions $\mathbf{c}^{\bullet+}$ from ionized aminoguanidine.

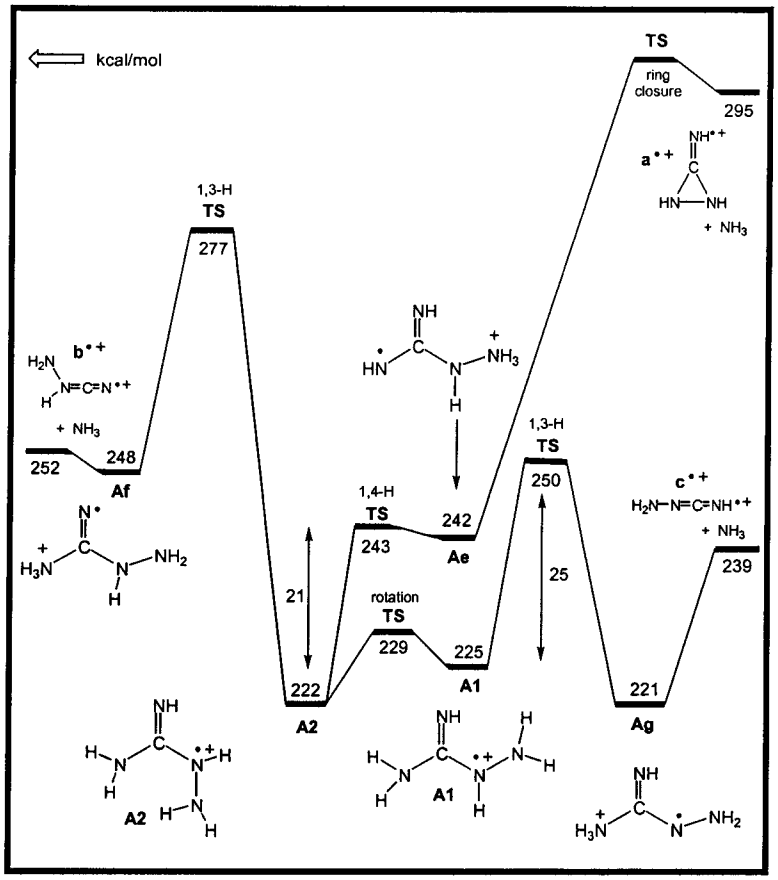

Figure 3.3. Potential energy diagram derived from the CBS-QB3 (298K) calculations describing the mechanistic loss of NH_3 from ionized aminoguanidine.

The NR spectrum of the m/z 57 ion of putative structure $\mathbf{c}^{\bullet+}$ is presented in Figure 3.1b. The spectrum displays an intense survivor ion signal at m/z 57 and the base peak at m/z 28. The intense survivor ion signal suggests that aminocarbodiimide **c** is a stable species in the gas phase, in line with the theoretical calculations, see Table 3.1 and Figure 3.4. The spectrum also shows

signals at m/z 16 ($NH_2^{\bullet}$) and 41 ($HNCN^{\bullet}$) of higher intensity than those in the CID spectrum. These peaks may result from the dissociation of a fraction of the 57 neutrals prior to reionization.

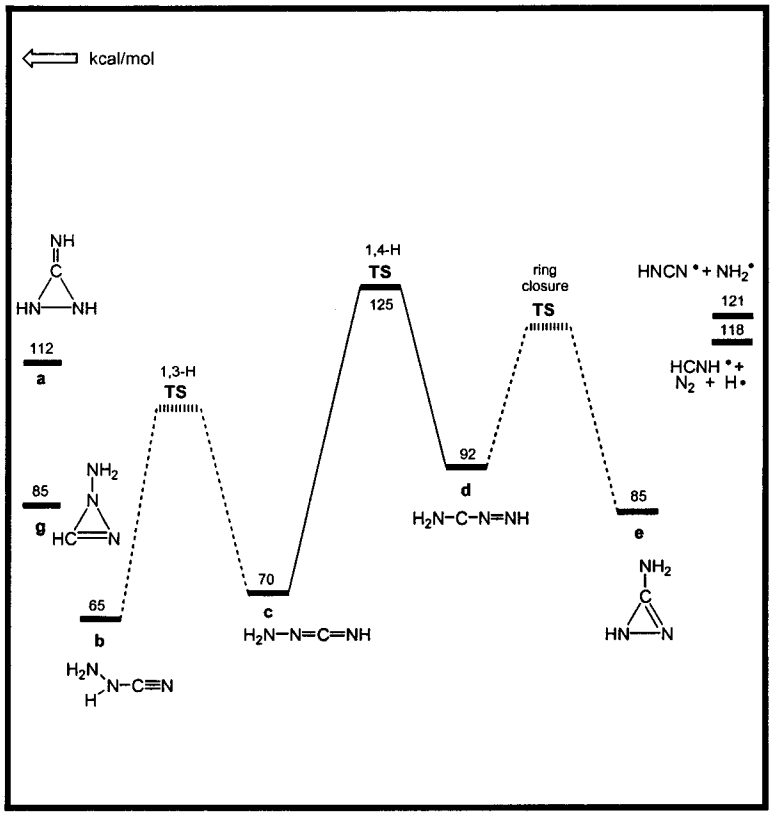

Figure 3.4. Potential energy diagram derived from the CBS-QB3 (298K, Table 1) calculations describing the isomerization reactions of the CH_3N_3 neutrals.

The potential energy diagram of the neutral system shows the energies of the neutral isomers and the dissociation products. It is seen that **b** is slightly more stable than **c**, whereas **a** lies higher in energy than both **b** and **c**. The TS for the isomerization **b** → **c** could not be located.

The CID spectrum of the survivor ion of putative structure $\mathbf{c}^{\bullet+}$ is closely similar to the 3ffr CID spectrum of the source generated ions, compare Figure 3.1c and d. This provides evidence that the incipient neutrals **c** do not isomerize

upon neutralization and so we conclude that aminocarbodiimide is a stable species in the gas phase .

From the potential energy diagram of Figure 3.2, it follows that ionized aminonitrilimine, $H_2N\text{-}C{=}N{=}NH^{\bullet+}$ ($\mathbf{d}^{\bullet+}$) and its cyclic counterpart C-amino-isodiazirine $\mathbf{e}^{\bullet+}$ both lie in deep potential wells. The isomers differ in energy by 5 kcal/mol and are separated by an isomerization barrier of 46 kcal/mol. A possible route to the formation of $\mathbf{e}^{\bullet+}$ involves dissociative ionization of 3-amino-1,2,4-triazole (loss of HCN) or 5-aminotetrazole (loss of N_2) :

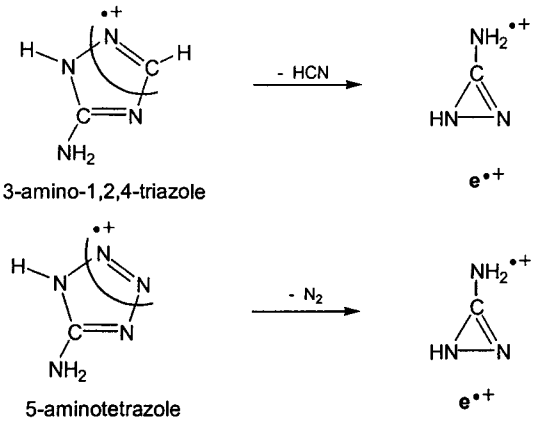

The CID spectra of the m/z 57 ions of the two precursor molecules are closely similar, see Figure 3.5a and b. The base peak in the CID spectra at m/z 28 corresponds to the formation of $HCNH^+$ ions by loss of N_2 and $H^{\bullet}$. In the high mass region, the spectra show peaks at m/z 41 and 42 with an intensity ratio of 1 : 2. In the low mass region, the peak at m/z 13 (CH^+) has nearly the same intensity as the m/z 16 (NH_2^+) peak. Considering the above mechanistic proposals for the structure of the ions and the fact that their CID spectra, compare Figure 3.5a and b, are closely similar, it seems likely that we are dealing with C-aminoisodiazirine ions $\mathbf{e}^{\bullet+}$.

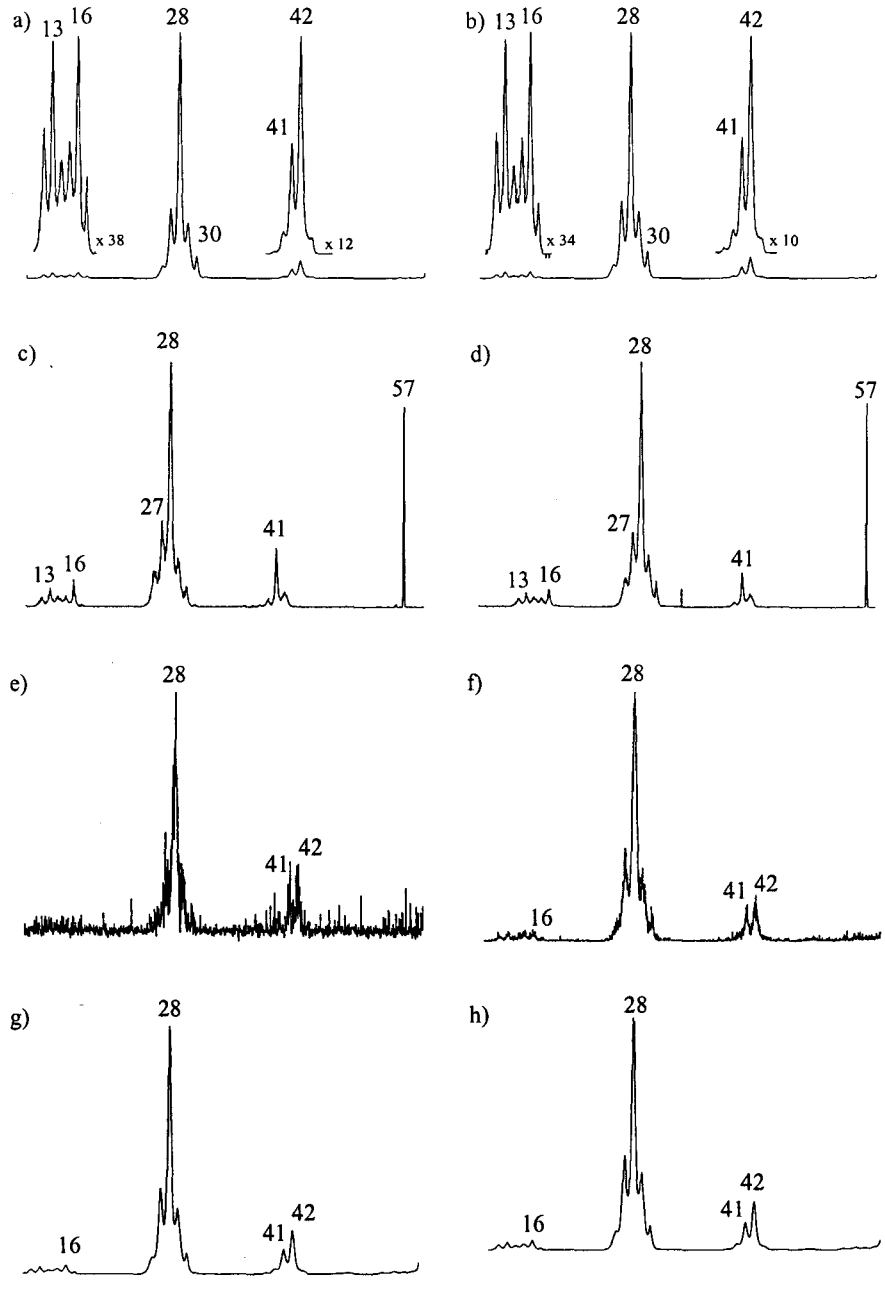

Figure 3.5. a) 2ffr CID spectrum; c) NR spectrum; e) NR/CID spectrum and g) 3ffr CID spectrum of the m/z 57 ions of ionized 5-aminotetrazole. b) 2ffr CID spectrum; d) NR spectrum; f) NR/CID spectrum and h) 3ffr CID spectrum of the m/z 57 ions of ionized 3-amino-1,2,4-triazole.

The NR spectra of the m/z 57 ions of putative structure $\mathbf{e}^{\bullet+}$ from 3-amino-1,2,4-triazole and 5-aminotetrazole are also nearly identical. The spectra show an abundant survivor ion signal indicating that neutrals **e** are stable species in the gas phase, see Figure 3.5c and d. The CID spectra of the survivor ion signals are closely similar to their respective 3ffr CID spectra of the source generated ions. This indicates that the neutrals do not isomerize upon neutralization and confirms that C-aminoisodiazirine is a stable species. The calculations presented in the potential energy diagram of the neutral system, shown in Figure 3.4, support these findings.

As discussed in Chapter 2, ionized 3,5-diamino-1,2,4-triazole readily loses H_2NCN. The resulting m/z 57 product ion could be either the aminonitrilimine ion $\mathbf{d}^{\bullet+}$ or its cyclic isomer $\mathbf{e}^{\bullet+}$:

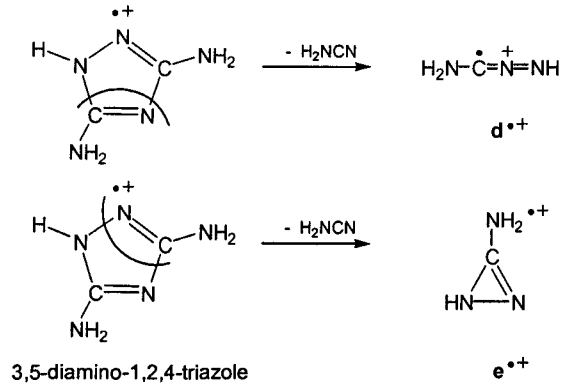

Considering that $\mathbf{d}^{\bullet+}$ and $\mathbf{e}^{\bullet+}$ differ in energy by only 5 kcal/mol, it seems likely that this precursor molecule will generate a mixture of the two ions. The potential energy diagram of Figure 3.2 indicates that ions $\mathbf{d}^{\bullet+}$ and $\mathbf{e}^{\bullet+}$ lie in fairly deep potential wells. Nevertheless, the isomerization barrier $\mathbf{d}^{\bullet+} \rightarrow \mathbf{e}^{\bullet+}$ lies lower in energy than that for $\mathbf{d}^{\bullet+} \rightarrow \mathbf{h}^{\bullet+}$, where $\mathbf{h}^{\bullet+}$ is the direct precursor to the formation of m/z 28 $HCNH^+$ ions by loss of N_2 and $H^{\bullet}$.

In the CID spectrum of the m/z 57 ions the fragment ion at m/z 28 ($HCNH^+$) represents the base peak, see Figure 3.6a. Peaks at m/z 41 (loss of

$NH_2^{\bullet}$) and 42 (loss of NH) also appear in this spectrum and the ratio of their intensities is approximately 1 : 0.9. This CID spectrum only differs from that of the aminocarbodiimide ion $\mathbf{c}^{\bullet+}$ in the peak intensity ratio of the m/z 41 and 42 peaks. The potential energy diagram of Figure 3.2 indicates that ions $\mathbf{d}^{\bullet+}$ and $\mathbf{c}^{\bullet+}$ can communicate via 1,4-H shift but the associated barrier is quite high. This makes it likely that the m/z 42 : 41 peaks intensity ratio reflects the fact that the m/z 57 ions from 3,5-diamino-,1,2,4-triazole represent a mixture of ions $\mathbf{e}^{\bullet+}$ and $\mathbf{d}^{\bullet+}$.

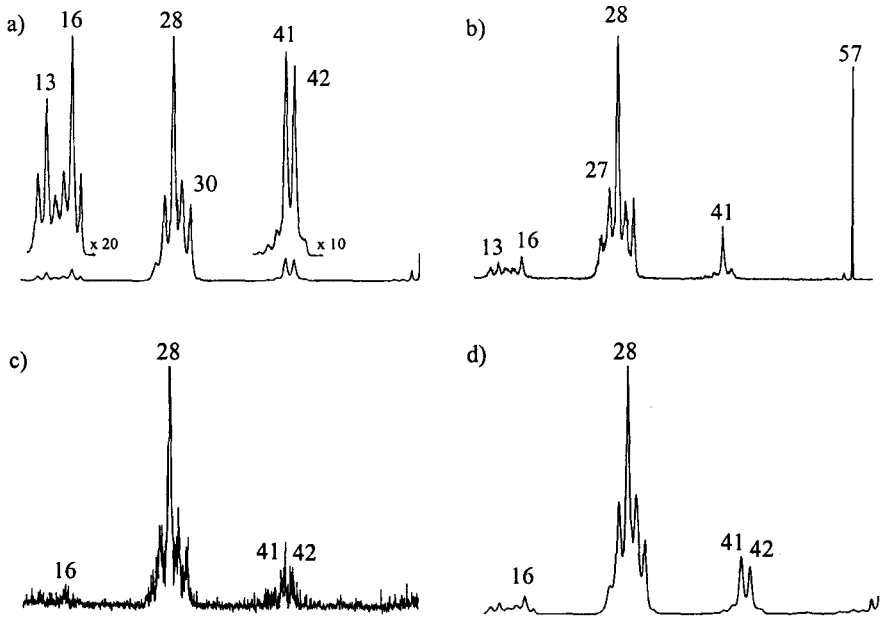

Figure 3.6. a) 2ffr CID spectrum; b) NR spectrum; c) NR/CID spectrum and d) 3ffr CID spectrum of the m/z 57 ions of ionized 3,5-diamino-1,2,4-triazole.

The NR spectrum of the m/z 57 ions displays an abundant survivor ion signal while the peak at m/z 28 represents the base peak, see Fig. 3.6b. As mentioned above, the enhanced intensities of the peaks at m/z 16 and 41 relative to those in the CID spectrum, may result from the dissociation of mass 57 neutrals. The weak CID spectrum of the m/z 57 survivor ions is not significantly

different from the 3ffr CID spectrum of the source generated ions, compare Fig. 3.6c and d. This is compatible with, but does not prove, the proposal that a mixture of ions $\mathbf{d}^{\bullet+}$ and $\mathbf{e}^{\bullet+}$ is generated from the dissociative ionization of 3,5-diamino-1,2,4-triazole.

The 70 eV EI mass spectrum of 4-amino-1,2,4-triazole is dominated by the molecular ion but it also contains a modest fragment ion at m/z 57. The MI spectrum of the molecular ion indicates that this fragment ion is generated by loss of HCN. Considering the structure of the molecular ion, loss of HCN could yield m/z 57 ions of structure $\mathbf{i}^{\bullet+}$ or $\mathbf{g}^{\bullet+}$, ionized N-aminoisodiazirine, as shown below :

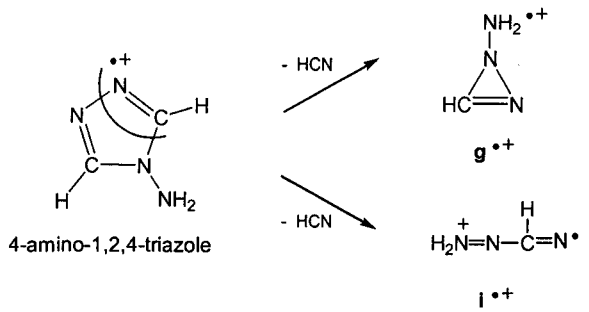

The potential energy diagram of Figure 3.2 indicates that the cyclic ion $\mathbf{g}^{\bullet+}$ is considerably less stable than the ionized biradical $\mathbf{i}^{\bullet+}$. In addition, the barrier for the isomerization $\mathbf{g}^{\bullet+} \rightarrow \mathbf{i}^{\bullet+}$ is very low so that $\mathbf{g}^{\bullet+}$ represents only a very shallow minimum. Therefore, it is most likely that the m/z 57 products ions are ions of structure $\mathbf{i}^{\bullet+}$.

The CID spectrum of the m/z 57 ions of putative structure $\mathbf{i}^{\bullet+}$ is presented in Figure 3.7a. The base peak at m/z 28, which corresponds with the formation of $HCNH^+$ ions by loss of N_2 and $H^{\bullet}$, is not of structure diagnostic value. However, compared with the spectra of the isomers $\mathbf{c}^{\bullet+}/\mathbf{d}^{\bullet+}/\mathbf{e}^{\bullet+}$, the spectrum shows two characteristic differences. First, it contains a unique peak at m/z 43. This peak corresponds to the loss of a $N^{\bullet}$ atom and would be compatible with the direct bond cleavage reaction $\mathbf{i}^{\bullet+} \rightarrow H_2N\text{-}N{\equiv}CH^+ + N^{\bullet}$. Secondly, the m/z 30 peak

intensity is greatly enhanced. This, too, can readily be rationalized in terms of the proposed structure : loss of HCN from $\mathbf{i}^{\bullet+}$ would involve either a direct bond cleavage reaction or a fast 1,2-H shift yielding m/z 30 ions of structure $H_2N_2^{\bullet+}$ or $HN{=}NH^{\bullet+}$, respectively.

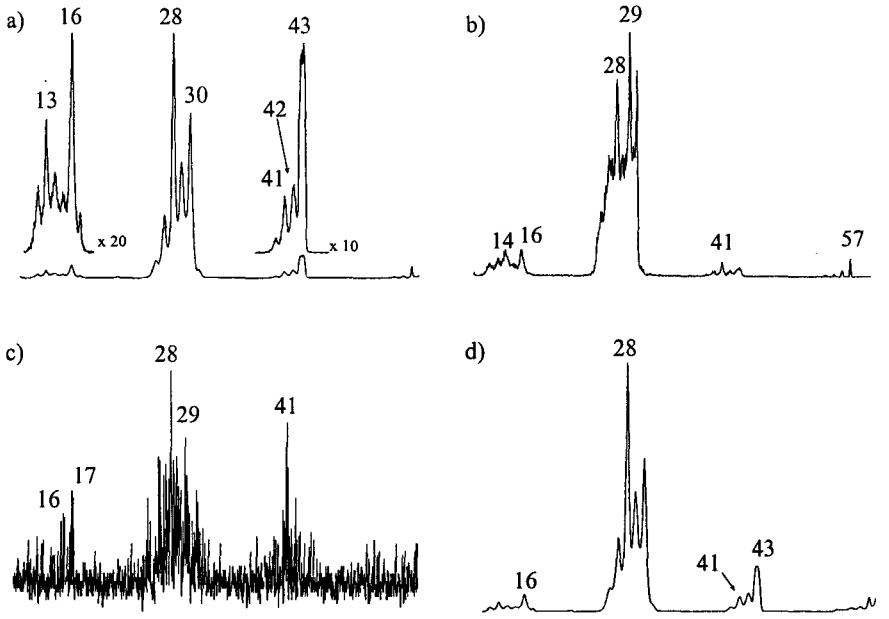

Figure 3.7. a) 2ffr CID spectrum; b) NR spectrum; c) NR/CID spectrum and d) 3ffr CID spectrum of the m/z 57 ions of ionized 4-amino,1,2,4-triazole.

The NR spectrum of the m/z 57 ion of putative structure $\mathbf{i}^{\bullet+}$ is shown in Figure 3.7 b. The spectrum shows only a weak survivor ion signal. This is not surprising, considering that the neutral counterpart of $\mathbf{i}^{\bullet+}$ is a high energy biradical that is prone to dissociate upon neutralization, possibly via $\mathbf{i}^{\bullet+} \rightarrow H_2NN{:} + HCN$. The low intensity of the survivor ion signal leads to a very weak survivor CID spectrum. The high noise level in this spectrum makes it difficult to interpret. However, we note that peaks at m/z 17 ($NH_3^{\bullet+}$) and m/z 41 (CHN_2^+) are clearly present. This would be compatible with the proposal that a small fraction of the high energy neutrals **i** rearrange via a 1,2-H shift into energy rich aminocyanamide neutrals **b**.

Conclusion

The structure, stability and isomerization behaviour of ten isomers of the family of $CH_3N_3^{\bullet+}$ ions was probed using the CBS-QB3 model chemistry. Four of the isomers, *viz.* the aminocarbodiimide ion $\mathbf{c}^{\bullet+}$, the aminonitrilimine ion $\mathbf{d}^{\bullet+}$, the C-aminoisodiazirine ion $\mathbf{e}^{\bullet+}$ and the ionized biradical, $H_2N{=}N\text{-}C(H){=}N^{\bullet+}$ ($\mathbf{i}^{\bullet+}$) were generated and characterized by tandem mass spectrometry as stable species in the gas phase. Analysis of the results of neutralization-reionization experiments leads to the conclusion that the neutral counterparts of $\mathbf{c}^{\bullet+}$ and $\mathbf{e}^{\bullet+}$ are stable and do not rearrange into other isomers. The neutral counterpart of $\mathbf{i}^{\bullet+}$ is not stable and the weak survivor peak in the NR spectrum of $\mathbf{i}^{\bullet+}$ probably results from neutrals **i** that have isomerized into aminocyanamide **b** via a 1,2-H shift. The latter neutral represents the global minimum on the CH_3N_3 potential energy surface.

References

[1] P. Sanchez-Andrada, I. Alkorta, J. Elguero. J. Mol. Struc. (Theochem) 544 (2001) 5.
[2] D. Tahmassebi. J. Chem. Soc., Perkin Trans. 2 (2001) 613.
[3] T. Fuchigami, E. Ichikawa. K. Odo. Bull. Chem. Soc. Japan. 46 (1973) 1765.
[4] M.A. McAlister, T.T.Tidwell. J. Am. Chem. Soc. 114 (1992) 6653
[5] M.W. Wong, C. Wentrup. J. Am. Chem. Soc. 115 (1993) 7743.
[6] (a) J.A. Montgomery Jr., M.J. Frisch, J.W. Ochterski, G.A. Petersson, J. Chem. Phys. 112 (2000) 6532 ; (b) J.A. Montgomery Jr., M.J. Frisch, J.W. Ochterski, G.A. Petersson, J. Chem. Phys. 110 (1999) 2822.
[7] M.J. Frisch, et al. Gaussian 98, Revision A.11.3, GAUSSIAN Inc., Pittsburgh PA, 2002.

Appendix to Chapter 3

Table 3.1. CBS-QB3 (298 K) computational results for the amino-substituted CH_2N_2 system.

Structure			CBS-QB3 (0 K)	ΔH_f (298 K)	E_{rel}
HN=C-N(H)-NH$^{\bullet+}$ (cyclic)	**a**$^{\bullet+}$		-203.39008	305.7	69.7
H_2N-N(H)-C≡N$^{\bullet+}$	**b**$^{\bullet+}$	[a]	-203.45886	263.1	27.1
H_2N-N=C=NH$^{\bullet+}$	**c**$^{\bullet+}$		-203.47960	250.3	14.3
H_2N-C=N=NH$^{\bullet+}$	**d**$^{\bullet+}$		-203.45075	264.4	28.4
H_2N-C=N-NH$^{\bullet+}$ (cyclic)	**e**$^{\bullet+}$		-203.44799	269.2	33.2
H_2N-C(H)-N≡N$^{\bullet+}$	**f**$^{\bullet+}$	[a]	-203.50148	236.0	0
H_2N-N-N=CH$^{\bullet+}$ (cyclic)	**g**$^{\bullet+}$	[a]	-203.38895	319.0	83.0
HN=C(H)-N=NH$^{\bullet+}$	**h**$^{\bullet+}$		-203.43979	287.3	51.3
H_2N-N=C(H)=N$^{\bullet+}$	**i**$^{\bullet+}$		-203.41936	299.8	63.8
TS (c to d)$^{\bullet+}$		[a]	-203.39229	316.5	80.5
TS (d to e)$^{\bullet+}$			-203.40271	310.2	74.2
TS (d to f)$^{\bullet+}$		[a]	-203.37352	328.8	92.8
TS (d to h)$^{\bullet+}$		[a]	-203.34464	347.3	111.3
TS (e to a)$^{\bullet+}$			-203.30597	371.0	135.0
HN=C-N(H)-NH (cyclic)	**a**		-203.76142	84.8	20.3
H_2N-N(H)-C≡N	**b**		-203.79455	64.5	0
H_2N-N=C=NH	**c**		-203.78588[f]	70.0	5.5
H_2N-C=N=NH	**d**		-203.75137	91.8	27.3
H_2N-C=N-NH (cyclic)	**e**		-203.75600	85.3	20.8
H_2N-C(H)-N≡N	**f**		-202.86379[g]		
H_2N-N-N=CH (cyclic)	**g**		-203.71892	111.9	47.4
TS (c to d)			-203.69769	124.7	60.2
$H_2NCH^{\bullet+}$	m/z 29		-94.10577	247.1	
N_2H^+		[e]		247.5	
$HCNH^+$	m/z 28		-93.55430	226.4	
$HNCN^{\bullet}$			-147.91569	76.2	
$HCNH^{\bullet}$			-93.81453	65.5	
$NH_2^{\bullet}$			-55.79117	45.0	
$H^{\bullet}$			-0.49982	52.1	

[a] Spin contamination occurs in the CBS-QB3 calculation beyond the acceptable range.
[b] CBS-QB3 (0 K) values in Hartrees; ΔH_f (298 K) values in kcal/mol.
[c] From R. Butt and J. Dannacher, Int. J. Mass Spectrom. Ion Process. 62 (1984) 1.
[d] M. Zhang, C. Wesdemiotis, M. Marchetti, P.O. Danis, J.C. Ray, B.K. Carpenter and F.W. McLafferty, J. Am. Chem. Soc. 111 (1989) 8341.
[e] S.G. Lias, J.E. Bartmess, J.F. Liebman, J.L. Holmes, R.O. Levin, W.G. Mallard, J. Phys. Chem. Ref. Data 17 (1988) Supplement 1
[f] Ref. 2. E^*_{total} from B3LYP/6-311+G(2d,p)//HF/6-31+G(d) level of theory is –204.114087.
[g] Ref. 4. E^*_{total} from HF/6-31+G*//HF/6-31G* level of theory.

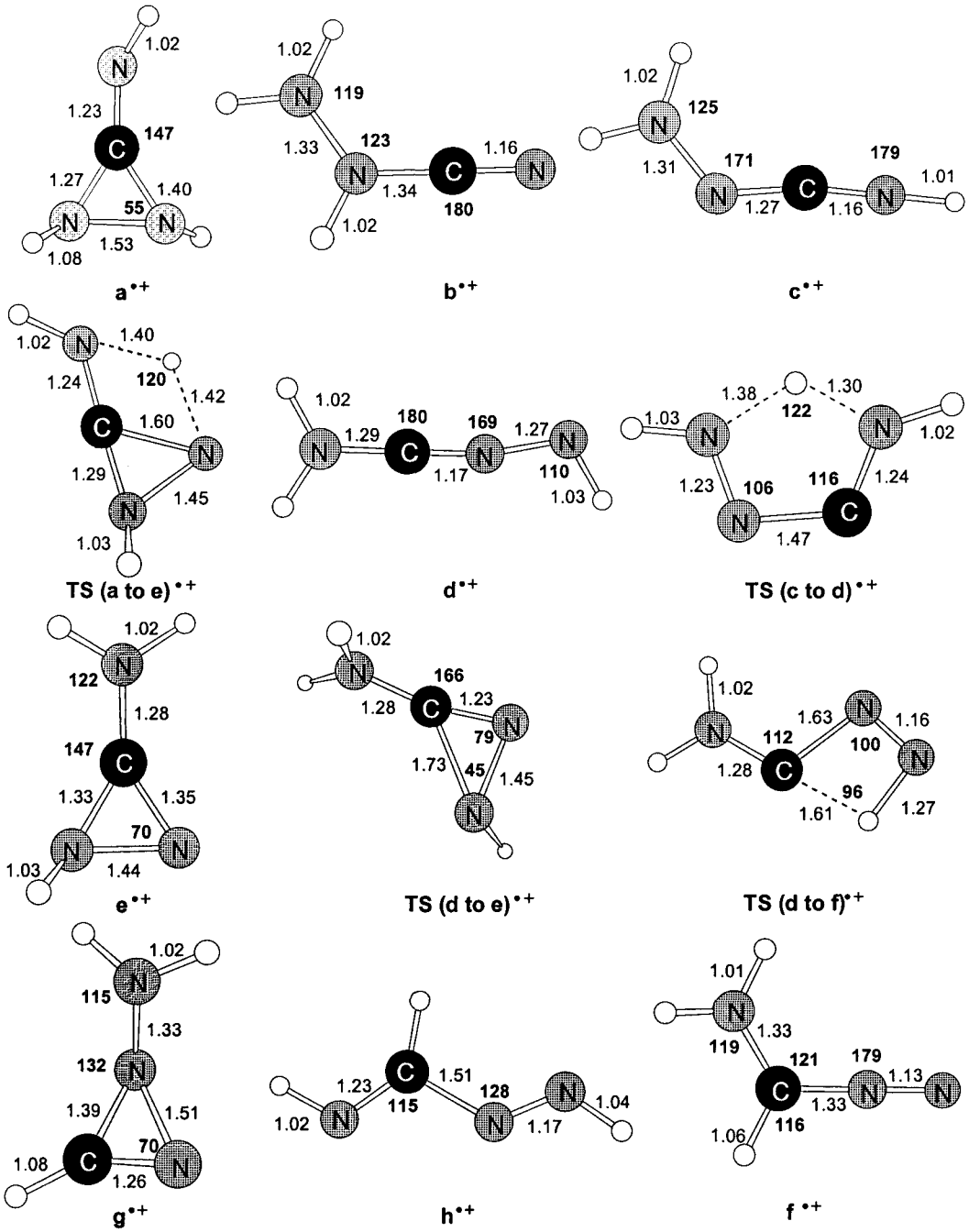

Figure A3.1. Selected optimized geometries for the $CH_3N_3^{\bullet+}$ ions and various transition states. Bond angles in degrees and bond lengths in Angstroms.

Chapter 4

Hydrogen-shift isomers of ionic and neutral N-containing heterocycles : a tandem mass spectrometry and computational study

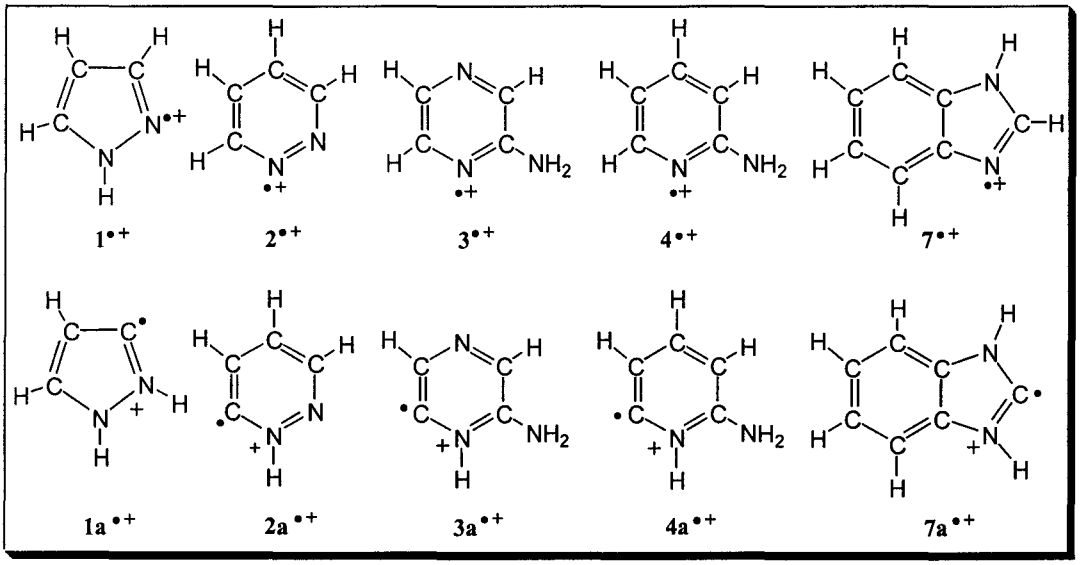

This Chapter describes the generation and characterization of the α-distonic ions of the ionized heterocyclic molecules shown in the Scheme above. The α-distonic ions were generated by dissociative ionization of suitable precursor molecules and identified as stable species in the gas phase through the use of tandem mass spectrometry. Neutralization-reionization experiments further show that their neutral counterparts are also stable species. Our CBS-QB3 derived calculations predict that these α-distonic ions are all higher in energy than their conventional counterparts and thus these systems appear to be less attractive to study molecule-assisted isomerization reactions (proton transport catalysis).

Introduction

The study of N-heterocyclic compounds in the gas phase has been an increasing research topic in the chemistry field mainly because of the biological importance of these types of compounds. Many biologically important species containing pyrazole, pyridazine, aminopyrazine and aminopyridine moieties are used as cancer therapy drugs, antioxidants and anticonvulsants [1-3]. As a consequence, numerous experimental and theoretical studies have been reported dealing with various physical and chemical properties of pyrazole, pyridazine, pyridine and their derivatives [4-6].

The study of these types of cyclic nitrogen-containing compounds in the gas phase has been extended to include not only ions of conventional structure but also their 1,2-hydrogen shift isomers. The 1,2-hydrogen shift isomers of ionized or neutral heterocycles such as pyridine [7], pyrazine [8], pyrimidine [9], imidazole [10] and thiazole [11] have been generated and characterized as being stable species in the gas phase by a combination of collision-induced dissociation (CID) and neutralization-reionization (NR) mass spectrometry.

We wanted to extend the study to see if the distonic ions of several other N-containing heterocyclic compounds, namely, pyrazole, pyridazine, aminopyrazine, aminopyridine and benzimidazole, can be identified as stable species in the gas phase. To do this we use sophisticated mass spectrometric techniques such as neutralization-reionization (NR) and collision induced dissociation (CID). Through computational analysis, we wanted to determine if these distonic ions are more stable than their conventional isomers, possibly allowing us to investigate the catalyzed isomerization of the isomeric ions via a mechanism termed proton-transport catalysis (PTC) as was done by our group on the pyridine system [12].

Experimental and Theoretical Methods

The mass spectrometric experiments were performed on the VG Analytical ZAB-R mass spectrometer of BEE geometry (E = electric sector, B = magnet).

Metastable ion mass spectra were recorded in the second field free region (2ffr); collision-induced dissociation mass spectra were recorded in the 2 and 3ffr using oxygen as collision gas. The CID mass spectra of the 2ffr metastable or collision-induced peaks were obtained in the 3ffr using O_2 as collision gas. For these experiments an accelerating voltage of 8 kV was used unless otherwise noted. CID spectra of reference ions having a translational energy close to that of product ions resulting from (MI or CID) dissociations in the 2ffr, were also obtained in the 3ffr. Neutralization-Reionization mass spectra were recorded using N,N-dimethylaniline as the reducing agent and oxygen gas for reionization. All spectra were recorded using a small PC-based data system developed by Mommers Technologies Inc. (Ottawa).

All samples, with the exception of pyrazole and pyridazine, were introduced into the mass spectrometer via a direct insertion-type solid probe equipped with a probe tube in which the sample is packed. Pyrazole and pyridazine were introduced via a direct insertion-type quartz probe fitted with a glass bulb. At indicated pressures (monitored by a remote ionization gauge) of typically 10^{-6} to 10^{-7} Torr, ions were formed by electron ionization.

Pyrazole, pyridine, aminopyrazine, 3-aminopyrazine-2-carboxylic acid **VI**, aminopyridine and benzimidazole were obtained from Aldrich. Pyrazole-3(5)-carboxylic acid **I**, methylpyrazole-3(5)-carboxylate **II**, pyridazine-3(6)-carboxylic acid **III**, 2-hydroxymethylpyridazine **IV**, methylpyridazine-3(6)-carboxylate **V**, methyl-2-aminopyridine-6-carboxylate **VII**, methyl-2-acetamidopyridine-6-carboxylate **VIII**, 2-acetamidopyridine **IX**, 3-acetamidopyridine **X**, 4-acetamidopyridine **XI**, methylbenzimidazole-2-carboxylate **XII**, benzimidazole-2-carboxylic acid **XIII** and 2-hydroxymethylbenzimidazole **XIV** were synthesized

by Thanasi Karapanayiotis and Dr. R.D. Bowen (University of Bradford, UK) in the context of a collaborative research project.

Structures and energies of the ions and neutrals, connecting transition states and dissociation products pertinent to this study, were probed by the standard CBS-QB3 model chemistry [13]. The calculations were performed using Gaussian 98 Revision A11.3 [14]. The calculated energies are presented in Tables 4.1 - 4.5 (see Appendix) and the potential energy diagrams of Figures 4.2 and 4.4. In the Appendix, Figures A4.1 - A4.5 show the optimized geometries of several ions and their isomers studied in this Chapter. Frequency calculations gave the correct number of negative eigenvalues for all minima and transition states and the spin contamination was within the acceptable range (any exceptions are noted in the Tables). The connections of the transition states have been checked by geometry optimizations and frequency calculations.

Results and Discussion

1. Pyrazole

From our CBS-QB3 derived calculations, it is observed that the α-distonic ion of pyrazole $\mathbf{1a}^{\bullet+}$ is less stable than its conventional isomer pyrazole $\mathbf{1}^{\bullet+}$ by 12 kcal/mol (Table 4.1, Figure 4.1). This value agrees remarkably well with that found by Flammang and co-workers [15] using (U)B3LYP/6-311++G(d,p) + ZPE calculations. From Figure 4.1, it follows that an energy barrier of 59 kcal/mol separates the isomeric ions. This barrier for isomerization was reported by Flammang and his team to be 58 kcal/mol [15].

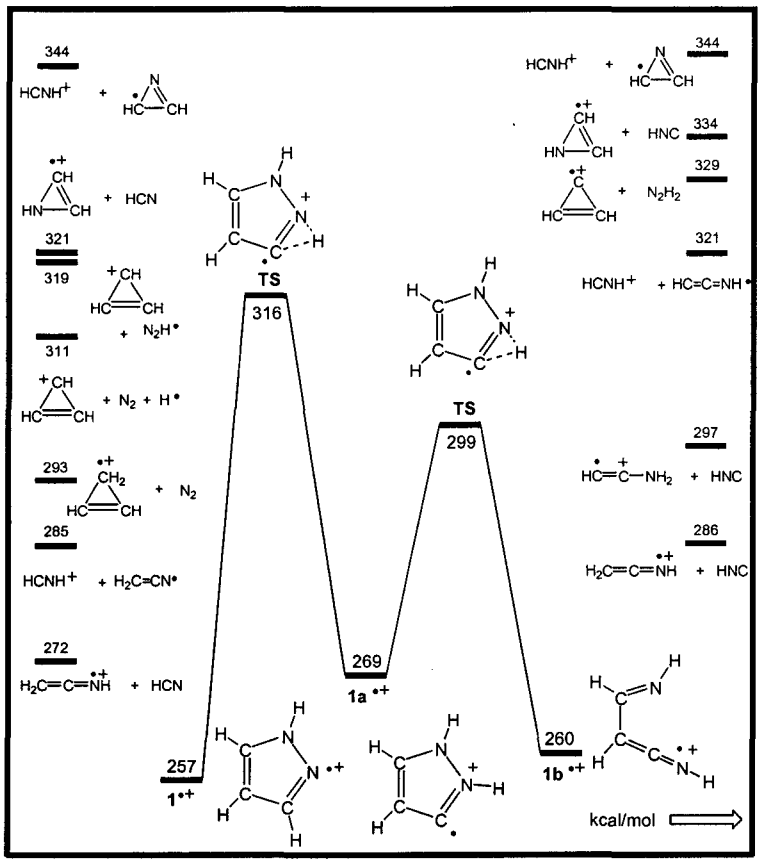

Figure 4.1. Potential energy diagram of the CBS-QB3 (298K) calculations for pyrazole, its isomers and their respective dissociation products.

The 70 eV electron impact (EI) mass spectrum of pyrazole-3(5)-carboxylic acid **I** shows a prominent peak at m/z 68 which is proposed to be α-distonic (ylid) ion, pyrazole-3-ylidene $\mathbf{1a}^{\bullet+}$, generated by the decarboxylation of **I** via a 1,4-H shift reaction :

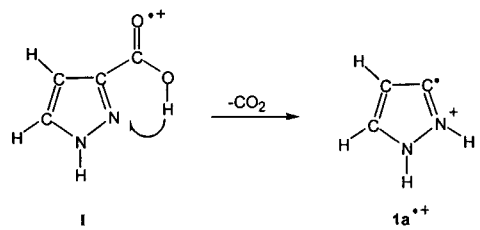

I $\qquad$ $\mathbf{1a}^{\bullet+}$

Electron impact ionization of methyl pyrazole-3(5)-carboxylate **II** also yields m/z 68 ions, proposed to have the ylid ion structure $\mathbf{1a}^{\bullet+}$, by consecutive losses of CH_2=O and CO, shown below:

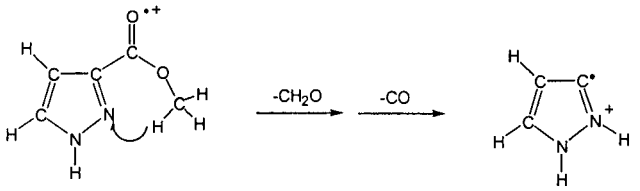

II $1a^{\bullet+}$

Pyrazole ions $\mathbf{1}^{\bullet+}$ are generated from 70eV electron impact ionization of the neutral molecule. The metastable ion spectra of ions $\mathbf{1}^{\bullet+}$ and $\mathbf{1a}^{\bullet+}$ show four metastable dissociations: loss of a $H^{\bullet}$ radical (m/z 67), loss of HCN (m/z 41), loss of N_2 (m/z 40) and formation of $HCNH^+$ ions (m/z 28), see Fig. 4.2a and b. The base peak in the MI of pyrazole lies at m/z 41 indicating that the [H,C,N] elimination is the reaction of lowest energy requirement. The potential energy diagram, shown in Figure 4.1, shows that the loss of HCN lies considerably higher than the loss of HNC and suggests that the pyrazole ions must isomerize into the α-distonic isomer before dissociating to give ions at m/z 41, whereas, the MI spectrum of pyrazole-2-ylidene $\mathbf{1a}^{\bullet+}$ is dominated by a $H^{\bullet}$ radical loss (base peak) followed by loss of HNC.

The CID mass spectra of the $\mathbf{1a}^{\bullet+}$ ions at m/z 68 from both precursors (**I** and **II**) were obtained and found to be nearly identical, see Fig. 4.2d. The CID spectrum of the $\mathbf{1a}^{\bullet+}$ ions clearly shows important differences when compared to the CID spectrum of ionized pyrazole $\mathbf{1}^{\bullet+}$ (Fig. 4.2c). Although both CID spectra show the loss of N_2 as the base peak, the small differences allow for differentiation of the α-distonic isomer from the conventional radical cation. The potential energy diagram shows that pyrazole-2-ylidene $\mathbf{1a}^{\bullet+}$ must rearrange into its conventional isomer, pyrazole $\mathbf{1}^{\bullet+}$, prior to loss of N_2 to give $C_3H_4^{\bullet+}$ ions at m/z 40.

The m/z 41 peaks in the CID spectra of ions $\mathbf{1}^{\bullet+}$ and $\mathbf{1a}^{\bullet+}$ seem to be of equal intensity and may well correspond to an [H,C,N] elimination. From the calculations, in the collision-induced dissociation process, it is expected (and

seems reasonable) that ions $\mathbf{1a}^{\bullet+}$ lose only HNC ions since this dissociation reaction lies much lower in energy than the reaction for the HCN loss. In contrast,

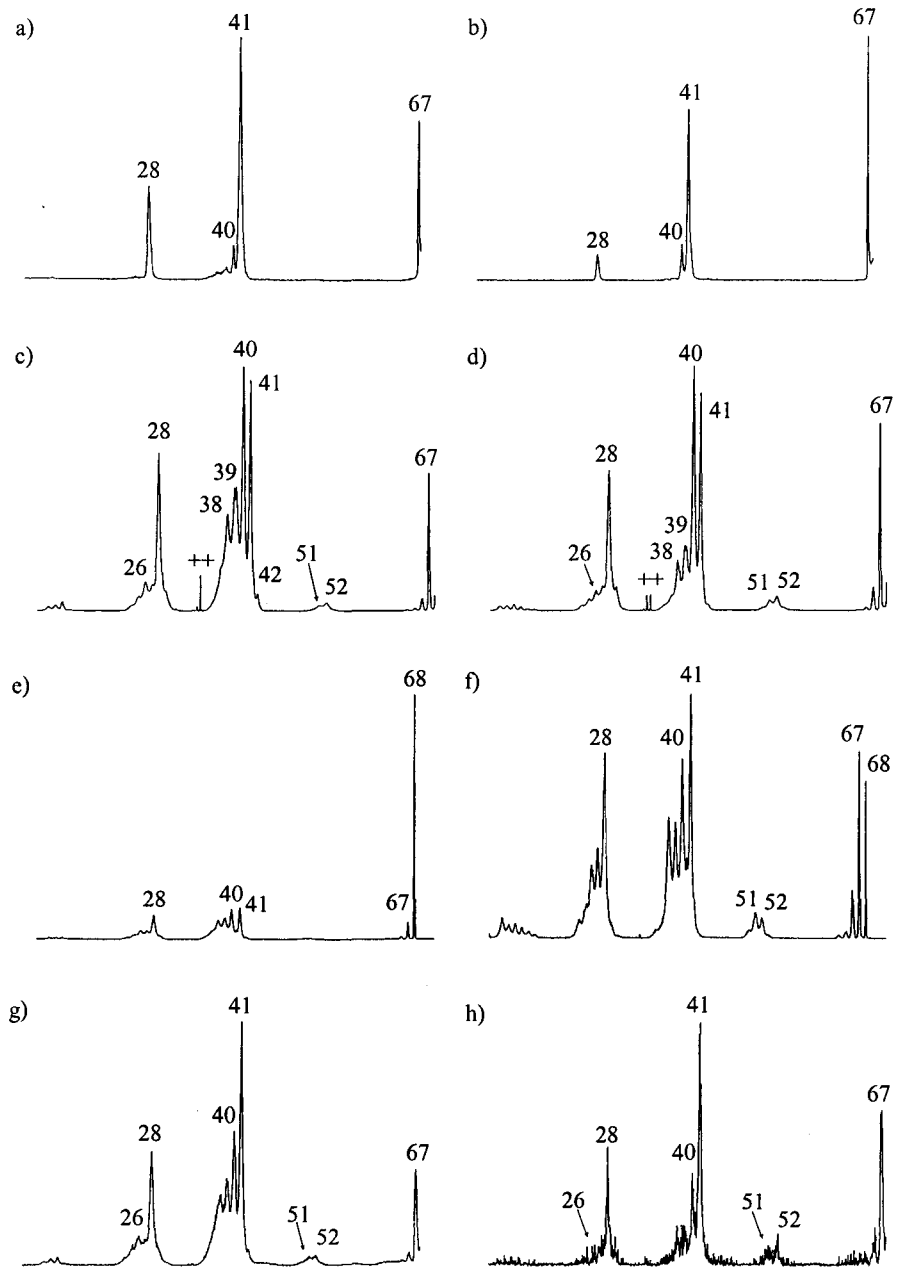

Figure 4.2. MI spectra of a) pyrazole ion $\mathbf{1}^{\bullet+}$ and b) the ylid ion of pyrazole $\mathbf{1a}^{\bullet+}$; CID spectra of c) $\mathbf{1}^{\bullet+}$ and d) $\mathbf{1a}^{\bullet+}$; NR spectra of e) $\mathbf{1}^{\bullet+}$ and f) $\mathbf{1a}^{\bullet+}$; NR/CID spectra of g) $\mathbf{1}^{\bullet+}$ and h) $\mathbf{1a}^{\bullet+}$.

ions $\mathbf{1}^{\bullet+}$ can in principle lose both HNC and HCN in a mixture since the dissociation reaction for loss of HCN lies about 5 kcal/mol higher in energy than the isomerization barrier of $\mathbf{1}^{\bullet+} \rightarrow \mathbf{1a}^{\bullet+}$. In this context, it should be noted that a PEPICO study [16] indicates that low energy (metastable) pyrazole ions lose HCN, at an energy which is very close to the calculated transition state of $\mathbf{1}^{\bullet+} \rightarrow \mathbf{1a}^{\bullet+}$. The CID spectrum of pyrazole shows a more pronounced loss of C_2H_2 to give ions at m/z 42.

The signal at m/z 39 seen in the CID spectrum may be attributed to the formation of cyclic $C_3H_3^+$ cations by loss of $N_2H^{\bullet}$ or N_2 and $H^{\bullet}$. For ionized pyrazole $\mathbf{1}^{\bullet+}$, this loss occurs via a direct bond cleavage mechanism whereas the ylid ions $\mathbf{1a}^{\bullet+}$ must undergo a 1,2-H shift rearrangement before dissociating, i.e. isomerize into pyrazole ions. This may explain why this signal is more prevalent in the CID spectrum of pyrazole. In the CID of pyrazole, it is observed that the signal at m/z 38 is more intense relative to the base peak as compared to the CID of $\mathbf{1a}^{\bullet+}$ and corresponds to the loss of N_2H_2.

Both isomers produce $HCNH^+$ ions at m/z 28 via a double direct bond cleavage reaction and this signal at m/z 28 is more pronounced in the CID spectrum of $\mathbf{1}^{\bullet+}$. To generate the products of lowest energy requirement, both ions $\mathbf{1}^{\bullet+}$ and $\mathbf{1a}^{\bullet+}$ must undergo a 1,2-H transfer prior to dissociating. Ionized pyrazole $\mathbf{1}^{\bullet+}$ rearranges and dissociates by loss of $H_2C\text{-}CN^{\bullet}$ to give $HCNH^+$ ions at m/z 28, whereas ions $\mathbf{1a}^{\bullet+}$ lose $HC{=}C{=}NH^{\bullet}$ neutrals to form the same ions. The dissociation reaction of $\mathbf{1a}^{\bullet+}$ lies much higher in energy than that of $\mathbf{1}^{\bullet+}$ which may explain the difference in intensity of the m/z 28 peaks in the MI and CID spectra of the two isomeric species.

One other difference is that in the CID of ionized pyrazole, the m/z 26 peak is more intense relative to the signal m/z 27 signal. Loss of NH and $NH_2^{\bullet}$ from $\mathbf{1}^{\bullet+}$ and $\mathbf{1a}^{\bullet+}$ yield ions at m/z 52 and 51, respectively. The signal at m/z 52 is slightly more intense in the CID spectrum of the m/z 68 ions having the α-

distonic ion structure, $\mathbf{1a}^{\bullet+}$, and is indicative of the structural connectivity of pyrazole-2-ylidene in that it contains two NH moieties available for cleavage.

Confident that ions are generated having the proposed ylid ion structure $\mathbf{1a}^{\bullet+}$ through dissociative ionization of **I** and **II**, the stability of the neutrals was probed using neutralization-reionization techniques. Figures 4.2e and f display the NR spectra of $\mathbf{1}^{\bullet+}$ and $\mathbf{1a}^{\bullet+}$. Although quite different from one another, the NR spectra of the isomeric ions show abundant survivor ion signals at m/z 68 providing evidence that both isomers are stable species in the gas phase. From the CBS-QB3 calculations, the neutral conventional isomer **1** is more stable than its neutral ylid **1a** by 50 kcal/mol and these neutrals are separated by an energy barrier of 79 kcal/mol. To confirm that there are no isomeric impurities in the survivor ion signal, CID experiments were performed on these ions in the 3ffr. Upon collisional activation, the survivor ions of $\mathbf{1}^{\bullet+}$ produce a CID spectrum that is similar to the 3ffr CID spectrum confirming three points : these ions do not isomerize upon neutralization, they survive the reionization process and they are stable species in the gas phase, see Fig. 4.2g and h. However, the survivor CID spectrum of the m/z 68 ions generated from **I** and **II** differs significantly from the 3ffr CID spectrum of the source generated ions. This suggests that the survivor ion represents a mixture of isomers. The CBS-QB3 calculations on the neutral system indicate that the ring-opened ylid, **1b**, is much more stable than **1a** and that these neutrals are separated by a barrier of only 10 kcal/mol. This implies that neutrals **1a** and **1b** may interconvert upon neutralization. Thus it is likely that the survivor ions in the NR are in fact a mixture of **1a** and **1b**.

2. Pyridazine

The EI mass spectra show that dissociative electron impact ionization of pyridazine-3(6)-carboxylic acid **III** and 3-hydroxymethylpyridazine **IV** produces ions at m/z 80 by the loss of CO_2 and CH_2=O, respectively. Methyl pyridazine-3(6)-carboxylate **V** undergoes consecutive losses of CH_2=O and CO to generate

ions at m/z 80 in its EI mass spectrum. These losses from **III**, **IV** and **V** result in ions at m/z 80 proposed to have the α-distonic ion structure, $\mathbf{2a}^{\bullet+}$, see Scheme 4.1.

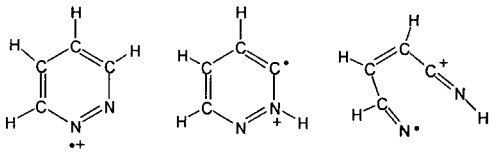

$\mathbf{2}^{\bullet+}$ $\mathbf{2a}^{\bullet+}$ $\mathbf{2b}^{\bullet+}$

Scheme 4.1

To probe the structure of these ions of putative structure $\mathbf{2a}^{\bullet+}$, their MI and CID spectra were obtained and compared with those of the pyridazine radical cation, $\mathbf{2}^{\bullet+}$, produced simply by 70 eV EI of pyridazine. It follows, from the results of Figure 4.3a and b, that the MI spectra are uniquely different. Low energy ions $\mathbf{2}^{\bullet+}$ exclusively lose N_2 to produce $C_4H_4^{\bullet+}$, most probably ionized methylene cyclopropene [17] (from the results presented in Table 4.2, it follows that this is the most stable $C_4H_4^{\bullet+}$ isomer). In contrast, ions $\mathbf{2a}^{\bullet+}$ only lose [C,H,N] to produce m/z 53 ions. Their structure was probed in a double-collision experiment and the resulting CID spectrum was found to be closely similar to that of the $H_2C{=}C{=}C{=}NH^{\bullet+}$ isomer studied by Lavorato et al.[7]. Here, too we are dealing with the most stable isomer of the set, see Table 4.2. The m/z 53 ions formed from $\mathbf{2a}^{\bullet+}$ are proposed to be generated by loss of HCN via the following mechanism:

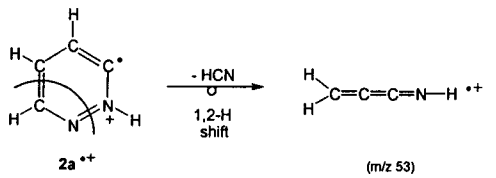

$\mathbf{2a}^{\bullet+}$ (m/z 53)

Figure 2.4, the potential energy diagram for this system of ions, indicates that $\mathbf{2}^{\bullet+}$ and $\mathbf{2a}^{\bullet+}$ are separated by a high barrier for the 1,2-H shift. The associated transition state is clearly higher than that for the loss of N_2 from $\mathbf{2}^{\bullet+}$. The loss of

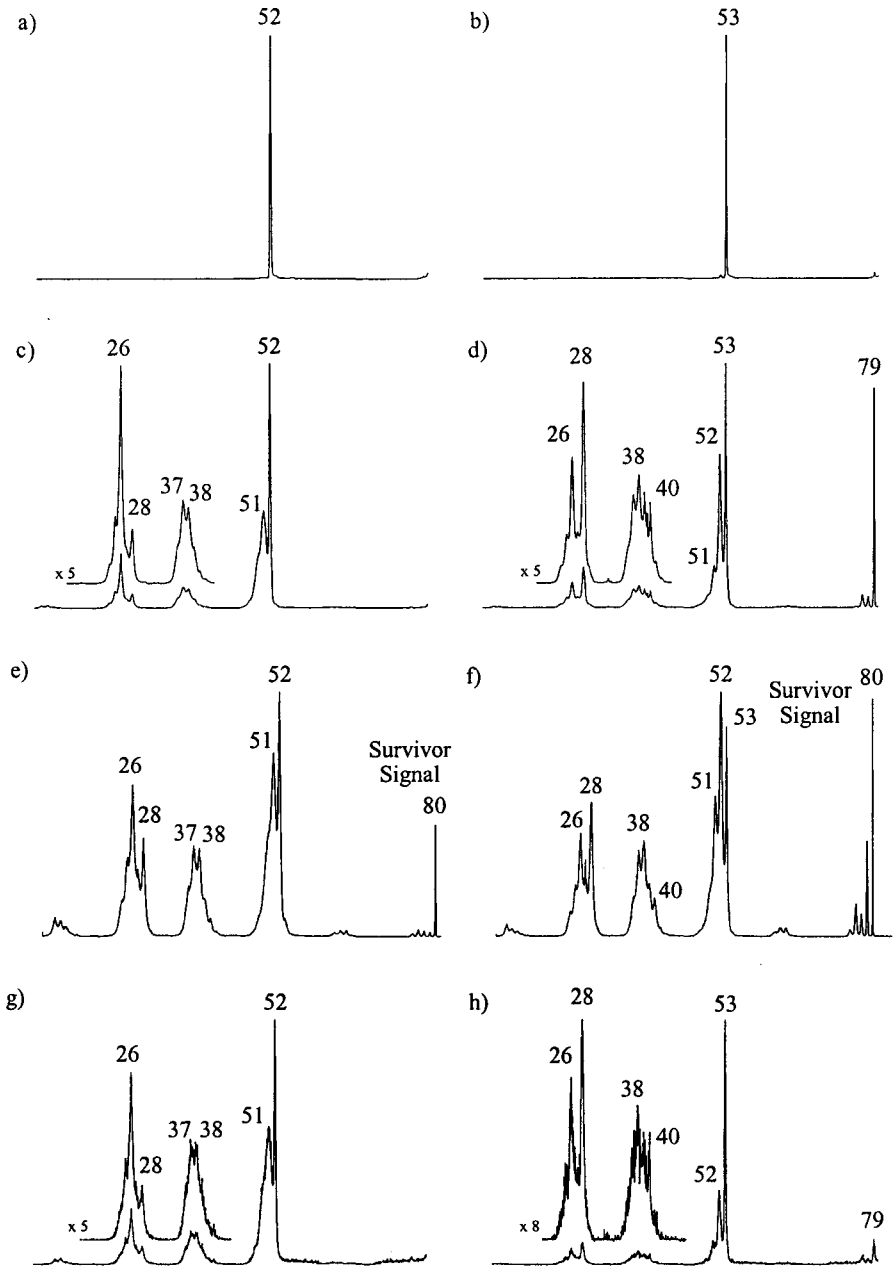

Figure 4.3. MI spectra of a) pyridazine ion $\mathbf{2}^{\bullet+}$ and b) pyridazine-3-ylidene $\mathbf{2a}^{\bullet+}$; CID spectra of c) $\mathbf{2}^{\bullet+}$ and d) $\mathbf{2a}^{\bullet+}$; NR spectra of e) $\mathbf{2}^{\bullet+}$ and f) $\mathbf{2a}^{\bullet+}$; NR/CID spectra of g) $\mathbf{2}^{\bullet+}$ and h) $\mathbf{2a}^{\bullet+}$.

HCN from $\mathbf{2a}^{\bullet+}$ may involve isomerization into the open structure $\mathbf{2b}^{\bullet+}$ via a low lying transition state. The ensuing loss of HCN involves a 1,2-H shift that has not been calculated but which clearly must lie below the TS for the isomerization $\mathbf{2}^{\bullet+} \rightarrow \mathbf{2a}^{\bullet+}$.

In line with the observations on the metastable ions, the CID spectra of $\mathbf{2}^{\bullet+}$ and $\mathbf{2a}^{\bullet+}$ are also characteristically different, see Figure 4.3c and d. Ions $\mathbf{2}^{\bullet+}$ show no loss of HCN, whereas this reaction dominates the CID spectrum of $\mathbf{2a}^{\bullet+}$. The signal at m/z 28 is clearly enhanced in the CID spectrum of $\mathbf{2a}^{\bullet+}$. This indicates that $HCNH^+$ cations are formed in greater abundance from $\mathbf{2a}^{\bullet+}$, in agreement with the proposed connectivity of the ion. The weak signals at m/z 40 and 41 appear in the CID spectrum of $\mathbf{2a}^{\bullet+}$ but not in that of $\mathbf{2}^{\bullet+}$ and correspond to minor processes that yield high energy ions.

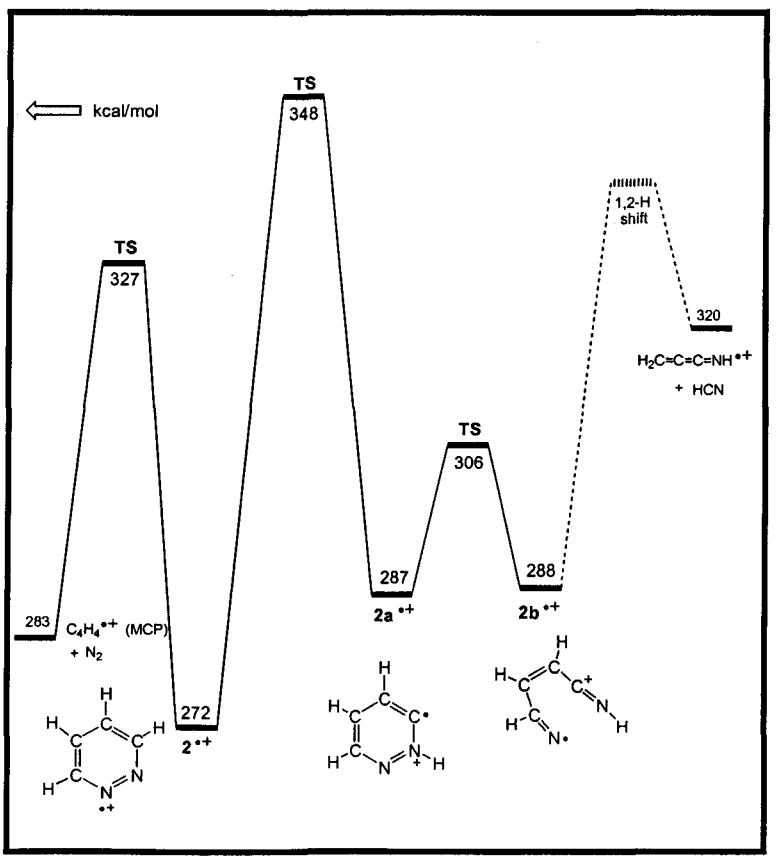

Figure 4.4. Potential energy diagram derived from the CBS-QB3 (298k) calculations of pyridazine and its isomers.

Thus there is little doubt that ions of putative structure $\mathbf{2a}^{\bullet+}$ communicate with $\mathbf{2}^{\bullet+}$ prior to collisional activation. However, ions $\mathbf{2a}^{\bullet+}$ are not necessarily isomerically pure : as discussed above, see Figure 4.4, they may represent a mixture of ions $\mathbf{2a}^{\bullet+}$ and $\mathbf{2b}^{\bullet+}$, the open chain ylid of $\mathbf{2a}^{\bullet+}$.

Next, the technique of neutralization-reionization mass spectrometry was used to generate and characterize the neutral counterparts of the m/z 80 ions of **III**, **IV** and **V**. As pointed out above, the ions may be a mixture of $\mathbf{2a}^{\bullet+}$ and $\mathbf{2b}^{\bullet+}$ and thus a survivor signal could correspond to either **2a** or **2b** or a mixture thereof. However, all attempts to calculate the absolute heat of formation of the open structure of the neutral ylid, **2b**, were unsuccessful as the optimized geometry became a cyclic structure resulting from a ring closure at the two radical sites. Thus theory suggests that ions $\mathbf{2b}^{\bullet+}$ do not have a stable neutral counterpart and leads to the conclusion that the survivor ions may be pure $\mathbf{2a}^{\bullet+}$.

In Figure 4.3f, the neutralization-reionization mass spectra of the m/z 80 ions of pyridazine and of **III**, **IV** and **V** are shown. It is seen that the spectra display intense survivor ions signals. The survivor ions from **III**, **IV** and **V** were subjected to CID and the resulting survivor CID spectra appear to be closely similar to the 3ffr CID spectra of the source generated ions, compare Fig. 4.3f and h. Based on this information, it may be tentatively concluded that the original main beam of ions consists of isomerically pure ions $\mathbf{2a}^{\bullet+}$. The NR spectrum of ions $\mathbf{2}^{\bullet+}$ also shows an abundant survivor ion signal and the NR/CID experiments confirm that the pyridazine neutral does not isomerize upon neutralization, see Fig. 4.3e and g.

3. 2-Aminopyrazine

Generation of the 1,2-hydrogen shift isomer of 2-aminopyrazine, 2-aminopyrazine-3-ylidene, $\mathbf{3a}^{\bullet+}$, may be expected to occur by dissociative ionization (EI) of an appropriately substituted aminopyrazine such as the readily

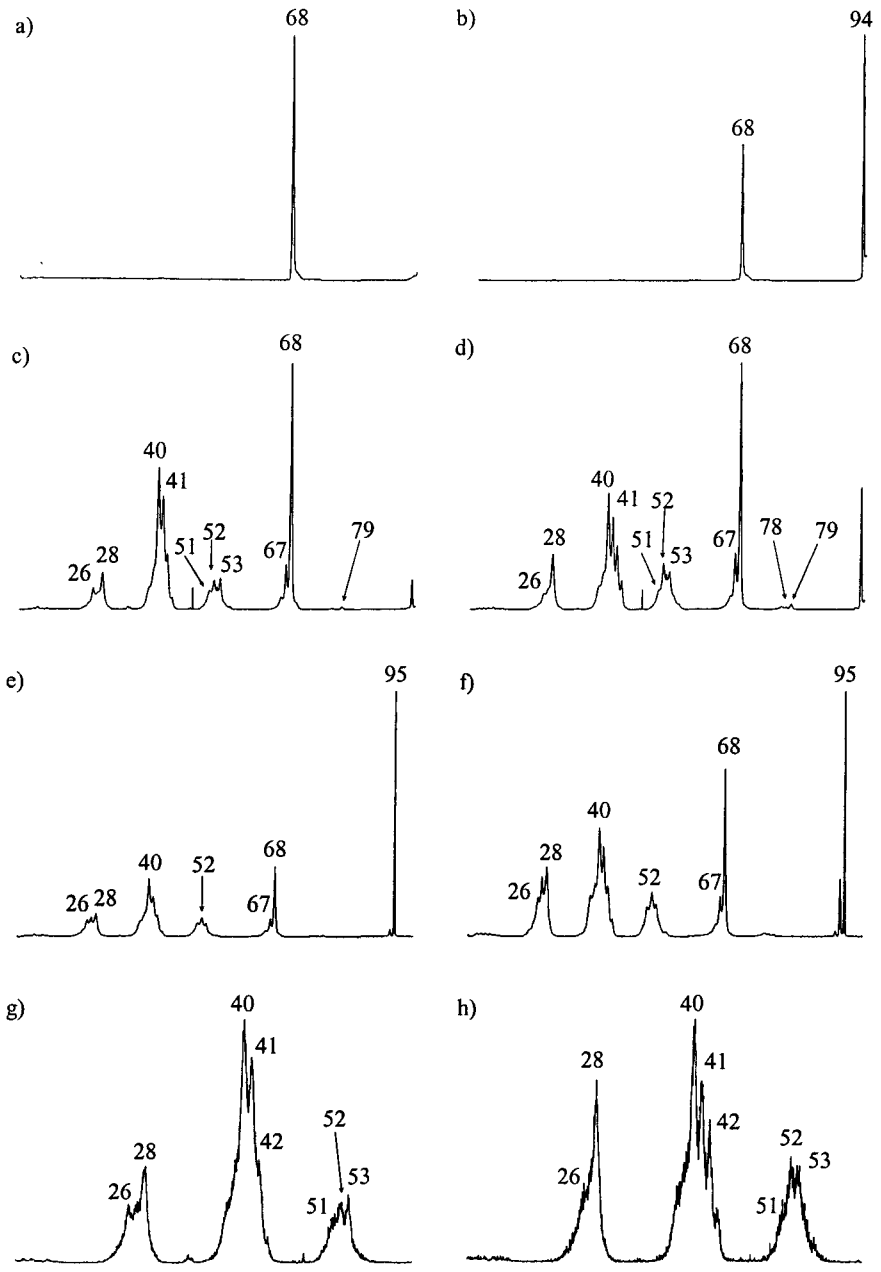

Figure 4.5. MI spectra of a) 2-aminopyrazine ion $\mathbf{3}^{\bullet+}$ and b) 2-aminopyrazine-3-ylidene $\mathbf{3a}^{\bullet+}$; CID spectra of c) $\mathbf{3}^{\bullet+}$ and d) $\mathbf{3a}^{\bullet+}$; NR spectra of e) $\mathbf{3}^{\bullet+}$ and f) $\mathbf{3a}^{\bullet+}$; Partial NR/CID spectra of g) $\mathbf{3}^{\bullet+}$ and h) $\mathbf{3a}^{\bullet+}$.

available 3-aminopyrazine-2-carboxylic acid **VI** (see Scheme 4.2 below), which has a sizeable $C_4H_5N_3^{\bullet+}$ peak at m/z 95 in its EI mass spectrum. 2-Aminopyrazine $\mathbf{3}^{\bullet+}$ shows in its MI spectrum loss of HCN as the only metastable process whereas a $H^{\bullet}$ radical loss dominates the MI spectrum of ion $\mathbf{3a}^{\bullet+}$ in addition to the loss of HNC at m/z 68, see Figure 4.5b.

Scheme 4.2

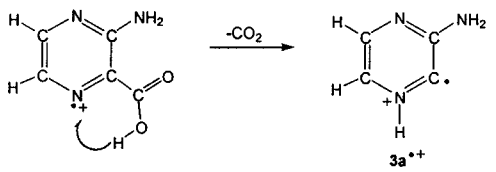

The collision induced dissociation spectrum of the m/z 95 ions obtained according to Scheme 4.2 is compared to that of 2-aminopyrazine radical cations, $\mathbf{3}^{\bullet+}$, which are produced by 70 eV EI of 2-aminopyrazine, see Figure 4.5. The m/z 95 ions generated from the two precursors give rise to reasonably similar spectra in that they both display a [C, H, N] elimination to yield ions at m/z 68. The CID mass spectrum of the m/z 68 ions from 2-aminopyrazine-3-ylidene$^{\bullet+}$ is closely similar to the CID mass spectrum of ionized imidazole. Thus, it seems likely that the ions generated by the loss of HNC from $\mathbf{3a}^{\bullet+}$ are imidazole ions.

The CID mass spectra of $\mathbf{3}^{\bullet+}$ and $\mathbf{3a}^{\bullet+}$ show some subtle differences, see Fig. 4.5c and d. First, the m/z 95 ions expected to have the ylid ion structure produce peaks at m/z 42 and 43 that are much more defined and have greater intensities as compared to the CID of $\mathbf{3}^{\bullet+}$. Secondly, the peak ratio of m/z 26 : 28 is larger (0.6 : 1) in the CID of $\mathbf{3a}^{\bullet+}$ as compared to that in the CID of $\mathbf{3}^{\bullet+}$ (0.3 : 1). Ions $\mathbf{3}^{\bullet+}$ give a more intense peak at m/z 51 relative to the peak at m/z 52 in their CID spectrum and they do not generate a peak at m/z 78 which appears in the CID spectrum of $\mathbf{3a}^{\bullet+}$.

These structure characteristic differences in the collision induced dissociation spectra allow us to differentiate the two isomeric ions. The CBS-QB3

calculations (Table 4.3) show that 2-aminopyrazine-3-ylidene, $\mathbf{3a}^{\bullet+}$, is less stable than the conventional isomer, $\mathbf{3}^{\bullet+}$, by 23 kcal/mol. However, the barrier for isomerization of these two isomers is larger (c. 70 kcal/mol, E_{rel} from B3LYP level of theory) than the dissociation reaction of lowest energy requirement. Thus isomerization of these ions prior to dissociation is not observed.

Confident that the 2-aminopyrazine-3-ylidene ion, $\mathbf{3a}^{\bullet+}$, was generated, we wanted to characterize and determine the stability of the neutral ylid ion and the conventional isomer using neutralization-reionization mass spectrometry. The neutral ylid, **3a**, is a stable species in the gas phase as the NR mass spectrum shows an abundant survivor ion signal at m/z 95 (the base peak), see Fig. 4.5f. Neutral molecules of 2-aminopyrazine, **3**, are also abundantly generated which is apparent by the intense recovery ion signal in the NR spectrum of Fig. 4.5e. The survivor ion signal in the NR experiment indicates that these neutrals survive the NR process and are stable species in the gas phase.

To probe the structure of the survivor ions generated in the NR experiments, we ran CID experiments in the 3ffr. In Figures 4.5g and h, the CID spectra of the survivor ions (m/z 95) of $\mathbf{3}^{\bullet+}$ and $\mathbf{3a}^{\bullet+}$ are closely similar to their respective 3ffr CID spectra confirming that these ions are stable species, in agreement with the CBS-QB3 calculations of Table 4.3. In addition, it is concluded that the **3a** neutrals do not isomerize into the more stable 2-aminopyrazine neutrals **3**.

4. 2-Aminopyridine

The 2-aminopyridine-6-ylidene ion $\mathbf{4a}^{\bullet+}$ is proposed to be generated by dissociative ionization of methyl-2-aminopyridine-6-carboxylate **VII** and methyl-2-acetamidopyridine-6-carboxylate **VIII** as outlined in Scheme 4.3:

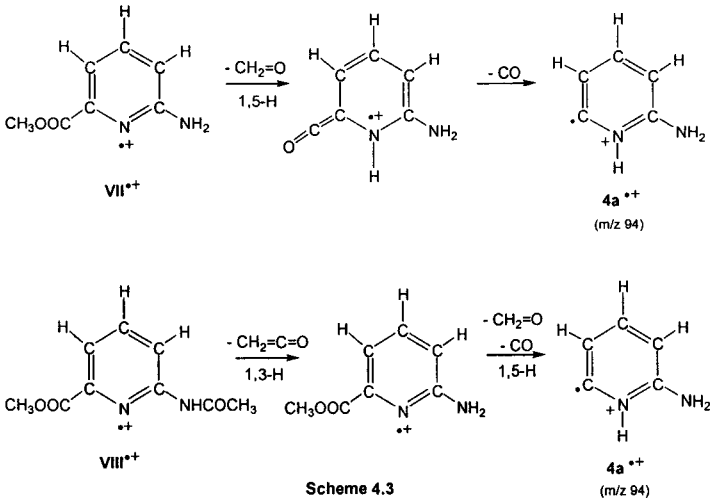

The metastable ion spectrum of the molecular ions of **VII**$^{\bullet+}$ shows the loss of CH_2=O at m/z 122 (base peak) followed by the loss of CO at m/z 94. The MI spectrum of **VIII**$^{\bullet+}$ shows intense signals at m/z 152 (loss of CH_2=C=O) and m/z 94 (subsequent losses of CH_2=O and CO). From the computational analysis, it follows, see Table 4.4, that the ylid ion **4a**$^{\bullet+}$ lies higher in energy than its conventional isomer, 2-aminopyridine **4**$^{\bullet+}$. The isomeric ions are separated by a very high energy barrier of 76 kcal/mol.

The 2-aminopyridine radical cation is generated by electron impact ionization of the neutral molecule and by dissociative ionization of 2-acetamidopyridine **IX** by the following Scheme:

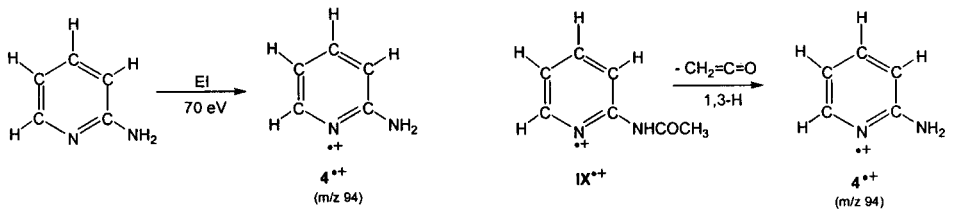

The MI spectrum of the molecular ion of **IX**$^{\bullet+}$ shows a predominant loss of ketene, CH_2=C=O, at m/z 94.

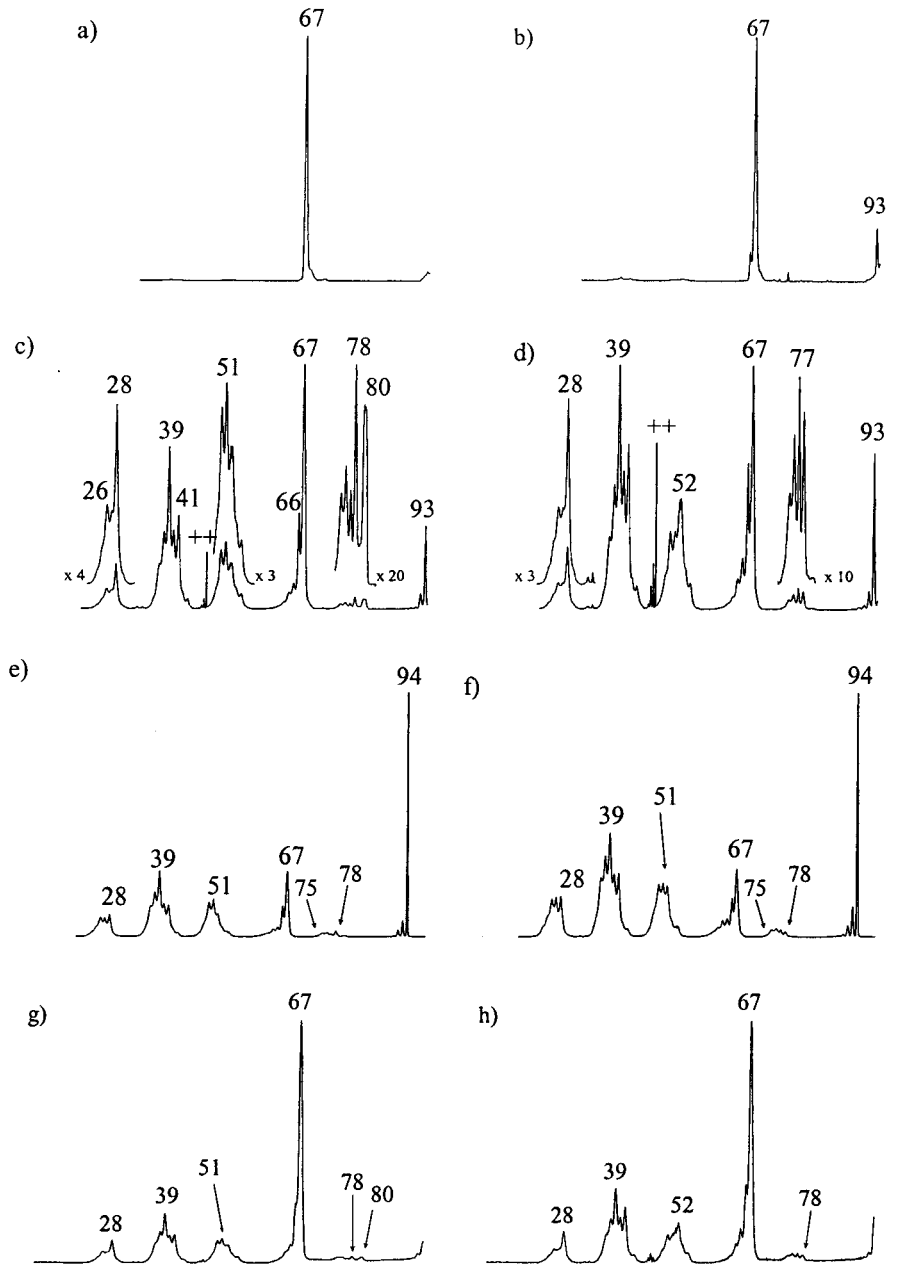

Figure 4.6. MI spectra of a) 2-aminopyridine ion $\mathbf{4}^{\bullet+}$ and b) 2-aminopyridine-6-ylidene ion $\mathbf{4a}^{\bullet+}$; CID spectra of c) $\mathbf{4}^{\bullet+}$ and d) $\mathbf{4a}^{\bullet+}$; NR spectra of e) $\mathbf{4}^{\bullet+}$ and f) $\mathbf{4a}^{\bullet+}$; NR/CID spectra of g) $\mathbf{5}^{\bullet+}$ and h) $\mathbf{4a}^{\bullet+}$.

The metastable ion spectrum of the m/z 94 ions, proposed to have the ylid ion structure $\mathbf{4a}^{\bullet+}$ (from **VII** and **VIII**), shows a predominant loss of HNC (or HCN), in addition to the less pronounced $H^{\bullet}$ and $HCNH^{\bullet}$ radical losses (m/z 93

and 66, respectively), see Figure 4.6b. The MI spectrum of $\mathbf{4}^{\bullet+}$ ions shows the loss of HCN at m/z 67 as the only metastable process, see Fig. 4.6a.

The CID mass spectrum of ions $\mathbf{4a}^{\bullet+}$ shows significant differences from the CID spectrum of $\mathbf{4}^{\bullet+}$ ions, compare Fig. 4.6c and d. The most apparent difference is the peak intensity ratio of the m/z 51 : 52 signal which is larger in the CID of the $\mathbf{4a}^{\bullet+}$ ions. In the higher mass region, the peak at m/z 78 dominates the peak cluster in that region of the CID spectrum of the $\mathbf{4}^{\bullet+}$ ions. Apart from these differences, the spectrum shows a signal at m/z 80 signal ($N^{\bullet}$ loss) which is a tell-tale peak as it does not appear in the CID spectrum of $\mathbf{4a}^{\bullet+}$.

The neutralization-reionization (NR) spectra of $\mathbf{4}^{\bullet+}$ and $\mathbf{4a}^{\bullet+}$ display abundant recovery ion signals at m/z 94 (base peak), see Fig. 4.6e and f. The subsequent CID experiment (NR/CID) performed on both survivor ion signals (Fig. 4.6g and h) are closely similar to their respective 3ffr CID spectra of the source generated ions, suggesting that neither ion $\mathbf{4}^{\bullet+}$ nor $\mathbf{4a}^{\bullet+}$ isomerizes during the NR process and thus the ions retain their structural integrity.

Dissociative ionization of 3-acetamidopyridine **X** also shows the loss of ketene giving ions at m/z 94. The same m/z 94 ions are generated abundantly in the EI mass spectrum of ionized 3-aminopyridine. The MI spectra of the m/z 94 ions of both precursors are closely similar and show a $H^{\bullet}$ loss at m/z 93 and a loss of HCN at m/z 67, see Fig. 4.7a. The structure characteristic CID spectra of the m/z 94 ions (Fig. 4.7) produced by 3-aminopyridine and 3-acetamidopyridine are nearly identical, indicating that ketene loss from **X** generates 3-aminopyridine ions $\mathbf{5}^{\bullet+}$.

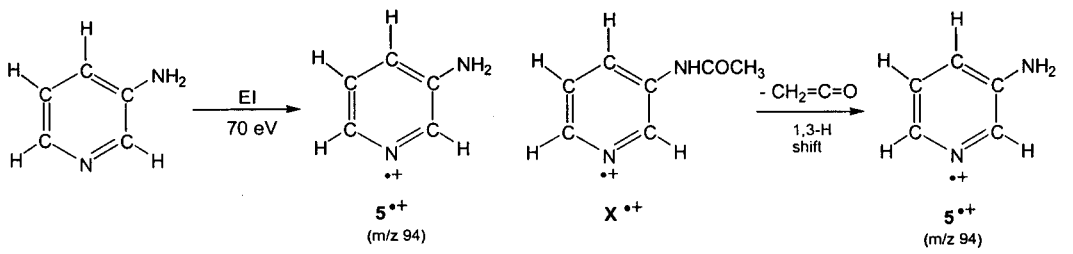

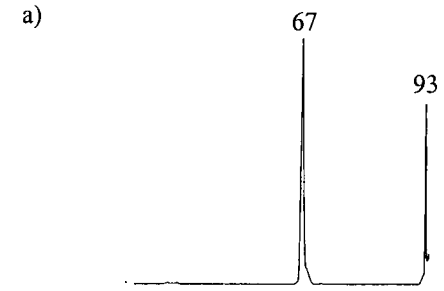

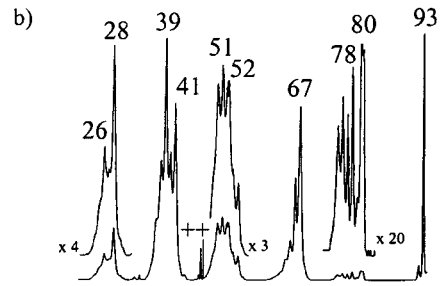

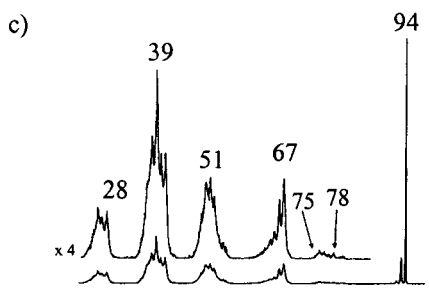

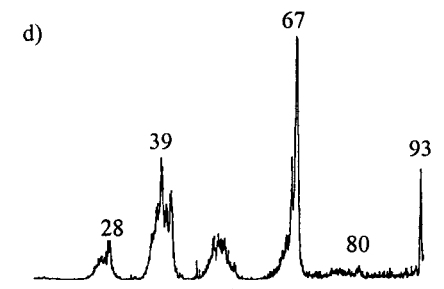

Figure 4.7. a) MI spectrum of 3-amino-pyridine ion $\mathbf{5}^{\bullet+}$; b) CID spectrum of $\mathbf{5}^{\bullet+}$; c) NR spectrum of $\mathbf{5}^{\bullet+}$ and d) NR/CID spectrum of $\mathbf{5}^{\bullet+}$.

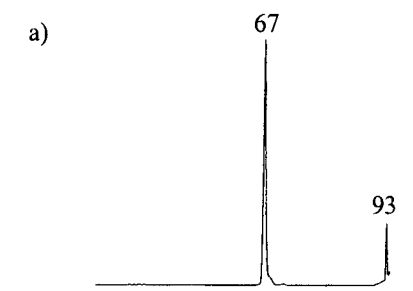

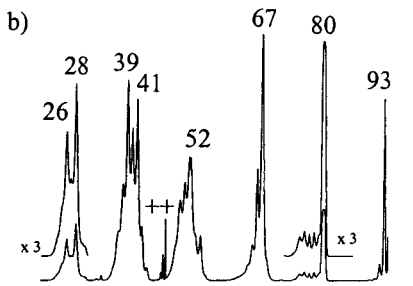

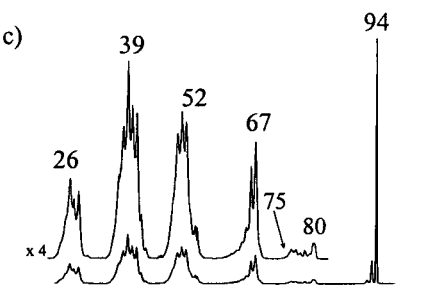

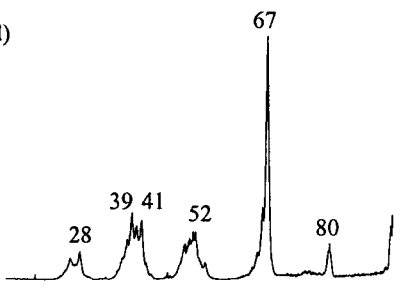

Figure 4.8. a) MI spectrum of 4-amino-pyridine ion $\mathbf{6}^{\bullet+}$; b) CID spectrum of $\mathbf{6}^{\bullet+}$; c) NR spectrum of $\mathbf{6}^{\bullet+}$ and d) NR/CID spectrum of $\mathbf{6}^{\bullet+}$.

Based on their CID spectra, both the ionized ortho (2-) and meta (3-) substituted aminopyridines can be differentiated from the para (4-) substituted aminopyridine. As in the above experiments, the 4-aminopyridine ion is generated directly by electron impact ionization of its neutral counterpart and also by dissociative ionization of 4-acetamidopyridine by the loss of ketene in the following Scheme :

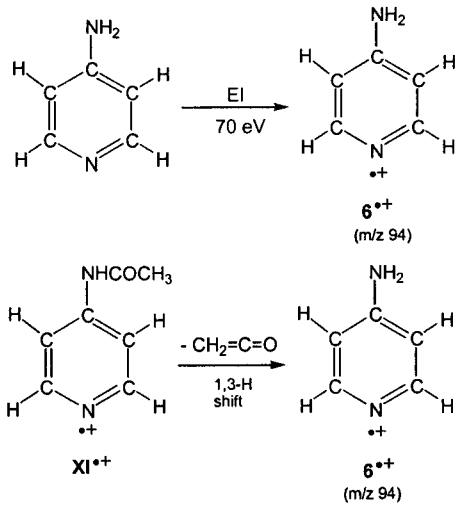

The EI mass spectrum of 4-aminopyridine shows an abundant molecular ion at m/z 94 and is otherwise dominated by a signal at m/z 67 (HCN loss). The EI mass spectrum of 4-acetamidopyridine **XI** shows an intense molecular ion but an even more intense ketene loss to give ions at m/z 94. Both precursors generate m/z 94 ions that have closely similar MI spectra showing an increased loss of HCN at m/z 67, see Figure 4.8a. But more significant is the fact that both CID spectra are nearly identical indicating that the loss of ketene CH_2=C=O from **XI** occurs via 1,3-H shift to generate 4-aminopyridine ions.

The representative CID spectra of the m/z 94 ions of 2- and 3-aminopyridine are characteristically different from the CID spectrum of 4-aminopyridine indicating that these three isomers can be distinguished from one another, see Figures 4.6b, 4.7b and 4.8b. The spectra show that the differences occur in the peak intensity ratio of the m/z 50, 51 and 52 peaks, 26, 27 and 28

peaks and in the high mass region, m/z 75 to 80 peaks. The peak intensity ratio of the m/z 50 : 51 : 52 signals vary in all three spectra. For 2- and 3- aminopyridine, the m/z 51 peak is the most intense and in the para-substituted 4-aminopyridine, the most intense peak in this cluster is the m/z 52 peak. In all three spectra, the m/z 78 ($-NH_2^{\bullet}$) and the m/z 26 peak vary in intensity and another interesting difference is the intensity of the doubly charged ion in all three spectra. One significant difference in these spectra is the shape and intensity of the m/z 80 signal proposed to be the expulsion of a ring nitrogen atom. This peak is very broad and flat-topped in all three CID spectra and is an excellent example of an oxygen effect. The elimination of the ring nitrogen results from using O_2 as the collision gas in the 2ffr collision cell in the CID experiment. When the same experiment is performed using He as the collision gas, there is no observable loss of $N^{\bullet}$ at m/ 80 confirming that the expulsion of $N^{\bullet}$ occurs from using O_2 as a target gas. This type of loss is also observed in the CID spectrum of pyridine N-oxide ions studied by our group [18], in which these ions lose an oxygen atom ($O^{\bullet}$) to give ions at m/z 79.

Moreover, the NR experiments of 2-, 3- and 4-aminopyridine reveal that each neutral isomer is a stable species in the gas phase since each respective NR spectrum shows the survivor ion signal as the base peak, see Fig. 4.6c, 4.7c and 4.8c. The survivor ions generated in these experiments produce upon collisionally induced dissociation, NR/CID spectra (Fig. 4.6d, 4.7d and 4.8d) that are closely similar to each of their respective 3ffr CID spectra providing evidence that each isomer retains its structural integrity (i.e. does not isomerize during the NR process) and confirming that each isomer, 2-, 3- and 4-aminopyridine is stable in the gas phase.

5. Benzimidazole

Benzimidazole radical cations, $\mathbf{7}^{\bullet+}$, generated by 70 eV electron impact ionization of the neutral counterparts, produce a mass spectrum with abundant

molecular ions at m/z 118. This EI mass spectrum is otherwise dominated by a loss of HCN at m/z 91 and other less intense signals at m/z 63 and 64. The α-distonic ion of benzimidazole, benzimidazole-3-ylidene, **7a**$^{\bullet+}$, is proposed to be generated by dissociative ionization of the methyl ester of benzimidazole-2-carboxylic acid **XII** via the following mechanism:

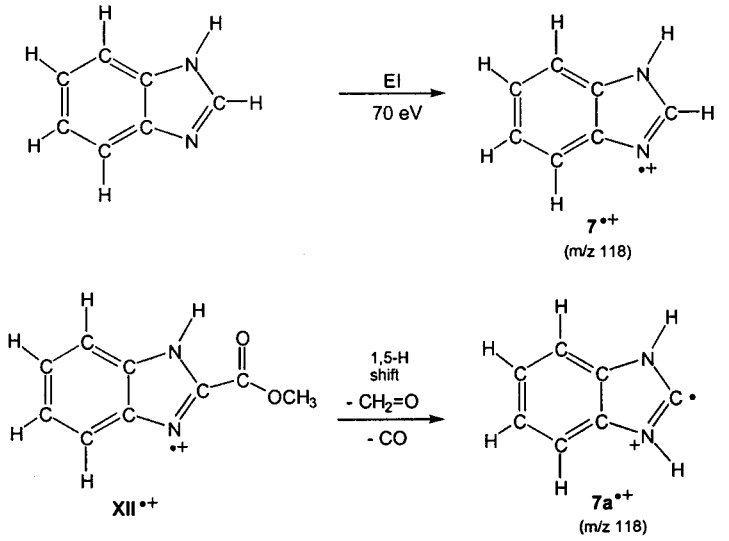

The EI mass spectrum of **XII** shows the m/z 118 peak as the base peak that we expect is the ylid ion **7a**$^{\bullet+}$. Loss of CH_2=O from the molecular ions generates the less intense signal at m/z 146 which is the direct precursor to generate benzimidazole-3-ylidene ions **7a**$^{\bullet+}$ by loss of CO.

The α-distonic ion of benzimidazole, **7a**$^{\bullet+}$, is less stable its conventional isomer, **7**$^{\bullet+}$, by c. 20 kcal/mol and the barrier for isomerization of **7**$^{\bullet+}$ into **7a**$^{\bullet+}$ is considerably higher at 75 kcal/mol (E_{rel} from B3LYP level of theory). Our theoretical calculations predict that the two isomeric ions do not interconvert prior to dissociating.

Collision induced dissociation experiments are used to characterize ions from their distonic isomers based on their structure. Benzimidazole ions selected by the magnet and transmitted into the 2ffr where they enter the collision cell

pressurized with O_2 gas, fragment to give a CID spectrum that is dominated by the loss of a $H^{\bullet}$ radical (m/z 117), loss of HCN (m/z 91), loss of $HCNH^{\bullet}$ (m/z 90) and generate ions at m/z 64 ($C_5H_4^{\bullet+}$) and m/z 63 ($C_5H_3^{+}$).

The CID spectrum of benzimidazole shows distinctive differences from the m/z 118 ions of the methyl-benzimidazole-2-carboxylate **XII**$^{\bullet+}$, see Fig. 4.9c and d.

One obvious difference is the peak intensity ratio of the m/z 63 and m/z 64 peaks. In the CID of the proposed ylid ions **7a**$^{\bullet+}$, both peaks are of equal intensity, however, the m/z 63 peak in the benzimidazole CID spectrum is slightly more intense than the m/z 64 peak. The peaks in the cluster m/z 74 to 78, in the CID of ions **7a**$^{\bullet+}$, decrease in intensity with increasing mass, whereas the peak at m/z 75 dominates the same peak cluster in the CID spectrum of **7**$^{\bullet+}$. In the CID spectrum of the m/z 118 ions of benzimidazole **7**$^{\bullet+}$, the signal at m/z 52 is more intense whereas in the CID of **7a**$^{\bullet+}$, the signal at m/z 50 signal has greater intensity. One other more subtle distinction that is observed is the peak intensity ratio of the m/z 26:28 peaks in both spectra. This ratio is larger in the CID of the α–distonic ion **7a**$^{\bullet+}$ as compared to the same ratio in the benzimidazole **7**$^{\bullet+}$ CID spectrum.

In an attempt to generate the ylid ions via dissociative ionization of the carboxylic acid of benzimidazole, **XIII**$^{\bullet+}$, and the hydroxymethyl derivative, **XIV**$^{\bullet+}$, the attempts were unsuccessful as a result of the suspected thermal decomposition of the neutral carboxylic acid derivative and the fact that the ions of the hydroxymethyl derivative lose formaldehyde to give benzimidazole ions.

The neutralization-reionization experiments prove that **7** and **7a** neutrals are stable species in the gas phase since the recovery signal ('survivor' ion signal) in the NR spectra of ions **7**$^{\bullet+}$ and **7a**$^{\bullet+}$ is the base peak, see Figure 4.9e and f. The survivor CID spectra of **7**$^{\bullet+}$ and **7a**$^{\bullet+}$ (Fig. 4.9g and h) confirms that both neutral isomers are stable species in the gas phase and do not isomerize during the neutralization-reionization process, in agreement with our CBS-QB3 calculations.

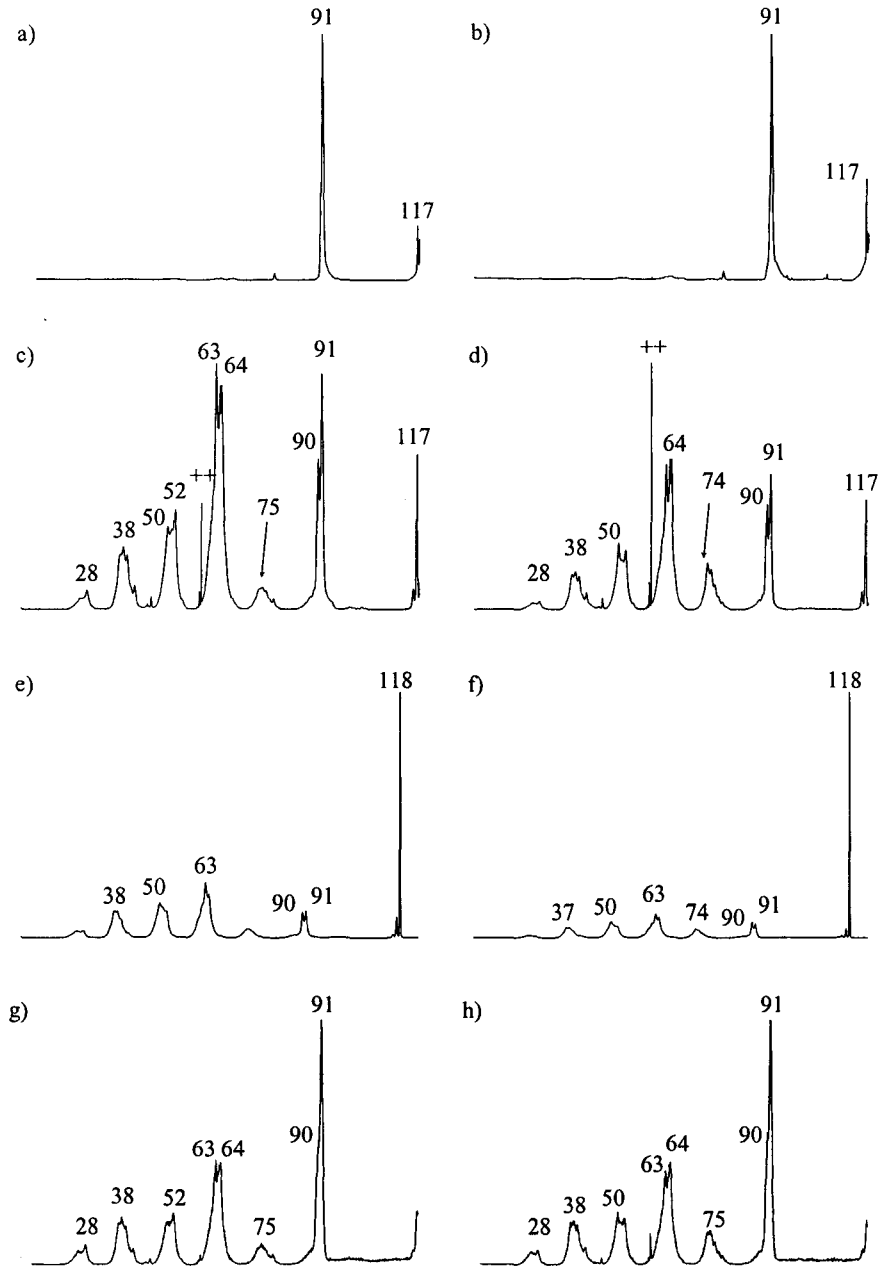

Figure 4.9. MI spectra of a) benzimidazole ion $\mathbf{7}^{\bullet+}$ and b) benzimidazole-2-ylidene ion $\mathbf{7a}^{\bullet+}$; CID spectra of c) $\mathbf{7}^{\bullet+}$ and d) $\mathbf{7a}^{\bullet+}$; NR spectra of e) $\mathbf{7}^{\bullet+}$ and f) $\mathbf{7a}^{\bullet+}$; NR/CID spectra of g) $\mathbf{7}^{\bullet+}$ and h) $\mathbf{7a}^{\bullet+}$.

Neutral benzimidazole **7** is more stable than its neutral ylid **7a** by about 25 kcal/mol and these neutral isomers are separated by a high energy isomerization barrier of 100 kcal/mol concluding that the neutrals **7** and **7a** do not interconvert upon neutralization.

Conclusion

The α-distonic ions of several heterocyclic nitrogen-containing compounds can be differentiated by their conventional isomers through the use of collision induced dissociation mass spectrometry. From neutralization-reionization experiments on the ylid ions and their conventional isomers, it follows that the ylid ions have stable neutral counterparts, as predicted by the theoretical calculations.

The CBS-QB3 calculations show that the ylid ions of the molecules studied in this Chapter are slightly less stable than their conventional counterparts. This makes it difficult to study proton transport catalysis in these systems of ions because the substrate ylid ions cannot be generated by direct ionization.

References

[1] P.G. Baraldi, G. Balboni, M.G. Pavani, G. Spalluto, M.A. Tabrizi, E. De Clercq, J. Balzarini, T. Bando, H. Sugiyama, R. Romagnoli. J. Med. Chem. 44 (2001) 2536.

[2] I. Devillers, G. Dive, C. De Tollenaere, B. Falmagne, B. de Wergifosse, J-F. Rees, J.Marchand-Brynaert, Bioorg. Med. Chem. Lett. 11 (2001)2305.

[3] D.J. Hogenkamp. PCT Int. Appl. (2001) 31 pp.

[4] a) I. Homsek, I. Kolaric, A. Pejcic, B. Kolaric. (Institute-drug delivery lab, ICN) Book of Abstracts, 219th ACS National Meeting, San Francisco, CA, March 26-30, 2000. (2000), COMP-170; b) M. Moreno-Manas, R.M. Sebastian, A. Vallribera, J.F. Piniella, A. Alvarez-Larena, M.L. Jimeno, J. Elguero. New J. Chem. 25 (2001) 329.

[5] F. Billes. J. Molec. Struct. (Theochem) 579 (2002) 191; b) A. Guven, C. Ogretir. J. Molec. Struct. (Theochem) 427 (1998) 65.

[6] a) B. Brodbeck, B. Pullmann, S. Schmitt, M. Nettekoven. Tetrahedron Letters. 44 (2003) 1675; b) B. Osmialowski, K.Laihia, E. Virtanen, M. Nissinen, E. Kolehmainen, R. Gawinecki. J. Molec. Struct. 654 (2003) 61.

[7] a) D. Lavorato, J.K. Terlouw, G.A. McGibbon, T.K. Dargel, W. Koch, H. Schwarz. Int. J. Mass Spectrom. Ion Process. 179-180 (1998) 7; b) D. Lavorato, J.K. Terlouw, T.K. Dargel, W. Koch, G.A. McGibbon, H. Schwarz. J. Am.Chem. Soc. 118 (1996) 11898.

[8] T.K. Dargel, W. Koch, D. Lavorato, G.A. McGibbon, J.K. Terlouw, H. Schwarz. Int. J. Mass Spectrom. Ion Process. 185-187 (1999) 925.

[9] D.J. Lavorato, J.K.Terlouw, G.A. McGibbon, T.K. Dargel, W. Koch, H. Schwarz. Int. J. Mass Spectrom. 210/211 (2001) 43.
[10] G.A. McGibbon, C. Heinemann, D. Lavorato, H. Schwarz. Angew. Chem., Int. Ed. Engl. 36 (1997) 1478.
[11] G.A. McGibbon, J. Hrusak, D.J. Lavorato, H. Schwarz and J.K. Terlouw. Chemistry – A European Journal. 3 (1997) 232.
[12] M.A. Trikoupis, D.J. Lavorato, J.K. Terlouw, P.J.A. Ruttink, P.C. Burgers. Eur. Mass Spectrom. 5 (1999) 431.
[13] a) J.A. Montgomery Jr., M.J. Frisch, J.W. Ochterski, G.A. Petersson, J. Chem. Phys. 110 (1999) 2822; b) ibid, 112 (2000) 6532.
[14] M.J. Frisch, et al. Gaussian 98, Revision A.11.3, GAUSSIAN Inc., Pittsburgh PA, 2002.
[15] R. Flammang, M. Barbieux-Flammang, H.T. Le, P. Gerbaux, J. Elguero, M.T. Nguyen. Chem. Phys. Lett. 347 (2001) 465.
[16] J. Main-Bobo, S. Olesik, W. Gase, T. Baer, A.A. Mommers, J.L. Holmes. J. Am. Chem. Soc. 108 (1986) 677.
[17] R. Buff and J. Dannacher. Int. J. Mass Spectrom. Ion Process. 62 (1984) 1.
[18] M.A. Trikoupis, P.Gerbaux, D.J. Lavorato, R. Flammang, J.K. Terlouw. Int. J. Mass Spectrom. 217 (2002) 1.
[19] S.G. Lias, J.E. Bartmess, J.F. Liebman, J.L. Holmes, R.O. Levin, W.G. Mallard. J. Phys. Chem. Ref. Data 17 (1988) Supplement 1.

Appendix to Chapter 4

Table 4.1. CBS-QB3 computational results for pyrazole, its isomers and dissociation products.

Structure			CBS-QB3 (0 K)	ΔH_f (298 K)	Exp. [c]	E_{rel}
pyrazole$^{\bullet+}$	**1**$^{\bullet+}$	[a]	-225.48120	257.2	258	0
pyrazole-3-ylidene$^{\bullet+}$	**1a**$^{\bullet+}$	[a]	-225.46209	269.2		12
open chain pyrazole-3-ylidene$^{\bullet+}$	**1b**$^{\bullet+}$	[a]	-225.47903	259.5		2
TS (**1** to **1a**)$^{\bullet+}$			-225.38653	316.2		59
TS (**1a** to **1b**)$^{\bullet+}$		[a]	-225.41423	299.2		42
pyrazole	**1**		-225.82315	42.4	44	0
pyrazole-3-ylidene	**1a**		-255.74427	91.9		50
open chain pyrazole-3-ylidene	**1b**		-225.78227	69.0		27
TS (**1** to **1a**)			-225.69780	121.2		79
TS (**1a** to **1b**)			-225.72759	102.5		60
CH_2=C=NH$^{\bullet+}$	m/z 41				240	
HC=C-$NH_2^{\bullet+}$	m/z 41	[a]	-132.13375	265.2		
HC=C(H)-NH$^{\bullet+}$ (cyclic)	m/z 41		-132.09549	288.8		
$C_3H_4^{\bullet+}$ (cyclic)	m/z 40		-116.02723	292.9	289	
HC=C-NH^+ (cyclic)	m/z 40					
HC=C=NH^+	m/z 40		-131.45990	323.9		
$C_3H_3^+$ (cyclic)	m/z 39		-115.50059	258.9	257	
$C_3H_2^{\bullet+}$ (cyclic)	m/z 38				281	
$HCNH^+$	m/z 28		-93.55430	226.4	226	
H_2C-CN$^{\bullet}$	m = 40				59	
HC=C=NH$^{\bullet}$	m = 40		-131.82460	94.9		
HC-N=CH$^{\bullet}$	m = 40		-131.78845	117.1		
HN-C=CH$^{\bullet}$	m = 40		-131.74833	142.4		
HN=NH (E)	m = 30		-110.48443	48.2	51	
$N_2H^{\bullet}$	m = 29		-109.88581	59.6		
HCNH$^{\bullet}$	m = 28		-93.81453	65.5		
HCN	m = 27		-93.28750	31.7	32.3	
HNC	m = 27		-93.26616	45.5	48	
HC≡CH	m = 26		-77.18740	55.9	54.7	
H$^{\bullet}$			-0.49982	52.1	52.1	

[a] Spin contamination occurs in the CBS-QB3 calculation above the value of 0.825.
[b] CBS-QB3 (0 K) values in Hartrees; ΔH_f (298 K) values in kcal mol^{-1}.
[c] from Ref. 19.

Table 4.2. CBS-QB3 computational results for the pyridazine system.

Structure			CBS-QB3 (0 K)	ΔH_f (298 K)	Exp. [e]	E_{rel}
pyridazine$^{\bullet+}$	**2**$^{\bullet+}$		-263.51456	271.5	(266)	0
pyridazine-3-ylidene$^{\bullet+}$	**2a**$^{\bullet+}$	[a]	-263.49011	286.7		15
open chain pyridazine-3-ylidene$^{\bullet+}$	**2b**$^{\bullet+}$	[a]	-263.48980	288.4		17
pyridazine	**2**		-263.84063	66.8	66.5	
pyridazine-3-ylidene	**2a**		-263.78433	102.2		
TS (2 to 2a)$^{\bullet+}$			-263.39314	347.8		76
TS (2a to 2b)$^{\bullet+}$		[a]	-263.45977	306.3		35
TS (2$^{\bullet+}$ **→ C_4H_4**$^{\bullet+}$ **+ N_2)**		[c]			(327)	
$H_2C{=}C{=}C{=}NH^{\bullet+}$	m/z 53	[a]	-170.16623	280.9		
$HC{=}CH{-}C{=}NH^{\bullet+}$	m/z 53	[a]	-170.15455	287.6		
$H_2C{=}CH{-}C{\equiv}N^{\bullet+}$	m/z 53	[a]	-170.13796	297.9		
$HC{\equiv}C{-}CH{=}NH^{\bullet+}$	m/z 53	[a]	-170.11929	310.1		
$HC{=}CH{-}CH{=}N^{\bullet+}$	m/z 53	[a]	-170.06730	342.7		
cyclobutadiene$^{\bullet+}$	m/z 52	[d]	-154.08685	290.8	296	
methylene cyclopropene$^{\bullet+}$	m/z 52		-154.09989	283.0	(289)	
$H_2C{=}C{=}C{=}CH_2^{\bullet+}$	m/z 52		-154.09057	289.1	(294)	
$H_2C{=}CH{-}C{\equiv}CH^{\bullet+}$	m/z 52	[d]	-154.08526	292.5	294	

Table 4.3. CBS-QB3 computational results for the aminopyrazine system, its isomers and dissociation products.

Structure			CBS-QB3 (0 K)	ΔH_f (298 K)	Exp. [e]	E_{rel}
2-aminopyrazine$^{\bullet+}$	**3**$^{\bullet+}$	[a]	-318.84714	238.8		0
2-aminopyrazine-3-ylidene$^{\bullet+}$	**3a**$^{\bullet+}$	[a]	-318.80947	262.1		23
2-aminopyrazine	**3**		-319.15775	43.3		0
2-aminopyrazine-3-ylidene	**3a**		-319.09503	82.7		39
TS (**3** to **3a**)$^{\bullet+}$			-319.34989[f]			71[f]
imidazole$^{\bullet+}$	m/z 68		-225.51519	235.7	238	

[a] Spin contamination occurs in the CBS-QB3 calculation above the value of 0.825.
[b] CBS-QB3 (0 K) values in Hartrees; ΔH_f (298 K) values in kcal mol^{-1}.
[c] From Ref. 16.
[d] From M. Zhang, C. Wesdemiotis, M. Marcetti, P.O. Danis, J.C. Ray, Jr., B.K. Carpenter, F.W. McLafferty. J. Am. Chem. Soc. 111 (1989) 8341.
[e] from Ref. 19.

[f] E^{*}_{total} and E_{rel} from B3LYP level of theory.

Table 4.4. CBS-QB3 computational results for the aminopyridine system, its isomers and dissociation products.

Structure			CBS-QB3 (0 K)	ΔH_f (298K)	Exp. [c]	E_{rel}
2-aminopyridine$^{\bullet+}$	**4**$^{\bullet+}$	[a]	-302.82185	215.5	(213)	0
2-aminopyridine-6-ylidene$^{\bullet+}$	**4a**$^{\bullet+}$	[a]	-302.78265	236.0		21
TS (4 to 4a)$^{\bullet+}$		[a]	-302.70178	291.1		76
3-aminopyridine$^{\bullet+}$	**5**$^{\bullet+}$	[a]	-302.81192	221.9	(221)	6
4-aminopyridine$^{\bullet+}$	**6**$^{\bullet+}$	[a]	-302.80215	228.0	(225)	13
2-aminopyridine	**4**		-303.11919	29.0	28	0
2-aminopyridine-6-ylidene	**4a**		-303.04206	77.6		49
TS (4 to 4a)			-302.98248	115.1		86
3-aminopyridine	**5**		-303.10977	35.0	34	6
4-aminopyridine	**6**		-303.11341	32.6	31	4

Table 4.5. CBS-QB3 computational results for the benzimidazole system.

Structure			CBS-QB3 (0 K)	ΔH_f (298 K)	E_{rel}
benzimidazole$^{\bullet+}$	**7**$^{\bullet+}$	[a]	-378.89407	240.9	0
benzimidazole-3-ylidene$^{\bullet+}$	**7a**$^{\bullet+}$		-378.86795	257.3	16
TS (7 to 7a)$^{\bullet+}$			-379.54237[d]		75[d]
benzimidazole	**7**		-379.20729	44.1	0
benzimidazole-3-ylidene	**7a**		-379.20024	69.3	25
TS (7 to 7a)			-379.11886	99.5	55

[a] Spin contamination occurs in the CBS-QB3 calculation above the value of 0.825.
[b] CBS-QB3 (0 K) values in Hartrees; ΔH_f (298 K) values in kcal mol^{-1}.
[c] from Ref. 19.
[d] E^{*}_{total} and E_{rel} from B3LYP level of theory.

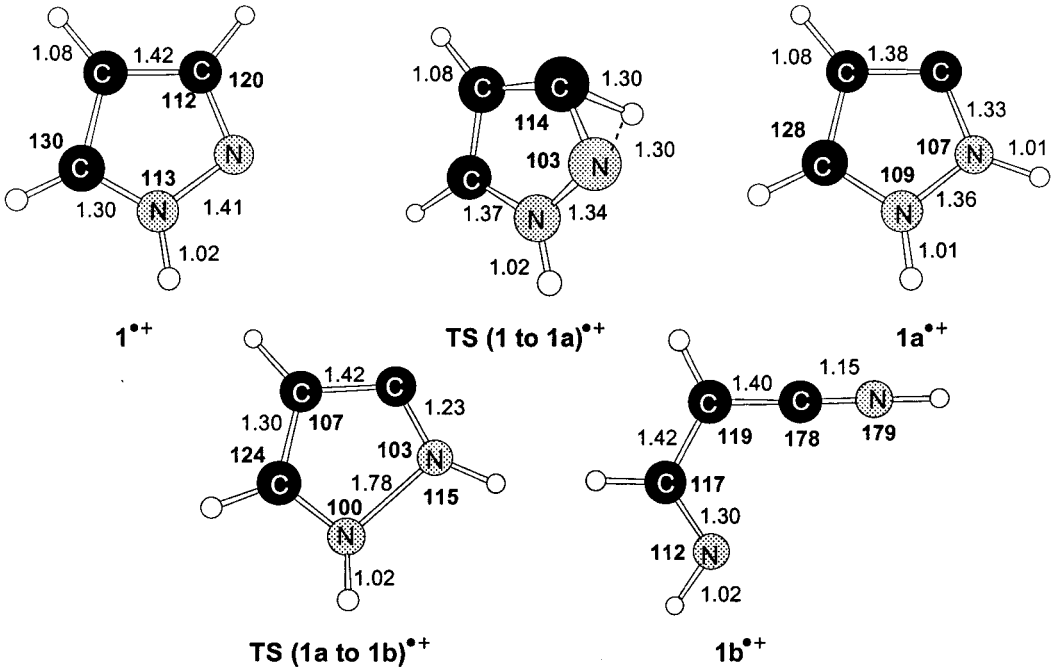

Figure A4.1. Selected optimized geometries of pyrazole and its isomers. Bonds angles in degrees and bond lengths in Angstroms.

Figure A4.2. Selected optimized geometries of pyridazine and its isomers. Bond angles in degrees and bond lengths in Angstroms.

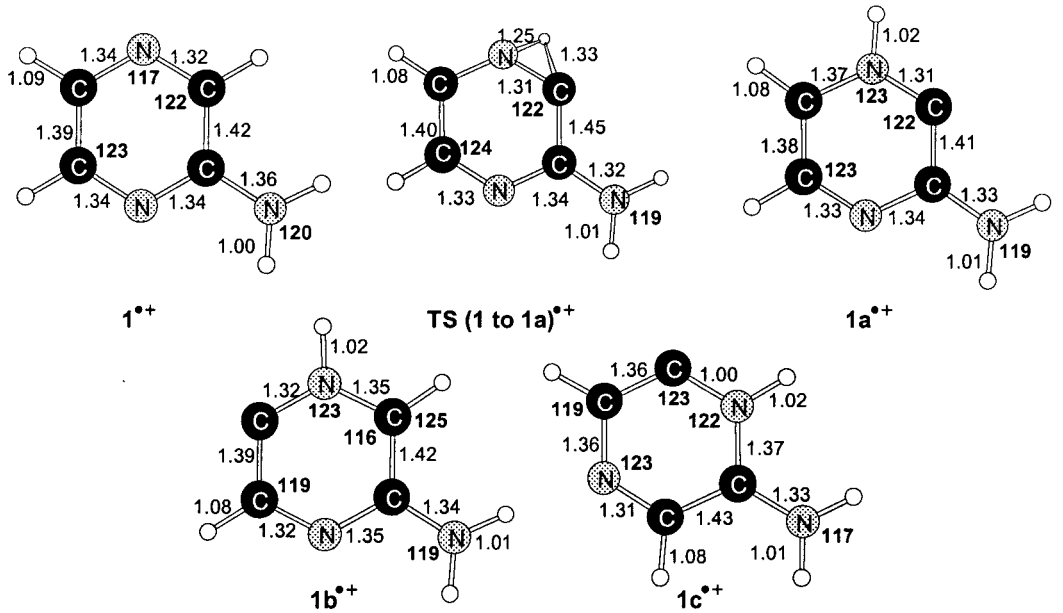

$1^{\bullet+}$ TS (1 to 1a)$^{\bullet+}$ $1a^{\bullet+}$

$1b^{\bullet+}$ $1c^{\bullet+}$

Figure A4.3. Selected optimized geometries of aminopyrazine and its isomers. Bond angles in degrees and bond lengths in Angstroms.

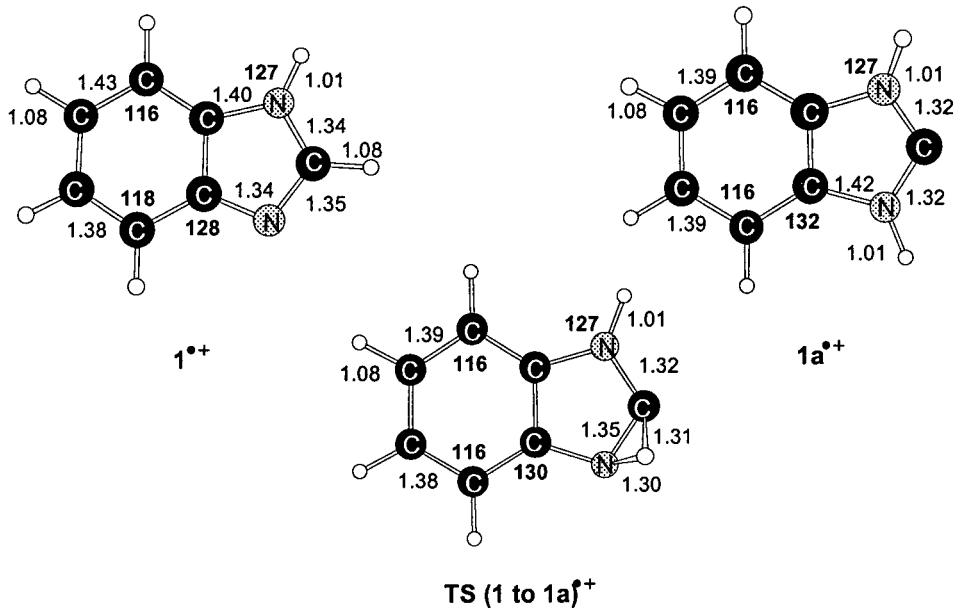

$1^{\bullet+}$ $1a^{\bullet+}$

TS (1 to 1a)$^{\bullet+}$

Figure A4.4. Selected optimized geometries of benzimidazole and its isomers. Bond angles in degrees and bond lengths in Angstroms.

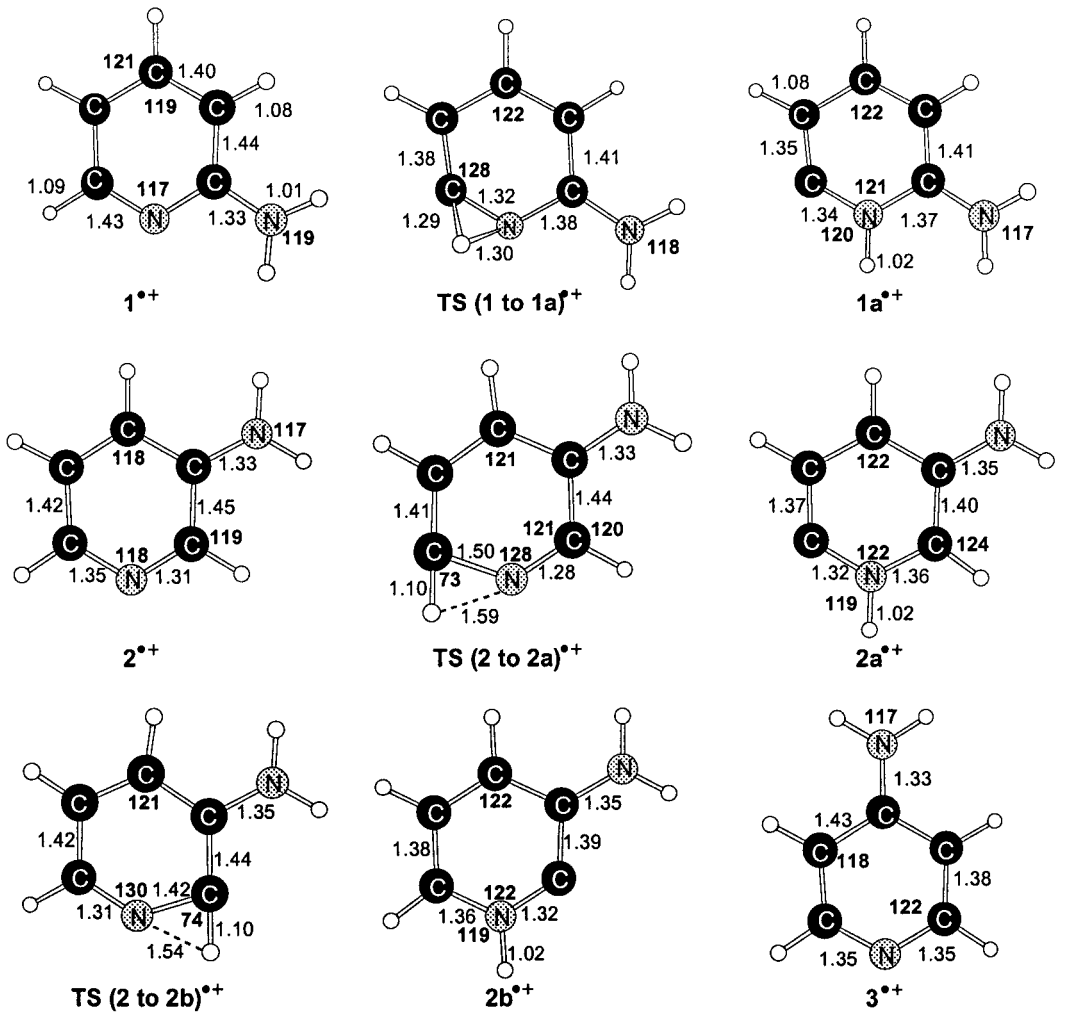

Figure A4.5. Selected optimized geometries of aminopyridine and its isomers. Bond angles in degrees and bond lengths in Angstroms.

Chapter 5

Generation and characterization of protonated silicic acid $Si(OH)_3^+$ and its neutral counterpart by tandem mass spectrometry and computational chemistry

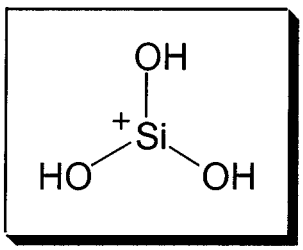

Dissociative electron ionization of triethoxysilane, $HSi(OC_2H_5)_3$, and tetraethoxysilane, $Si(OC_2H_5)_4$, generates m/z 79 ions of composition $[Si, O_3, H_3]^+$. From tandem mass spectrometry experiments and CBS-QB3 model chemistry calculations, it is concluded that these ions have the structure of protonated silicic acid, $Si(OH)_3^+$, $\mathbf{1a}^+$, for which ΔH_f(298 K) = -36.3 kcal mol^{-1} (for the anti-isomer). Low energy (metastable) ions $\mathbf{1a}^+$ dissociate via loss of H_2O and SiO_2 to yield m/z 61 ($HOSi{=}O^+$) and m/z 19 (H_3O^+) product ions, respectively. These reactions involve isomerization of $\mathbf{1a}^+$ into the stable isomers $HOSi(=O)OH_2^+$, $\mathbf{1b}^+$, and $[H_2O{\bullet\bullet}H{\bullet\bullet}O{=}Si{=}O]^+$, $\mathbf{1c}^+$, the proton-bound dimer of SiO_2 and H_2O. The dimer ion lies 77 kcal mol^{-1} higher in energy than $\mathbf{1a}^+$, in contrast to the carbon analogues $C(OH)_3^+$ and $[H_2O{\bullet\bullet}H{\bullet\bullet}O{=}C{=}O]^+$ which have comparable heats of formation. From neutralization-reionization experiments it is concluded that the $Si(OH)_3^\bullet$ radical is a stable species in the gas phase, having a calculated ΔH_f (298 K) = -191.1 kcal mol^{-1} (for the anti-isomer).

This work described here has been published previously in an article under the same title: Georgina Dimopoulos, R. Srikanth, R. Srinivas, and Johan K. Terlouw. Int. J. Mass Spectrom. 221 (2002) 219.

Introduction

Over the past several years, small silicon containing organic molecules and ions have attracted a great deal of attention of both experimentalists and theoreticians due to their importance as reactive intermediates in chemical reactions ranging from synthetic organic chemistry [1] to microprocessor manufacturing [2]. Besides, these species have been suggested to play an important role in interstellar chemistry. Two silicon-bearing molecules, SiO and SiS have been detected in interstellar clouds and four other silicon-containing molecules, SiC, c-SiC_2, SiC_4 and SiH_4, have been detected in circumstellar shells [3,4]. Amongst the experimental methods, neutralization-reionization mass spectrometry (NRMS) [5] has proven to be a powerful and versatile technique for investigating highly reactive elusive radicals/molecules which are fundamentally important. The NRMS methodology has been successfully used by Schwarz and co-workers to generate and characterize several small silicon-containing organic species [6]. Among the oxygen containing silicon species that have been characterized are SiOH/HSiO [7], CH_2OSi [8], $Si_xO_yH_z$ [7, 9], $(CH_3)_2SiOH$, CH_3SiOH [10], $SiOCH_3$ [11] and SiNCO [12].

Silicon containing species of the type H_xSiO_y are also known to be key intermediates in silane-oxygen flames and theoretical studies [13] on some of these have been reported in the literature. Such species have also been extensively studied by Bohme and coworkers [14], using the selected-ion flow tube (SIFT) technique. We recently reported on the characterization of ionic and neutral silicon dihydroxide , $Si(OH)_2^{+\bullet/0}$ and silanoic acid $HSi(O)OH^{+\bullet/0}$ by NRMS and computational chemistry [15]. Here we report on the characterization of $Si(OH)_3^+$ and its neutral counterpart in the gas phase by using a combination of tandem mass spectrometric methods and calculations using the CBS-QB3 model chemistry [16].

Experimental and Theoretical Methods

The mass spectrometric experiments were performed on VG Analytical Autospec M and ZAB-R mass spectrometers of EBE and BEE geometry, respectively (E = electric sector, B = magnet). Detailed information about these instruments has been previously reported [17,18].

Triethoxysilane (**I**) and tetraethoxysilane (**II**) (obtained from Aldrich) were used as precursor molecules for the m/z 79 $Si(OH)_3^+$ ions of the study. The expected elemental composition of the mass 79 ions in the 70 eV electron ionization (EI) mass spectra of **I** and **II** was confirmed with the Autospec using a resolution $m/\Delta m = 7000$ (10% valley definition).

The metastable ion (MI), collision-induced dissociation (CID) and neutralization-reionization (NR) spectra recorded on the instruments were similar. The NR/CID survivor spectrum was obtained with the ZAB-R instrument and for reasons of uniformity the related spectra presented in Figure 2 were also recorded on this instrument. The CID spectra were recorded using oxygen as collision gas. The NR spectra were recorded using *N*, *N*-dimethylaniline (ZAB-R) or Xenon (Autospec M) as reducing agents and oxygen gas for reionization. The ZAB-R spectra were recorded using a small PC-based data system developed by Mommers Technologies Inc. (Ottawa).

Structures and energies of the H_3SiO_3 and H_3CO_3 ions and neutrals pertinent to this study, connecting transition states and dissociation products were probed by the standard CBS-QB3 model chemistry [16]. The calculations were performed using Gaussian 98 Revision A.7 [19]. The calculated energies are presented in Table 5.1 (see Appendix) and the potential energy diagram of Figure 5.1. Detailed geometries of selected species are displayed in the Appendix, Figure A5.1 (the complete set of geometries is available upon request). Frequency calculations gave the correct number of negative eigenvalues for all minima and transition states and the spin contamination was within the acceptable range. The

connections of the transition states have been checked by geometry optimizations and frequency calculations.

Results and Discussion

1. The generation and characterization of the $Si(OH)_3^+$ ion.

The 70 eV EI mass spectra of triethoxysilane, $HSi(OC_2H_5)_3$ (**I**), and tetraethoxysilane, $Si(OC_2H_5)_4$ (**II**), both display a sizeable (~ 40% of the base peak) peak at m/z 79, corresponding to ions of elemental composition [Si, O_3, H_3]$^+$. From an analysis of the MI and CID spectra of all potential precursor ions, it follows that the m/z 79 ions from $\mathbf{I}^{\bullet+}$ are generated by the reaction sequence: $164^{\bullet+}$ ($\mathbf{I}^{\bullet+}$) $\rightarrow$ 163^+ $\rightarrow$ 135^+ $\rightarrow$ 107^+ $\rightarrow$ 79^+, i.e. loss of $H^\bullet$, followed by three consecutive C_2H_4 losses. For $\mathbf{II}^{\bullet+}$, the m/z 79 ions are also generated by the route 135^+ $\rightarrow$ 107^+ $\rightarrow$ 79^+, while m/z 135 is generated via two pathways: $208^{\bullet+}$ ($\mathbf{II}^{\bullet+}$) $\rightarrow$ 163^+ $\rightarrow$ 135^+ (consecutive losses of $C_2H_5O^\bullet$ and C_2H_4) and $208^{\bullet+}$ ($\mathbf{II}^{\bullet+}$) $\rightarrow$ 179^+ $\rightarrow$ 135^+ (consecutive losses of $C_2H_5^\bullet$ and $CH_3C(H)=O$).

If the ethylene losses involve β-hydrogen rearrangements, the resulting m/z 79 ions would have the structure $Si(OH)_3^+$, $\mathbf{1a}^+$, i.e. silicic acid $(HO)_2Si=O$ protonated at the Si=O moiety. Its carbon analogue, *viz.* carbonyl protonated carbonic acid, $C(OH)_3^+$, $\mathbf{2a}^+$, has been identified as a stable species in the gas phase. The CID spectrum of this ion is characteristically different from that of its isomer $[O=C=O\cdots H\cdots OH_2]^+$, $\mathbf{2c}^+$, the proton-bound dimer of CO_2 and H_2O [20]. A third isomer, hydroxyl protonated carbonic acid, $HOC(=O)OH_2^+$, $\mathbf{2b}^+$, has so far eluded experimental observation. Semi-empirical calculations [21] indicate that this ion lies higher in energy than $\mathbf{2a}^+$, by 33 kcal mol^{-1}, and is separated by a high barrier for interconversion. Very recently reported [22] high-level ab initio results on this system yield ΔH_f(298 K) $\mathbf{2a}^+$ = 35.9 kcal mol^{-1} (for the anti-isomer); ion $\mathbf{2b}^+$ was found to lie 25 kcal mol^{-1} higher in energy with an interconversion barrier of 52 kcal mol^{-1}. The proton-bound dimer $\mathbf{2c}^+$, on the other hand, is reported to lie 4 kcal mol^{-1} lower in energy. Our CBS-QB3 computational results (Table 5.1)

which provide ΔH_f(298 K) values for $\mathbf{2a}^+$, $\mathbf{2b}^+$ and $\mathbf{2c}^+$ of 35, 61 and 33 kcal mol^{-1}, respectively, are in good agreement with the G2 results of the above study [22]. Thus ions $\mathbf{2a}^+$ and $\mathbf{2c}^+$ are of comparable stability, while $\mathbf{2b}^+$ lies c. 27 kcal mol^{-1} higher in energy. In this context, we note that the ΔH_f for the proton-bound dimer ion $\mathbf{2c}^+$ can also be estimated from the empirical relationship of ref. 23, which correlates the hydrogen bond energy and the proton affinity (PA) difference between the dimer components in heterogeneous proton-bound dimers. This procedure yields, using the appropriate PA values from ref. 24a, $\Delta H_f(\mathbf{2c}^+)$ = 29 kcal mol^{-1}, which is fairly close to the computationally derived value.

In view of these observations, it seemed reasonable to assume that ions $\mathbf{2b}^+$ and $\mathbf{2c}^+$ have stable silicon analogues, *viz.* $HOSi(=O)OH_2^+$, $\mathbf{1b}^+$, and $[O=Si=O\cdots H\cdots OH_2]^+$, $\mathbf{1c}^+$. These could conceivably be (co)generated in the dissociative ionization of $\mathbf{I}^{\bullet+}$, as is depicted in Scheme 5.1 for the ethylene loss from the m/z 107 ion, the immediate precursor of the m/z 79 ions.

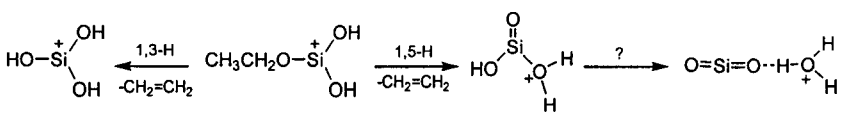

$\mathbf{1a}^+$ (m/z 79) — (m/z 107) — $\mathbf{1b}^+$ (m/z 79) — $\mathbf{1c}^+$ (m/z 79)

Scheme 5.1

Our calculations, see Table 5.1, show that all three ions $\mathbf{1a}^+$ - $\mathbf{1c}^+$ are minima on the potential energy surface as are the high energy isomers $\mathbf{1d}^+$ and $\mathbf{1e}^+$ which were not further considered. For ions $\mathbf{1a}^+$ - $\mathbf{1c}^+$, unlike the situation with the carbon analogues, the proton-bound dimer $[O=Si=O\cdots H\cdots OH_2]^+$ is now the least stable isomer of the set, lying 79 kcal mol^{-1} higher in energy than the anti-isomer of $Si(OH)_3^+$. This makes it unlikely that this isomer is co-generated in the C_2H_4 loss from m/z 107. This is probably also true for the hydroxyl protonated silicic acid isomer $\mathbf{1b}^+$, which lies 48 kcal mol^{-1} higher in energy than $\mathbf{1a}^+$ while the isomerization barrier $\mathbf{1b}^+ \rightarrow \mathbf{1a}^+$ is fairly low, 22 kcal mol^{-1} (see Table 5.1). Thus, it is likely that both $\mathbf{I}^{\bullet+}$ and $\mathbf{II}^{\bullet+}$ yield m/z 79 ions of structure $Si(OH)_3^+$, $\mathbf{1a}^+$.

Nevertheless, the (identical) MI spectra of the mass 79 ions from $\mathbf{I}^{\bullet+}$ and $\mathbf{II}^{\bullet+}$ provide clear evidence that ions $\mathbf{1b}^+$ and/or $\mathbf{1c}^+$ participate in the dissociation of low energy ions $\mathbf{1a}^+$. The MI spectrum (2ffr, 10 keV ions) displays two peaks, at m/z 61 and m/z 19 with an intensity ratio of 7:1. Both peaks have a Gaussian shape. For the loss of H_2O, yielding the m/z 61 ion $HOSi{=}O^+$, the kinetic energy (KER) release measured from the width at half-height, $T_{0.5}$ [25], is 17 meV. For the loss of SiO_2, yielding the m/z 19 H_3O^+ ion, the KER is slightly but significantly higher, $T_{0.5}$ = 23 meV. It is reasonable to expect that the loss of water involves participation of either $\mathbf{1b}^+$ or $\mathbf{1c}^+$. The less abundant m/z 19 H_3O^+ ions on the other hand, could well be generated by direct bond cleavage from the proton-bound dimer $\mathbf{1c}^+$.

To further probe this proposal, we have calculated the minimum energy requirements for the above metastable dissociations and the two direct bond cleavage reactions that dominate the CID spectrum discussed below. The results are combined in the potential energy diagram of Figure 5.1.

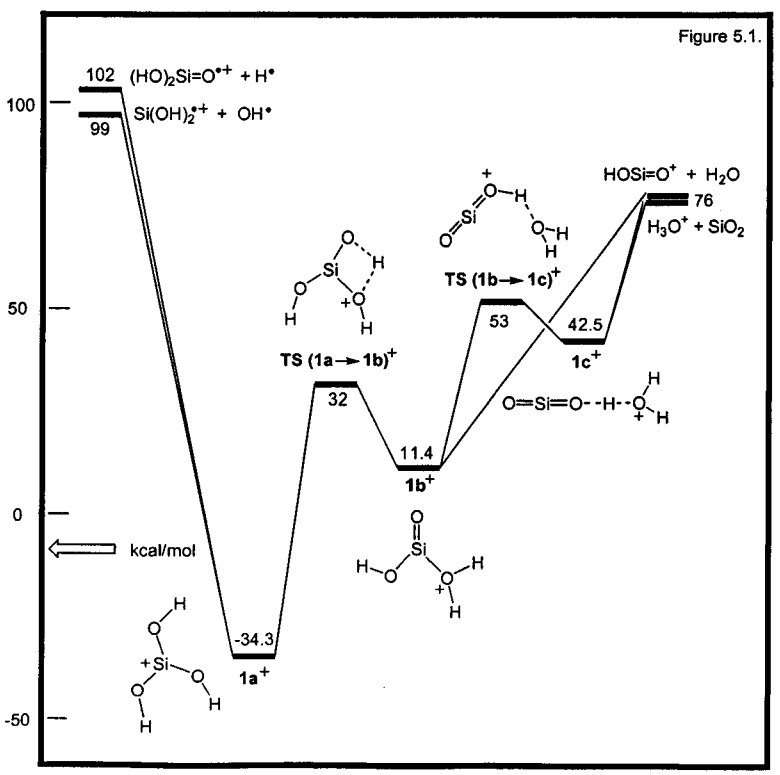

It is seen that ions $\mathbf{1a}^+$ can freely interconvert with their hydroxyl protonated silicic acid isomer $\mathbf{1b}^+$, at energies well below that required for the H_2O and SiO_2 losses observed in the MI spectrum, while that for the two direct bond cleavage reactions lies even higher in energy. We further note that the energy level for $H_3O^+ + SiO_2$ lies slightly below that for $HOSi{=}O^+ + H_2O$. This implies that the PA of SiO_2 (for which no experimental value is available) is only marginally lower than that of H_2O, 165 kcal mol^{-1} [24a]. In line with this, in the optimized geometry of the proton-bound dimer $[O{=}Si{=}O{\cdots}H{\cdots}OH_2]^+$, the bridging H is a little closer to the H_2O molecule (1.021 Å vs 1.273 Å for $H{\cdots}O{=}Si{=}O$, see Figure A5.1). (For the carbon analogue, $[O{=}C{=}O{\cdots}H{\cdots}OH_2]^+$, where the PAs of the bridged molecules differ considerably, by 36 kcal mol^{-1} [24a], the $O{=}C{=}O{\cdots}H$ and $H{\cdots}OH_2$ distances are 1.518 and 1.022 Å respectively.)

We further note that the calculated stabilization energy of the proton-bound dimer, c. 33 kcal mol^{-1}, is close to that for symmetric O-H-O bridged proton-bound dimers, ~ 30.5 kcal mol^{-1} [23]. However, a facile interconversion of $\mathbf{1b}^+$ into the proton-bound dimer apparently does not occur: if the dimer ion were generated from $\mathbf{1b}^+$ below the threshold for dissociation by loss of H_2O, then H_2O and SiO_2 would be lost to the same extent. This does not occur: loss of H_2O dominates the MI spectrum and moreover the associated KER is smaller than that for the loss of SiO_2. Thus, although $TS(\mathbf{1b} \rightarrow \mathbf{1c})^+$ is calculated to lie below the energy levels for the loss of H_2O and SiO_2, the isomerization $\mathbf{1b}^+$ to $\mathbf{1c}^+$ suffers from a substantial kinetic hindrance.

The CID spectra of the source generated m/z 79 ions from the two ethoxysilanes are identical. A representative spectrum is presented in Figure 5.2a. In line with the proposal, that the stable m/z 79 ions are ions $\mathbf{1a}^+$ which can easily interconvert with $\mathbf{1b}^+$ but not $\mathbf{1c}^+$, the spectrum displays intense peaks at m/z 78, 62 and 61. Note that m/z 19 ions are barely detectable. Other major peaks are m/z 45 ($SiOH^+$) and m/z 44 ($SiO^{\bullet+}$) which are obviously secondary fragment ions. The spectra also contain a weak doubly charged ion, at m/z 39.

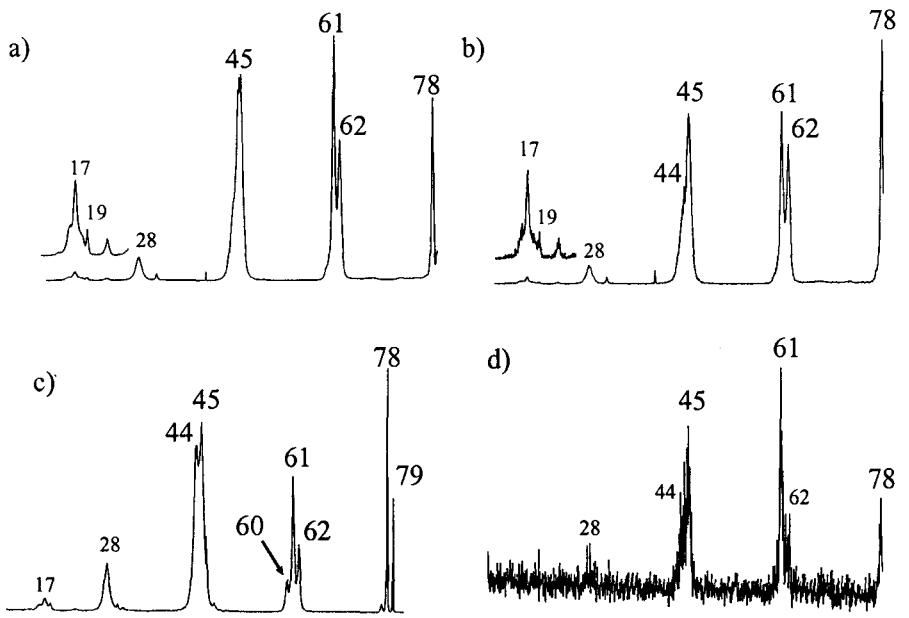

Figure 5.2. a) CID spectrum (3ffr) of 8 keV source generated m/z 79 ions $Si(OH)_3^+$; b) CID spectrum (3ffr) of m/z 79 $Si(OH)_3^+$ ions generated from 10 keV m/z 107 metastable ions $C_2H_5OSi(OH)_2^+$; c) NR spectrum (2ffr) of 8 keV m/z 79 $Si(OH)_3^+$ ions ; d) CID spectrum (3ffr) of the m/z 79 survivor ion in the NR spectrum of Fig. 2c.

Loss of C_2H_4 is the only dissociation of the metastable m/z 107 ions $C_2H_5OSi(OH)_2^+$ and the internal energy content of the resulting m/z 79 ions is expected to be lower than that of the source generated ions. The energy required for loss of C_2H_4 via a 1,3-H shift leading to $\mathbf{1a}^+$, see Scheme 5.1, is estimated to be ~ 30 kcal mol^{-1} [26], considerably less than that required to form $\mathbf{1b}^+$ via a 1,5-H shift, ~ 45 kcal mol^{-1}, see Figure 5.1. Therefore, the metastably generated m/z 79 ions from the m/z 107 precursor ion may well represent isomerically pure ions $\mathbf{1a}^+$. The CID spectrum of these ions is presented in Figure 5.2b. The spectrum is closely similar to that of Fig. 5.2a but, as seen from the enhanced m/z 62: m/z 61 peak intensity ratio, the low energy ions are less prone to lose H_2O upon collisional activation. This supports the proposal that the metastably generated m/z 79 ions are (largely) $\mathbf{1a}^+$, whereas the source generated ions consist of $\mathbf{1a}^+$ in admixture with $\mathbf{1b}^+$.

2. Characterization of the neutral species $Si(OH)_3^{\bullet}$.

The neutralization-reionization mass spectra of ions $\mathbf{1a}^+$ from both precursors are identical and a representative spectrum is shown in Figure 5.2c. The spectrum displays a fairly abundant recovery signal at m/z 79 (45 % of the base peak at m/z 78). Among ions $\mathbf{1a}^+$ - $\mathbf{1c}^+$, only $\mathbf{1a}^+$ is expected to have a stable neutral counterpart and thus the presence of a sizeable recovery signal indicates that the $Si(OH)_3^{\bullet}$ radical is a stable species on the μs time scale of the NR experiment. This is in line with our calculations which show that $Si(OH)_3^{\bullet}$, **1a**, is a stable minimum on the potential energy surface with a ΔH_f (298 K) of –191 kcal mol^{-1} (for the anti-isomer). The calculations further indicate, see Table 5.1, that the neutral counterpart of $\mathbf{1b}^+$ is only a shallow minimum, which lies 3 kcal mol^{-1} below the transition state for its isomerization into **1a**.

To eliminate the possibility that (part of) the recovery signal in the NR spectrum stems from an isobaric impurity [28], we have obtained its CID spectrum which is presented in Figure 5.2d. Although the weak spectrum suffers from a high noise level, there is little doubt that the survivor ions of Fig. 5.2c are silicon containing species of structure $Si(OH)_3^+$. Thus, while $Si(OH)_3^{\bullet}$ is a stable species on the μs timescale of the NR experiment, this is not the case for its carbon analogue $C(OH)_3^{\bullet}$. From the recently reported comprehensive NR study by Gerbaux and Tureček [22], it follows that collisional neutralization of protonated carbonic acid yields transient trihydroxymethyl radicals that dissociate rapidly by loss of a hydrogen atom, so that no survivor species are observed on a timescale ≥ 360 ns.

Two further points deserve comment: (i) comparison of the shapes of the peaks at m/z 78, 62 and 61 of the 2ffr CID spectra of $\mathbf{1a}^+$ with those of its NR spectrum shows that the m/z 78 NR peak is less broadened than its CID counterpart, whereas the width of the peaks at m/z 61 and 62 shows no change. This suggests that part of the m/z 78 ions $(HO)_2Si{=}O^{\bullet+}$ result from collisional ionization of neutral silicic acid molecules $(HO)_2Si{=}O$, generated by loss of $H^{\bullet}$

from $Si(OH)_3^{\bullet}$. This reaction is calculated to be endothermic, by 47 kcal mol^{-1} (Table 5.1) and would be associated with only a small reverse activation energy; (ii) the m/z 60 peak is not significant in the CID spectrum of $\mathbf{1a}^+$ and considering the high heat of formation of the $SiO_2^{\bullet+}$ ion, 222 kcal mol^{-1}, this is not surprising. The NR spectrum does display a (moderate) peak at m/z 60, which probably originates from collisional ionization of SiO_2. A thermochemically attractive route for its formation involves dehydration of the incipient $Si(OH)_3^{\bullet}$ radical into $HOSi{=}O^{\bullet}$ followed by loss of $H^{\bullet}$. Loss of $OH^{\bullet}$ from $HOSi{=}O^{\bullet}$ into SiO has a slightly lower energy requirement and this may explain the enhanced intensity of the m/z 44 peak in the NR spectrum.

Conclusion

From the combined results of tandem mass spectrometric experiments and CBS-QB3 theoretical calculations, it is concluded that dissociative electron ionization of triethoxysilane, $HSi(OC_2H_5)_3$ and tetraethoxysilane, $Si(OC_2H_5)_4$, yields m/z 79 ions having the structure of protonated silicic acid , $Si(OH)_3^+$, $\mathbf{1a}^+$. The dissociation of metastable ions $\mathbf{1a}^+$ - via loss of H_2O and SiO_2 to form m/z 61 ($HOSi{=}O^+$) and m/z 19 (H_3O^+) ions - involves the participation of the high-energy isomers $HOSi(=O)OH_2^+$, $\mathbf{1b}^+$, and $[O{=}Si{=}O\cdots H\cdots OH_2]^+$, $\mathbf{1c}^+$, a proton-bound dimer. Neutralization-reionization experiments show that $Si(OH)_3^{\bullet}$, $\mathbf{1a}^{\bullet}$, is a stable species in the rarefied gas phase, in contrast to its carbon analogue, $C(OH)_3^{\bullet}$, [22].

References

[1] N. Auner, J. Weis, Organosilicon Chemistry: From Molecules to Materials. VCH Publishers. Weinheim. 1994.

[2] J.M. Jasinski, S.M. Gates. Acc. Chem. Res. 24 (1991) 9.

[3] D. Smith., Chem. Rev. 92 (1992)1473.

[4] H. Miyoshi, K. Matsumoto, K. Kameno, H. Takaba, T. Iwata. Nature 371 (1994) 395.

[5] For a recent review see: C.A. Schalley, G. Hornung, D. Schröder, H. Schwarz. Chem. Soc. Rev. 27 (1998) 91.

[6] N. Goldberg, H. Schwarz, in the Chemistry of Organic Silicon Compounds, Ed. Z. Rapoport, Y. Apeloig, Wiley. Chichester. 1988. Vol. 2, Chapter 18, 1106-1133.

[7] R. Srinivas, D. Sülzle, T. Weiske, H. Schwarz. J. Am. Chem. Soc. 113 (1991) 5970.

[8] R. Srinivas, D.K. Bohme, J. Hrusak, D. Schröder, H. Schwarz. J. Am. Chem. Soc. 114 (1992) 1939.
[9] R. Srinivas, D.K. Bohme, D. Sülzle, H. Schwarz. J. Phys. Chem. 95 (1991) 9836.
[10] V.Q. Nguyen, S.A. Schaffer, F. Tureček, C.E.C.A Hop. J. Phys. Chem. 99 (1995) 15454.
[11] M.C. Holthausen, D. Schröder, W. Zummack, W. Koch, H. Schwarz. J. Chem. Soc. Perkin Trans. 2 (1996) 2389.
[12] R. Srinivas, S. Vivekananda, D. Schröder, H. Schwarz. Chem. Phys. Lett. 316 (2000) 243.
[13] N.A. Richardson, J.C. Rienstra-Kiracofe, H.F. Schaefer. J. Am. Chem. Soc. 121 (1999) 10813.
[14] a) S. Wlodek, A. Fox, D. Bohme. J. Am. Chem. Soc. 109 (1987) 6663 ; b) D. Bohme, Int. J. Mass Spectrom. 100 (1990) 719 ; c) Review on "Chemistry Initiated by Atomic Silicon Cations" in Advances in Gas-phase Ion Chemistry. N.G. Adams, L. Babcock. JAI Press. Vol.1 (1992) 225.
[15] R. Srikanth, K. Bhanuprakash, R. Srinivas. Chem. Phys. Lett. 360 (2002) 294.
[16] (a) J.A. Montgomery Jr., M.J. Frisch, J.W. Ochterski, G.A. Petersson, J. Chem. Phys. 112 (2000) 6532 ; (b) J.A. Montgomery Jr., M.J. Frisch, J.W. Ochterski, G.A. Petersson, J. Chem. Phys. 110 (1999) 2822.
[17] S. Vivekananda, R. Srinivas. Int. J. Mass Spectrom. Ion Processes 171 (1997) 79.
[18] H.F. van Garderen, P.J.A. Ruttink, P.C. Burgers, G.A. McGibbon, J.K. Terlouw. Int. J. Mass Spectrom. Ion Processes 121 (1992) 159.
[19] M.J. Frisch, et al. Gaussian 98, Revision A.7, GAUSSIAN Inc., Pittsburgh PA, 1998.
[20] J. Hrušák, G.A. McGibbon, H. Schwarz, J.K. Terlouw. Int. J. Mass Spectrom. Ion Processes 160 (1997) 117.
[21] H. Egsgaard, L. Carlsen. J. Chem. Soc. Faraday Trans. 1 85 (1989) 3403.
[22] P. Gerbaux, F. Tureček. J. Phys. Chem. A 106 (2002) 5938.
[23] J.W. Larson, T.B. McMahon. J. Am. Chem. Soc. 104 (1982) 6255.
[24] (a) E.P.S. Hunter, S.G. Lias. J. Phys. Chem. Ref. Data 27 (1998) No. 3 ; (b) S.G. Lias, J.E. Bartmess, J.F. Liebman, J.L. Holmes, R.O. Levin, W.G. Mallard. J. Phys. Chem. Ref. Data 17 (1988) Supplement 1.
[25] J.L. Holmes, J.K. Terlouw. Org. Mass Spectrom. 15 (1980) 383.
[26] A typical value for a 1,3-H shift in even electron ions is 30 kcal mol^{-1}. Note also that the minimum energy requirement for loss of C_2H_4 from $C_2H_5OSi(OH)_2^+$ is 21 kcal mol^{-1} (from $\Delta H_f [C_2H_5OSi(OH)_2^+]$ = -41.8 kcal mol^{-1}, $\Delta H_f [Si(OH)_3^+]$ = -34.3 kcal mol^{-1}, CBS-QB3 (298 K) values, this work; $\Delta H_f [C_2H_4]$ = 13 kcal mol^{-1} [18b])
[27] C.L. Darling, H.B. Schlegel. J. Phys. Chem. 97 (1993) 8207.
[28] L.N. Heydorn, C.Y. Wong, R. Srinivas, J.K. Terlouw. Int. J. Mass Spectrom. 225 (2003) 11.

Appendix to Chapter 5

Table 5.1. CBS-QB3 [a] computational results for the key isomers of the $[Si, O_3, H_3]^{+/\bullet}$ system, some carbon analogues and dissociation products.

Structure			CBS-QB3 (0 K)	CBS-QB3 (Enthalpy)	ΔH_f (0 K)	ΔH_f (298 K)
$Si(OH)_3^+$		**1a$^+$ (syn)**	-516.14491	-516.13846	-31.4	-34.3
$Si(OH)_3^+$		**1a$^+$ (anti)**	-516.14790	-516.14162	-33.3	-36.3
$Si(OH)_3^\bullet$		**1a (anti)**	-515.39565	-516.38837	-188.8	-191.1
$HOSi(=O)OH_2^+$		**1b$^+$**	-516.07208	-516.06564	14.3	11.4
$HOSi(=O)OH_2^\bullet$		**1b**	-516.32300	-516.31565	-143.2	-145.5
$O=Si=O\cdot\cdot H\cdot\cdot OH_2^+$		**1c$^+$**	-516.02328	-516.01608	44.9	42.5
$HO(H)\underline{Si\text{-}O\text{-}O}H^+$		**1d$^+$**	-515.97150	-515.96540	77.4	74.3
$HO(H)SiO\text{-}OH^+$		**1e$^+$**	-515.95878	-515.95159	85.4	83.0
TS **1a$^+$ → 1b$^+$**			-516.04002	-516.03357	34.4	31.5
TS **1b$^+$ → 1c$^+$**			-516.00582	-515.99948	55.8	52.9
TS **1a → 1b**			-516.31712	-516.31097	-139.5	-142.6
$C(OH)_3^+$		**2a$^+$ (syn)**	-264.97708	-264.97205	44.2	40.9
$C(OH)_3^+$		**2a$^+$ (anti)**	-264.98696	-264.98213	38.0	34.6
$HOC(=O)OH_2^+$		**2b$^+$**	-264.94566	-264.94002	63.9	61.0
$O=C=O\cdot\cdot H\cdot\cdot OH_2^+$		**2c$^+$**	-264.99199	-264.98513	34.8	33.0
$(HO)_2Si=O^{\bullet+}$		m/z 78	-515.43169	-515.42530	50.8	48.9
$(HO)_2Si=O$			-515.82081	-515.81510	-193.3	-195.7
$Si(OH)_2^{\bullet+}$		m/z 62	-440.28228	-440.27705	93.4	91.8
$HOSi=O^+$		m/z 61	-439.63436	-439.62922	134.7	134.0
$HOSi=O^\bullet$	[b]		-439.96896	-439.96419	-75.3	-76.2
$O=Si=O^{\bullet+}$	[c]	m/z 60				221.6
$O=Si=O$	[b]		-439.37501	-439.37077	-67.9	-68.0
$SiOH^+$		m/z 45	-364.52633	-364.52639	151.2	150.9
$SiO^{\bullet+}$	[b]	m/z 44	-363.79760	-363.79428	243.3	243.5
SiO	[b]					-23.8
H_3O^+		m/z 19	-76.59652	-76.59265	145.2	143.6

[a] CBS-QB3 energies given in Hartrees, all other components are in kcal/mol; The calculated ΔH_f(298 K) values for $H^\bullet$, $OH^\bullet$ and H_2O used in Fig. 1 are 52.1, 6.9 and -58.2 kcal/mol, respectively.
[b] G2 (298 K) calculated values for SiO, SiO_2 and $HOSi=O^\bullet$ are -22.6, -66.2 and -72.9 kcal/mol, respectively [27]; For SiO and $SiO^{\bullet+}$ experimental values are available, -24.0 and 239.6 kcal/mol respectively [24b].
[c] For $SiO_2^{\bullet+}$ spin contamination occurs in the CBS-QB3 calculation. The G2 calculation does not suffer from spin contamination and yields 227.1 kcal/mol.

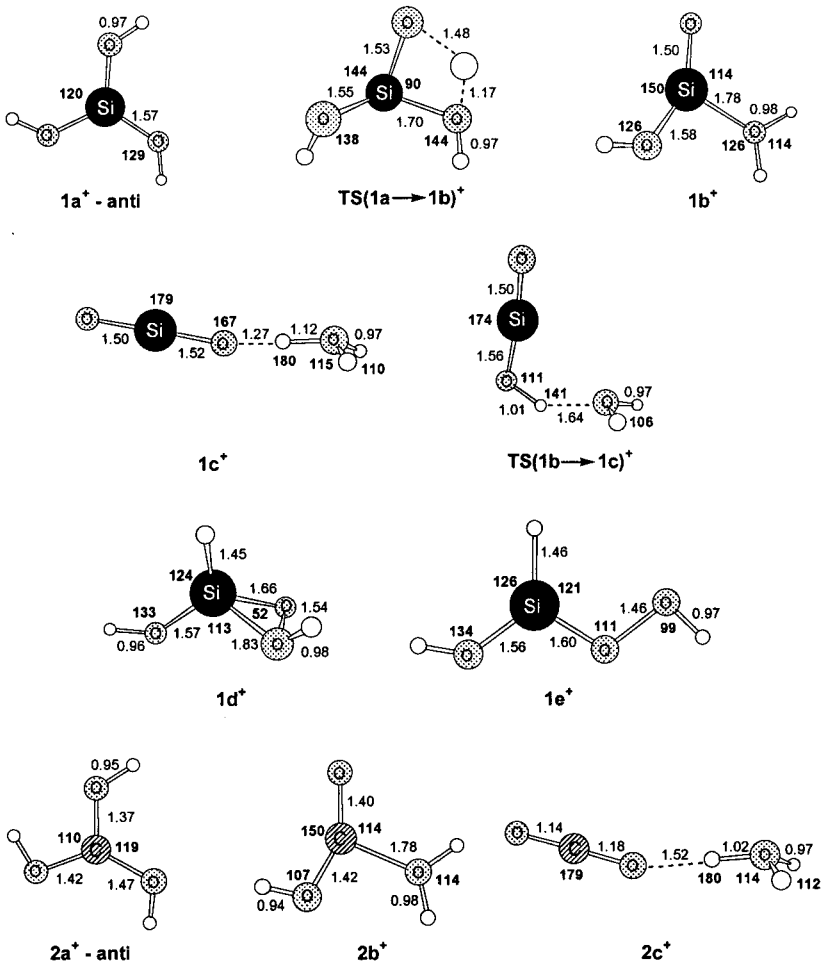

Figure A5.1: Selected optimized geometries of the protonated silicic acid, $Si(OH)_3^+$, isomers $\mathbf{1a}^+$ - $\mathbf{1e}^+$ and the carbon analogues $\mathbf{2a}^+$ - $\mathbf{2c}^+$. Bond angles in degrees and bond lengths in Angstroms.

SUMMARY

The research presented in this thesis is focused on a unified mass spectrometric and computational chemistry approach to problems of gas-phase ion chemistry. The structure, reactivity and stability of various ions and neutrals in the gas phase were studied.

In Chapter 2, it is shown that tandem mass spectrometry based experiments on the $CH_2N_2^{\bullet+}$ family of ions allow for the characterization and differentiation of the various isomers. Persuasive evidence is presented in Chapter 2 for the generation and characterization of the elusive carbodiimide ion, $HNCNH^{\bullet+}$, using collision-induced dissociation and collision-induced dissociative ioniziation mass spectrometry. CBS-QB3 calculations predict that $HNCNH^{\bullet+}$ and $H_2NCN^{\bullet+}$ are separated by a high energy barrier for the 1,3-H shift so that their unassisted interconversion does not occur. However, in agreement with theory, it is proposed that a single water molecule catalyzes the isomerization of the cyanamide ion into its more stable counterpart, the carbodiimide ion.

Using the results of a CBS-QB3 computational study on the $CH_3N_3^{\bullet+}$ isomeric ions, Chapter 3 describes the characterization and differentiation of the aminocarbodiimide ion, $H_2N\text{-}N{=}C{=}NH^{\bullet+}$, the aminonitrilimine ion, $H_2N\text{-}C{=}N{=}NH^{\bullet+}$, the C-aminoisodiazirine ion, $H_2N\text{-}\underline{C{=}N{=}N}H^{\bullet+}$, and the ionized biradical, $H_2N{=}N\text{-}C(H){=}N^{\bullet+}$, using collision-induced dissociation mass spectrometry. From CBS-QB3 calculations, these ions were identified as stable species in the gas phase. The stability of the neutrals was probed by neutralization-reionization experiments and it follows that the aminocarbodiimide ion and the C-aminoisodiazirine ion have stable neutral counterparts, in agreement with the computational results.

In Chapter 4, the α-distonic ions of several heterocyclic nitrogen-containing compounds were differentiated from their conventional isomers through the use of CID mass spectrometry. From NR experiments on the ylid ions

and their conventional isomers, it follows that the ylid ions have stable neutral counterparts, as predicted by theory. CBS-QB3 calculations show that the ylid ions of the molecules studied in Chapter 4 are slightly less stable than their conventional counterparts. This makes it difficult to study proton transport catalysis in these systems of ions because the substrate ylid ions cannot be generated by direct ionization.

Lastly, Chapter 5 presents the combined results of tandem mass spectrometric experiments and CBS-QB3 theoretical calculations for the generation and characterization of protonated silicic acid, $Si(OH)_3^+$, and its neutral counterpart. The metastable $Si(OH)_3^+$ ions dissociate by loss of H_2O and SiO_2 to form $HOSi{=}O^+$ and H_3O^+ ions, respectively. The dissociation reactions of $Si(OH)_3^+$ involve the participation of the high-energy isomers $HOSi(=O)OH_2^+$ and $[O{=}Si{=}O\cdots H\cdots OH_2]^+$ (a proton-bound dimer). NR experiments show that $Si(OH)_3^\bullet$ is a stable species in the rarefied gas phase.